NOTICE

The quality of this microform is heavily dependent upon the quality of the original thesis submitted for microfilming. Every effort has been made to ensure the highest quality of reproduction possible.

If pages are missing, contact the university which granted the degree.

Some pages may have indistinct print especially if the original pages were typed with a poor typewriter ribbon or if the university sent us an inferior photocopy.

Reproduction in full or in part of this microform is governed by the Canadian Copyright Act, R.S.C. 1970, c. C-30, and subsequent amendments.

AVIS

La qualité de cette microforme dépend grandement de la qualité de la thèse soumise au microfilmage. Nous avons tout fait pour assurer une qualité supérieure de reproduction.

S'il manque des pages, veuillez communiquer avec l'université qui a conféré le grade.

La qualité d'impression de certaines pages peut laisser à désirer, surtout si les pages originales ont été dactylographiées à l'aide d'un ruban usé ou si l'université nous a fait parvenir une photocopie de qualité inférieure.

La reproduction, même partielle, de cette microforme est soumise à la Loi canadienne sur le droit d'auteur, SRC 1970, c. C-30, et ses amendements subséquents.

Canada

Novel Designs and Theories for Holographic Fiber Networking Components

by Gang Yun

A THESIS

presented to the School of Graduate Studies and Research

in partial fulfillment of

the requirements for the degree of

DOCTOR OF PHILOSOPHY

in

Electrical Engineering

Department of Electrical Engineering

University of Ottawa

OTTAWA, ONTARIO, K1N 6N5

ISBN 0-315-83850-7

UNIVERSITÉ D'OTTAWA
UNIVERSITY OF OTTAWA

ABSTRACT

The author's major contributions presented in this Ph.D. thesis are three novel design techniques (or concepts) for implementation of efficient holographic fiber networking components. The first concept is termed as grating degeneration, which allows sharing of one holographic grating by more than one wave pair. This makes it possible to use a single grating as a number of 2×2 couplers in parallel, and the number of gratings required for fiber $N \times N$ couplers can be significantly reduced. The second concept is the so called sandwich structure. By using a sandwich structure, a multi-stage topology, instead of a complete mesh, can be incorporated in the construction of a grating system in a coupler. This again can simplify the structure of an $N \times N$ coupler, especially when combined with the grating degeneration technique. The third technique, called quasi-Bragg diffraction is introduced in this thesis for the construction of 16×16 couplers. It turns out that when designed properly, the number of gratings required by a 16×16 coupler can be reduced to two per slab. This is in comparison with the original design which uses four gratings in two of the four cascade slabs. The key technique is to use off-Bragg diffraction while keeping the violation of Bragg condition much higher for the unwanted waves than for the wanted waves. Apparently, this technique, as a concept, should not be restricted to 16×16 couplers. It may also be applied to other grating-based components. More generally, all of the three presented techniques should not be restricted only to star coupler designs, either. They may be applied to any multiple-grating-based component. An example is given in this thesis for applying grating degeneration to the construction of 8×8 wavelength routing couplers. It turns out that the sixteen gratings in the original design can be merged to only six actually required gratings in the final design.

Another aspect of the author's contribution is the development of a generalized diffraction theory. The major features of the theory are the rigorousness and the generality. On one hand, the theory is rigorously based on Maxwell's equations, which makes it a realistic model for simulations and analyses. On the other hand, the theory places no restrictions on light polarization, the incident wave direction and the parameters of

the grating system. This is vital to the design of a multi-grating system using grating degeneration because of the three-dimensional arrangement of the wave vectors. Besides, Jones matrices are used for a complete characterization of any grating-bearing slabs. This provides a great deal of convenience for grating performance analyses.

A general discussion is given at the beginning of the thesis on a few fundamental issues about the coupler connectivity design. It is suggested that a coupler can best be described by an idealized lossless coupler which is only subject to the first and the second law of thermal dynamics, and a matrix of coefficients representing the excess loss or any imperfections of a realistic coupler.

Two other projects that the author did during his Ph.D. program are also listed in this thesis as appendix A and B. One project was finished in the first year of the program. It is about the application of a non-imaging component—optical taper to the free-space / atmospheric optical links. The other project is a new configuration for indoor wireless communications. The author has several publications on both subjects, and the knowledge gained, especially the experience obtained in the experimental work has been helping the author to carry on an industry / university collaborative research project smoothly.

ACKNOWLEDGEMENT

Mere words cannot express the gratitude I feel to my supervisor, Dr. Mohsen Kavehrad. He has been a true mentor, and it is his constant encouragement, expert guidance and brilliant insights that has made the completion of this thesis possible. In addition, I would like to thank him for the financial support provided to me throughout the course of my Ph.D. research.

I would like to thank the members of my advisory committee, Dr. W. Steenaart and Dr. P. Galko for their valuable guidance and encouragement. A special note of thanks also goes to Dr. P. Galko for supervising my work on the IMAX project. It has been one of the most rewarding jobs I have done during the period of my Ph.D. study.

I would like to thank Dr. E. Simova for allowing me to quote some of the experimental results of her research work as a means of supporting the theories presented in this thesis. I also wish to thank her for the wonderful partnership I enjoyed in our joint research effort.

I wish to thank all my colleagues for the partnership and the numerous discussions that have helped me to carry out my work with far less difficulty. I would like to thank the staff of the Department of Electrical Engineering, University of Ottawa for their cheerful assistance. And I would like to acknowledge the financial support from the Department in the form of teaching assistant positions in the early days of my Ph.D. program.

My dear wife Lipping showed constant understanding and was extremely supportive. A mere acknowledgment by no means compensates the hardships she had to go through on account of this thesis.

Last, but not the least, my whole-hearted appreciation goes to Prof. Meiwen Yu of Beijing Institute of Technology, China, my first supervisor who lead me to the wonderful world of research. Also, I would like to thank the Canadian government for giving me the privilege of studying and working in such a wonderful country.

Contents

Chapter 1

Introduction: A General Discussion on Photonic Networking and Fiber Couplers

1.1 Optical Communications

The principal motivation in using optical-frequency-carriers for communications is the tremendous increase in transmission bandwidth. In communications systems, the amount of information transmitted is directly related to the modulation bandwidth of the carrier, which is limited to a fraction of the carrier frequency. Increasing the carrier frequency theoretically increases the available transmission bandwidth, and thus the information capacity. Frequencies of optical carriers are in the order of hundreds of THz, i.e., 10^5 times higher than those of RF or microwave carriers. This is extremely attractive to emerging applications which require transmission of large amounts of information [1]. In addition, optical carriers have other distinct characteristics. For instance, the short wavelength, resulting from the extremely high frequency, makes it possible to concentrate the transmitted power into a much smaller area or volume. This provides the possibility of building very compact systems. For example, antennae used for free-space applications

can be made much smaller than their counterparts in the microwave range. As another example, in comparison with the hair-thin fiber optical waveguides, the lateral size of waveguides in the microwave range is in the order of centimeters. All these are obviously inviting to communications engineers who consider compactness an important issue in developing new communications systems. Other desirable features, to name a few, associated with optical communications are higher security, the immunity to electromagnetic interference (EMI) and low transmission loss in certain media. These are all advantageous for meeting various system requirements.

Basically, three different media have been used for optical communication systems. They are free-space, atmosphere and optic fibers. Free-space is an ideal medium for lightwave propagation in the sense that it introduces no absorption, scattering or dispersion. The characteristics of this channel are so simple that it is sometimes called a "textbook" channel. Unfortunately, free-space only exists in outer space. A free-space optical link can thus only find applications in inter-satellite communications. The difficulty encountered so far in this application is the requirement for a precision pointing, tracking and acquisition (PTA) system. It is really a challenge to accurately direct a laser beam whose beamwidth can be easily made as small as 10^{-5} radians to a receiver tens of thousands of miles away.

Compared with free-space, the second type of medium – the atmosphere – is much more problem-prone. In the atmosphere, the drawbacks of optical waves become significant. Since the optical wavelengths are comparable with molecule or particle sizes, certain propagation effects are generated which are uncommon to radio and microwave frequencies. Bad weather conditions such as snow, rain or fog can easily degrade the performance of an atmospheric optical link to an unacceptable level. Even on a clear day, the atmospheric turbulence can add difficulties to the link alignment. Therefore, atmospheric optical links cannot replace existing microwave links in long-distance communications. Nevertheless, for short-distance communications, e.g., inter-building communications on a campus or in a downtown area, an atmospheric link can still be a very advantageous

choice. For a short link, say a link of a few hundred meters to a few kilometers, a large power margin can be obtained to decrease the link outage to an acceptable level. The major advantages of using an atmospheric optical link include large bandwidth, absence of electromagnetic interference and security. In fact, line-of-sight optical links can be even preferred to fiber links under certain circumstances, because no dig-up is required to lay the fiber cables.

Another kind of atmospheric application is indoor wireless communications systems. When radio wave regulations are in force, an optical indoor wireless system becomes desirable. There is apparently no concern about bad weather conditions and the channel characteristics are simpler than radio due to the very short wavelengths. However, multipath propagation fading may become a problem when the transmission rate is high. Besides, the power limit and the ambient light noise are typical problems encountered by optical indoor systems.

The author of this thesis has made contributions to both the outdoor and indoor applications of light transmission during his Ph.D. program. Two projects are briefly introduced in this thesis as appendices.

The third medium—optical fiber is the most important one of the three. The dramatic advance in fiber communications technology has been mainly due to the historical reduction of fiber attenuation. In the past two decades, the fiber attenuation has been reduced from hundreds of dB/km to below 0.2 dB/km [2]. Fiber links, owing also to the development of semiconductor single mode lasers, optical amplifiers and high performance optical receivers, etc., have firmly established the dominant position in long-haul communication trunk applications. Millions of kilometers of fiber have been installed. Now, has come the era of using optic fibers to build high-capacity communication networks. Generally speaking, because of the unique power division problem associated with fiber power distribution, the trend has been to use point-to-point fiber links to build fiber networks. One example is the 100 Mb/s fiber distributed data interface (FDDI) which uses an active ring architecture [3, 4]. The high performance, state of the art, Gigabits per second range

networks are mainly based on synchronous optical network (SONET) technology, which uses 2.488 Gb/s fiber links supported by bandwidth concatenation [5][6]. Compared with asynchronous fiber systems, a synchronous system does not require very high-speed electronic signal processing power and can thus achieve a higher transmission rate. Network flexibility can be achieved in the higher layers of the architecture with technologies such as ATM (asynchronous transfer mode [7]). However, when point-to-point links are used for networking, a problem arises. It is called the electronic bottleneck. Since the traffic of the whole network has to pass through the electronic circuit of the nodes, the throughput of the network is limited by the speed of electronics. It is known that the bandwidth at optical frequencies is several orders of magnitude higher than that in the electrical domain, the huge bandwidth of the fiber, about 60 THz, in the fiber 1.2 1.7 micron window, is actually left intact.

1.2 Photonic Networking

Great efforts have been made to make use of this huge fiber bandwidth. A network which has the ability to tap the huge fiber bandwidth is often called a lightwave network or a photonic network. It turns out that the most practical way of making use of the huge bandwidth of the fiber is to let each user use a small but different portion of the bandwidth at the same time. The most commonly used technologies are the wavelength division multiplexing (WDM)[8][9] and optical frequency division multiplexing (OFDM) [10]. WDM and OFDM are not much different conceptually. They are only different from the technology point of view. WDM usually refers to technologies with a channel spacing in the order of the wavelength resolution of optical filters; while OFDM can be considered as very dense WDM with a channel spacing in the order of the bit rate. When WDM/OFDM is used, it is required that the users are physically interconnected with a pure optical medium (with or without gain). In this case, even though each user still has a transmission speed limited by the electronics, it is given access to a fraction of the

entire fiber bandwidth. When a properly designed protocol is applied, different pairs of users can use different wavelengths in the optical band to communicate with each other at the same time. This way, concurrency is achieved and the network throughput can be multiplied. An alternative way of achieving concurrency is the use of very short optical pulses. Optical pulses have been generated as short as a few femtosecond (10^{-15} second) with mode-locked lasers [11][12]. Theoretically, optical time division multiplexing (OTDM) [13]-[15] or optical code division multiplexing (OCDM)[16]-[18] can be used to explore the vast fiber bandwidth. However, considering the state-of-the-art of the optical signal processing technology, these approaches seem to be much more difficult to implement. First, the mutiplexing and demultiplexing techniques are complicated. Second, a fiber simply may not have the bandwidth to transmit a femtosecond pulse, though people have been talking about tens of THz of available fiber bandwidth. The limiting element is dispersion. Dispersion gives the fiber a nonlinear phase transfer characteristic and reduces the temporal resolution. Unless an optical filter or something equivalent (e.g., SOLITON technology) can be implemented to compensate the dispersion, a very short optical pulse cannot be transmitted over a long distance. Hence, it can be concluded that, in the foreseeable future, WDM/OFDM will be the dominant technology in photonic network deployment.

Though the capacity of a fiber photonic network can be extremely large and the electronic bottleneck can be opened with WDM/OFDM technology, it can still be limited to far less than the bandwidth of the fiber itself by fundamental energy considerations. This is the so called power division problem. In a photonic network, each user transmits information by injecting power into the fiber medium. The power is distributed or divided in a certain way among other users according to network topology. Clearly, a given amount of signal power may be divided among a certain number of users before the received power level drops below the required minimum for an acceptable performance. The maximum bandwidth limited by the transmission power for each user can therefore be written as $P_t/(\mathcal{E}_b N)$, where P_t is the power transmitted by the user, $\mathcal{E}_b$ is the optical energy required

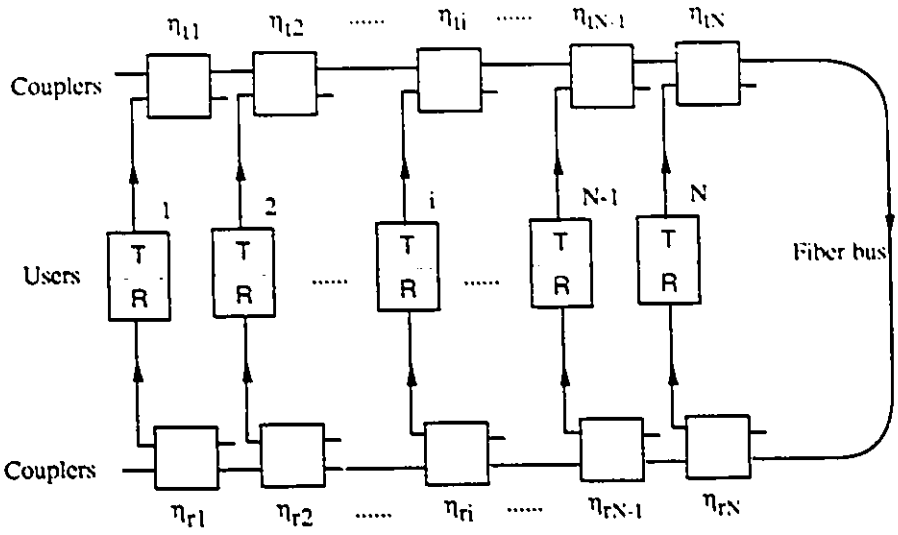

Figure 1.1: A unidirectional bus network.

for one bit of information and N is the number of users connected to the medium. The bandwidth decreases in proportion to $1/N$. This is in comparison to a point-to-point optical link, where the power-limited bandwidth is $P_t/\mathcal{E}_b$, which is much higher than a photonic network. In fact, this problem can be even worse, if the optical power is not divided in the right way. The power-limited bandwidth of each user can be much lower than what we have estimated. The major reason is that the fiber is a waveguide, not a conductor. One fundamental law about fiber waveguide is that it is impossible to combine the optical power from two (thus from more than two) pieces of fiber into one fiber. This makes it difficult to translate many high capacity networking concepts into practical implementation. For example, some favorable topologies in electrical networking such as a bus may become impractical. With the help of a simple performance evaluation, this can be well explained. Suppose a unidirectional bus network is built with 2×2 directional couplers which have an adjustable coupling coefficient η and an excess loss α, as it is shown in Fig. 1.1. The model of the coupler is shown in Fig. 1.2. In order to be fair to each user, the coupling coefficients are arranged as shown in the following equations:

$$\eta_{r1} = \eta_{t1} = 1 \tag{1.1}$$

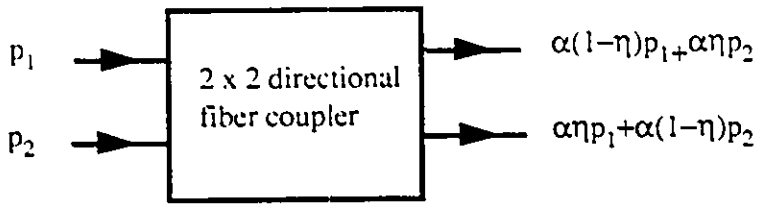

Figure 1.2: Model for a 2 × 2 directional coupler

$$\eta_{r2} = \eta_{t2} = \frac{1}{2} \tag{1.2}$$

...

$$\eta_{ri} = \eta_{ti} = \frac{1}{i} \tag{1.3}$$

...

$$\eta_{rN} = \eta_{tN} = \frac{1}{N} \tag{1.4}$$

where the subscript t stands for "transmission", and r stands for "reception". The power received by each receiver is:

$$P_r = \frac{P_t}{N^2}\alpha^M \tag{1.5}$$

where M ranges from 2 to 2N depending on how many couplers a message has to encounter through the network before reaching its destination, P_t and P_r are the transmitted and the received power of a user, respectively. Apparently, the worst situation happens when user number 1 transmits a message and the message is received by the same user. The power received in this worst case scenario is thus $\frac{P_t}{N^2}\alpha^{2N}$. We can compare this result with that of a star network. To make the comparison fair, we may use the same building blocks—2×2 directional couplers—to build the star network. The network is shown in Fig. 1.3. An ideal star network is one that evenly divides the power to all the users, so the power received by a user is P_t/N. In a non-ideal case, the excess loss introduced by the directional coupler should be considered. Therefore, the received power is:

$$P_r = \frac{P_t}{N}\alpha^{\log_2 N} \tag{1.6}$$

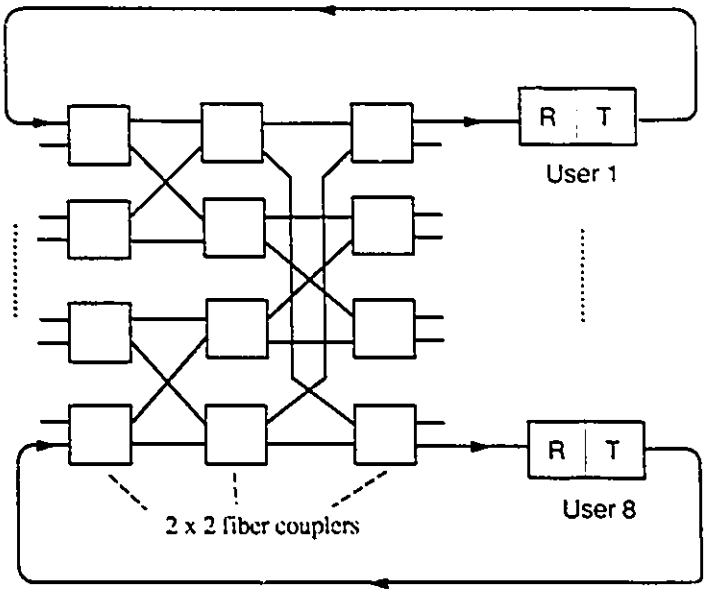

Figure 1.3: Star network interconnected with 2×2 couplers.

It can be seen that a star network has a higher efficiency in power distribution. The gain in power-limited bandwidth of a star topology over a bus is

$$G = \frac{P_{r,STAR}/\mathcal{E}_b}{P_{r,BUS}/\mathcal{E}_b} = N\alpha^{-2N+\log_2 N} \tag{1.7}$$

which increases sharply with an increase in the number of users, N. A calculated result is shown in Fig. 1.4, where excess losses of 1 dB and 0.1 dB are assumed for α. For $N = 16$, the gain is 10094 times in power-limited bandwidth, or about 40 dB in the received power for a given transmission rate.

The physical insight of the gain described in Eq. (1.7) can be easily explained. The first factor N represents the gain due to the fact that no power is allowed to be wasted from the network in a star topology; while in a bus network, since there is no such a thing as a power combiner, light power leaks through the unused ends of 2×2 couplers. The second factor $\alpha^{-2N+\log_2 N}$ represents the fact that a star topology is less vulnerable to excess loss. The excess loss increases linearly with the number of users N in a bus network and in a logarithmic manner in a star network because of the multi-stage parallel structure.

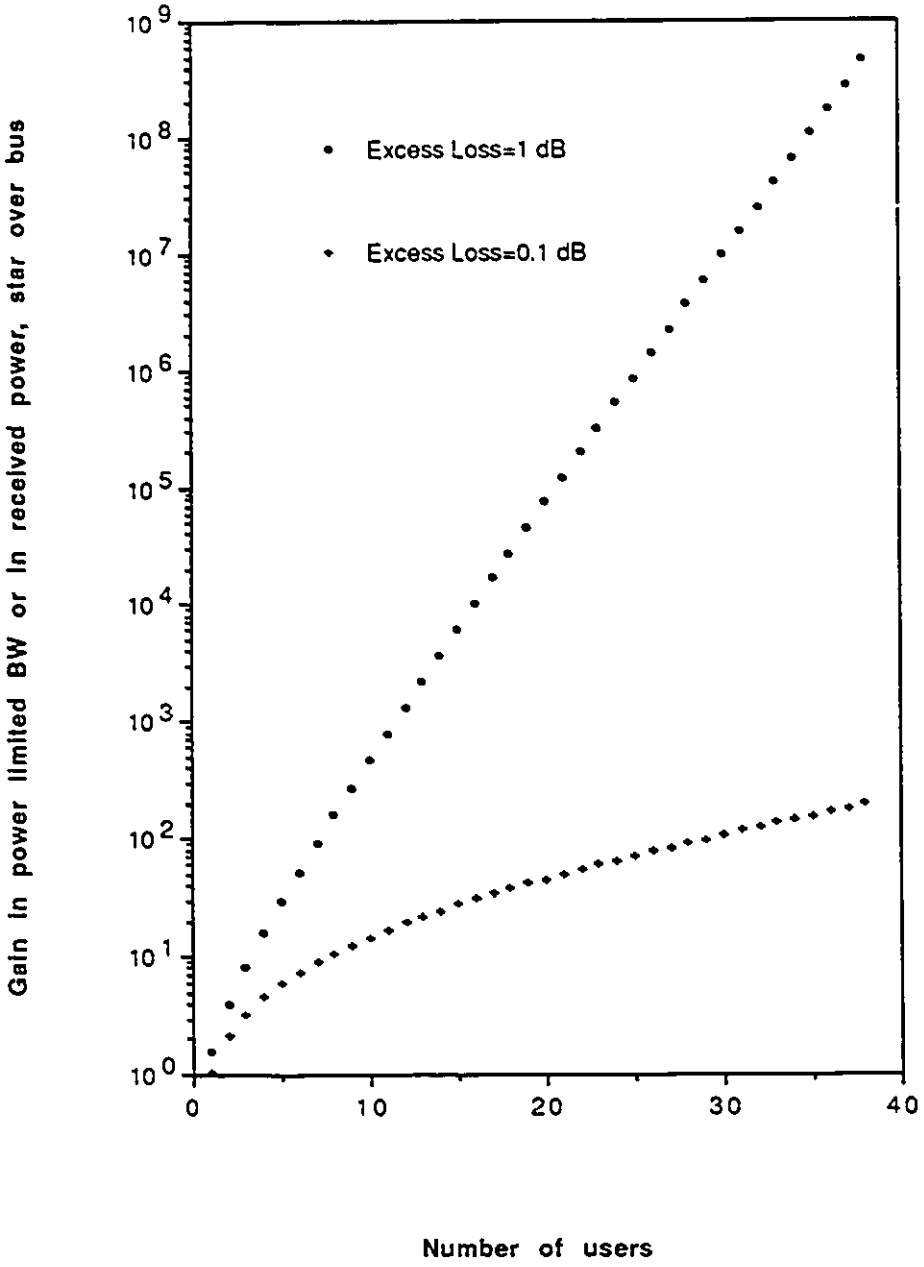

Figure 1.4: Gain of star topology over bus in the power-limited bandwidth for each user.

This shows that though a bus is a very desirable topology for electrical networks, it is not suitable for photonic networks, because it is simply a waste of the precious power. In comparison, a star is the most efficient topology in terms of the efficiency in power distribution. It is tolerant to excess loss, because the signals pass through only $\log_2 N$ element 2×2 couplers. The maximum throughput of a star network is $N \cdot \frac{P_t}{N\mathcal{E}_b} = \frac{P_t}{\mathcal{E}_b}$. As an example, assume $P_t = 5$ mW and $\mathcal{E}_b = 500$ photons/b, the power-limited throughput is about 50 Tb/s, which covers almost the whole fiber bandwidth. In practice, higher power or better receiver sensitivity is required to cover the same bandwidth because of the excess loss and fiber attenuation.

1.3 Fundamental Issues of Fiber Couplers

The key component of a star network is the passive star coupler. In [9], it is pointed out that optical gain cannot significantly improve the performance of a star coupler, because an optical amplifier is subject to the same power limitation as a laser transmitter. Therefore, a passive star coupler of a good quality is vital to the network performance. Generally, a star coupler is a component which has N fiber input ports and N output ports. At each output port a user can listen to the signals from all the input ports. Or on the other hand, a user can broadcast its signal through one input port to all the output ports. Some optical couplers, such as fan-in and fan-out couplers used in optical switching [19], are actually more specialized versions of star couplers. They are based on similar working mechanisms, and subject to basically the same restrictions. Optical star couplers can be classified as transmissive or reflective types [20]. The former has $2N$ fiber connections; while the later has only half as many. With a transmissive coupler, each user uses two fibers, one connected to the transmitter laser, the other connected to the receiver; with a reflective coupler, only one fiber is required for each user, because the traveling waves of both directions of the fiber are used for transmitting and receiving. In the latter case, a circulator or a 3 dB coupler may be used to separate the traffic of the

two opposite directions. A circulator is usually an expensive component, its use may not justify the saving in fiber; while the use of 3 dB couplers will introduce at least 6 dB loss in power.

From the point of view of practical implementation, a star network can use either a centralized configuration or a distributed one [21]. A centralized configuration uses a single, usually large, star coupler to support all the users. When the number of users increases, the total fiber length required increases linearly with N. To reduce the cost of the fiber, one may employ a number of smaller star couplers, with each supporting a cluster of users which are geometrically close to each other. The small star couplers are then connected such that a star topology can be maintained for all the network users. In fact, the difference between the centralized star or distributed star is just a matter of where the fiber connections are "stretched". Even in a centralized configuration, the star coupler may be made by interconnecting smaller star couplers with only short fibers. When these short fibers are extended in a certain way, we obviously will have a distributed network. Nevertheless, there are also ways to make integrated star couplers without making any inter-coupler connections. This issue will be discussed in the next chapter. In this section, we will first discuss some fundamental issues about constructing a star coupler. We will elaborate on a few concepts that could be confusing and discuss the fundamental laws that should be followed in an optical fiber coupler design. We will try not to limit the discussion to broadcasting star couplers.

In [9], it has been pointed out that it is not possible to build a power adder (i.e., a coupler) that combines two (or more) uncorrelated inputs and delivers them to its output; to do so would violate the second law of the thermodynamics. However, when the law is applied to coupler designs, some details have to be clarified. Consider the following facts that may confuse a designer:

1. If the wavelengths (or frequencies) of the two inputs are different, we can design a coupler to couple them into the same output fiber without any loss.

2. If the polarizations of the two inputs are known, a coupler can be made to couple them into the same output fiber without any loss.

3. If the inputs are from single mode fibers, they can be coupled into a multimode fiber losslessly.

These statements may not seem to be in harmony with the statement made in [9]. A more detailed investigation is needed to resolve this confusion. The key is to consider the very components of the light field inside a fiber. A mode in a fiber is defined as a possible field solution to Maxwell's equations [22] without considering the launching conditions. A fiber can have multiple modes, as in the case of multimode fiber. However, in a strict sense, even a single mode fiber can have more than one mode. This is because that though the light field in a single mode fiber has basically only one transverse mode, there is still more than one solution or mode characterized by quantities or field structure parameters other than the transverse mode. For example, either of the two orthogonal polarizations is by itself a solution to the Maxwell's equations and can be considered as a different mode. Similarly, the frequency can also distinguish different modes (in a general sense, longitudinal modes, there are uncountable number of them, because there are no constraints in the longitudinal direction). Here, in order to avoid possible confusion in terminology, we may call an elementary field solution to the Maxwell's equations an elementary mode. Notice that, to specify an elementary mode, its polarization and its longitudinal mode must be specified as well as its transverse mode. With this concept of elementary modes in mind, a more rigorous statement should be that two uncorrelated inputs carried by the same elementary mode cannot be coupled into the same elementary mode without a 3dB loss in power. In all the three statements listed above, different elementary modes are coupled into the same fiber, but not into the same elementary mode. Therefore, all of them can be done losslessly. However, coupling signals from single-mode fibers into a multimode fiber is obviously unreasonable and has hardly any practical value, neither does the use of polarization. In the former case, the use of multimode fiber cannot justify the use of single-mode fibers. In the latter case, only two orthogonal polarizations

are available, which means at most two signals can be multiplexed, and in practice, even this may not be possible because of the cross-talk between the two polarizations in single mode fibers. Hence, from a practical point of view, only the frequency is a variable (or dimension) for obtaining a different elementary mode. Couplers that make use of this variable are widely applied. As we all know, they are called wavelength multiplexers (or couplers). The key to such devices is a wavelength-sensitive element, e.g., a grating. There have been proposals that suggest the use of holographic gratings to accomplish wavelength routing in a WDM network. In Chapter 2, the contribution of the author on this subject will be presented. When WDM is applied, one interesting point is: under what condition can two light waves be considered to have the same frequency? For example, if the difference in frequency is 1 Hz, knowing that the frequency of light is in hundreds of THz, can we say that the two light waves have the same frequency? The author believes that the answer depends on the frequency resolution of the components (or sometimes, the system). If the component responds differently to this difference of 1 Hz, the two frequencies are different.

Another important point when applying the second law is that the two inputs mentioned above are assumed to be uncorrelated. Consider the example shown in Fig. 1.5: In (a), a beam splitter is used as a loss-free 1×2 coupler. If all the light waves are completely reversed, according to the principle of reversibility, the same coupler can be used as a lossless 2×1 coupler, as it is shown in Fig. 1.5.(b). However, this is not true, since in the case of a 2×1 coupler, the two input waves are not simply the reverse of the outputs of the 1×2 coupler due to the incoherency of the two inputs. The correct picture is the one shown in Fig. 1.5(c). Some loss must be accepted because the light beams will not cancel each other at any of the two output branches. Actually it will be more efficient if the splitter is used as a 2×2 coupler, instead of a 2×1 coupler. Now the question is: what kind of inputs can be considered as uncorrelated? On one hand, we may use the same elementary mode to carry both input signals and the two waves can be coherent because they have the same frequency. On the other hand, the modulating signals are

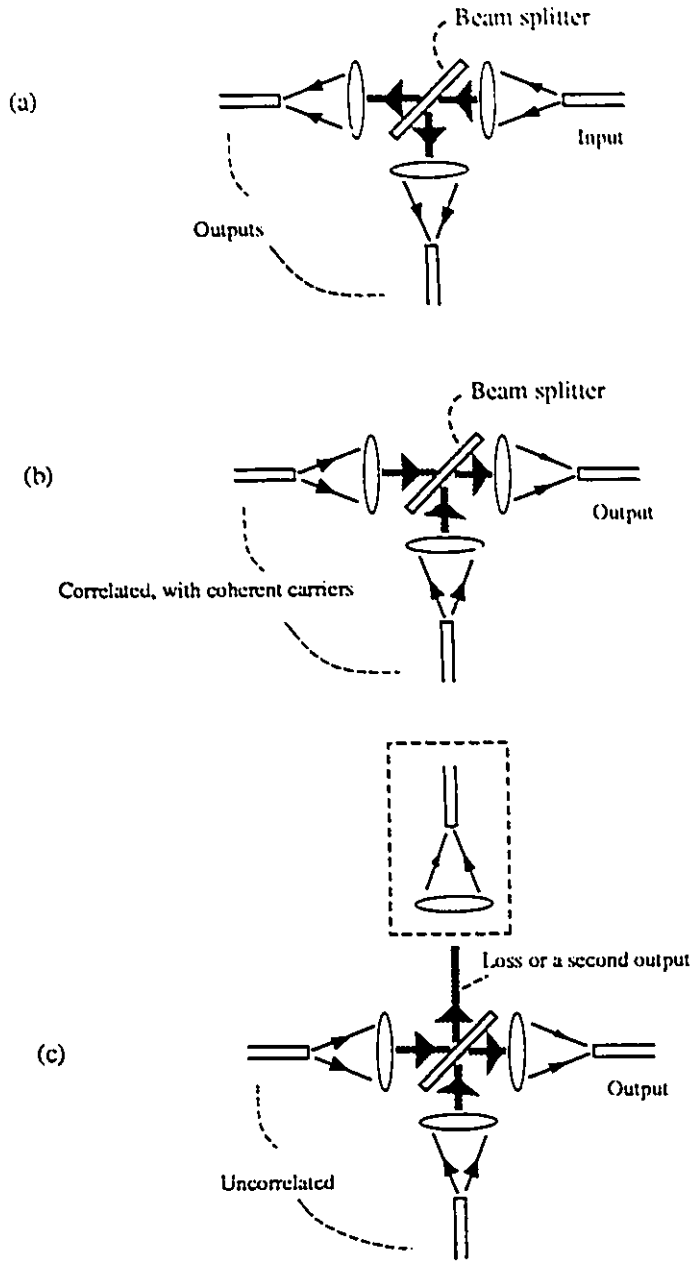

Figure 1.5: (a) A beam splitter used as a 1×2 coupler. (b) The reverse of (a), a postulated 2×1 coupler. (c) The reality—a 2×2 coupler or a 2×1 coupler with loss.

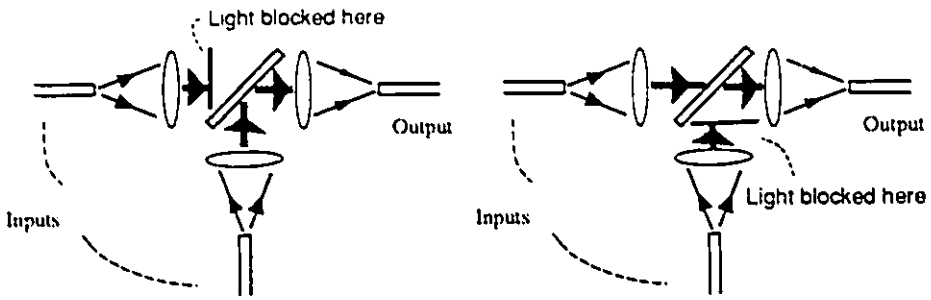

Figure 1.6: The functionality of a coupler should remain the same if one or some of the inputs are zero. This means that for a postulated loss-free 2×1 coupler, it is required that when one beam is totally blocked, the other beam can still be completely coupled into the intended output direction without any loss, and vice versa.

uncorrelated, because they carry information from different sources. This puzzle can be solved by investigating the original purpose of a coupler. It is desired to build a coupler with a certain functionality. Since the two inputs have uncorrelated modulations, the interference between the two waves will be random, so will the power distribution in both output ports. At one moment the power might be coupled totally into one fiber, but at the next, the other one. Apparently, the functionality of the coupler cannot depend on the interaction of the two input waves, even though the carriers can be coherent. Actually the random power distribution is one good example of the so called "beat noise" [23], which should be avoided. The way to avoid this noise is: either the users do not transmit at the same time, as in the case of Ethernet, or they use different wavelengths so that the carriers of the two signals are not coherent any more. With this idea in mind, the functionality of a postulated 2×1 coupler is best described by Fig. 1.6, where when one arm of the input is blocked, the input from the other arm can still be completely coupled into the output port. This is obviously not realistic. No passive splitters or mirrors can fulfill this function due to the Second Law of Thermodynamics.

To summarize, the second law of thermodynamics does not prevent the happening of a "casual" combination of two signal-carrying waves into one fiber at a particular time

interval. At the moment, when the phase and amplitude of the signals match, the output may appear in only one of the two output fibers. But this cannot happen "all the time", especially, it should not happen if transmission of one of the signals stops. This is, in the author's opinion, a simple interpretation of the statement "uncorrelated inputs". Next, we will use mathematical equations to describe the fundamental laws that have to be met by a coupler design.

The functionality or connectivity of a general coupler can be specified by a power coupling matrix C:

$$C = \begin{pmatrix} c_{11} & c_{12} & \cdots & c_{1N} \\ c_{21} & c_{22} & \cdots & c_{2N} \\ \vdots & \vdots & \ddots & \vdots \\ c_{N1} & c_{N2} & \cdots & c_{NN} \end{pmatrix} \tag{1.8}$$

where c_{ij} is the coupling coefficient from the j-th input to the i-th output. The matrix C relates the power of the N input ports $p_1, p_2, \ldots, p_N$ with that of the output $p'_1, p'_2, \ldots, p'_N$ in the following way:

$$\begin{pmatrix} p'_1 \\ p'_2 \\ \vdots \\ p'_N \end{pmatrix} = C \begin{pmatrix} p_1 \\ p_2 \\ \vdots \\ p_N \end{pmatrix} \tag{1.9}$$

Though C basically defines the functionality of a star coupler, other type of couplers can be expressed as special cases. For example, a $1 \times N$ splitter can be expressed as:

$$C = \begin{pmatrix} c_{11} & 0 & \cdots & 0 \\ c_{21} & 0 & \cdots & 0 \\ \vdots & \vdots & \ddots & \vdots \\ c_{N1} & 0 & \cdots & 0 \end{pmatrix} \tag{1.10}$$

while an $N \times 1$ coupler can be expressed as:

$$C = \begin{pmatrix} c_{11} & c_{12} & \cdots & c_{1N} \\ 0 & 0 & \cdots & 0 \\ \vdots & \vdots & \ddots & \vdots \\ 0 & 0 & \cdots & 0 \end{pmatrix} \tag{1.11}$$

Therefore, to design the connectivity of a coupler, N^2 variables $(c_{ij}, i, j = 1, 2, \ldots, N)$ or parameters have to be specified. However, the degrees of freedom are not as many, because the parameters are not independent. This is due to the restriction caused by two fundamental laws. The first fundamental law to be followed is conservation of energy. Applying this to matrix C yields:

$$\sum_{i=1}^{N} c_{ij} \leq 1 \qquad for \;\; j = 1, 2, \cdots, N \tag{1.12}$$

which means, the total output power is less than or equal to the total input power.

The second law that a coupler is subject to is the second law of thermodynamics, which states that in an isolated system, the entropy can only increase when any internal condition is changed. A passive coupler and the light waves passing through it as a whole can be considered as an isolated system. When the light waves propagate through the coupler, the entropy of the system cannot be decreased. Now the question is how to define the entropy of a lightwave system. For couplers with excess loss, this is difficult because of the heat produced by the coupler. However, the author finds that it is not so difficult to define the entropy for an ideal, loss-free coupler with a power coupling matrix:

$$\Pi = \begin{pmatrix} \eta_{11} & \eta_{12} & \cdots & \eta_{1N} \\ \eta_{21} & \eta_{22} & \cdots & \eta_{2N} \\ \vdots & \vdots & \ddots & \vdots \\ \eta_{N1} & \eta_{N2} & \cdots & \eta_{NN} \end{pmatrix} \tag{1.13}$$

Since the entropy is a measure of disorder, the entropy may be defined, not exclusively as:

$$S = \sum_i \frac{p_i}{p} \log \frac{p}{p_i} \tag{1.14}$$

where p is the total power defined as:

$$p = \sum_i p_i \tag{1.15}$$

Evidently, with this definition, the more is the light power concentrated in one (or a few) ports, the lower is the entropy. The second law of thermodynamics can then be stated as:

$$S' \geq S \tag{1.16}$$

where S is the entropy measured at the input side of the coupler, and S' is the entropy measured at the output side. It is apparent that when the power is evenly distributed among all the lightwaves, S has the maximum value, which means the degree of disorder is the highest. Some conclusions we discussed earlier can be easily drawn from expressions (1.14) through (1.16). For example, it is possible to split a light beam into N beams with an efficiency of 100%, but it is impossible to couple N beams into one beam without any excess loss. It also explains the example given earlier about the beam splitting couplers. Actually, with a passive device, it is not even possible to have the power coupled relatively more into one beam, because it means an entropy decrease in an isolated system.

Eq. (1.14) through Eq (1.16) are not in a convenient form to apply. S is defined in terms of the input or the output light power which may vary from case to case. If any of the inputs or the outputs is zero, Eq. (1.14) cannot be evaluated. Besides, it is the coupler that is under design, not the waves. In fact, what is really needed is an expression governing the matrix element η_{ij} which has nothing to do with the lightwaves. Therefore, we may consider a special case, namely:

$$p_1 = p_2 = \ldots = p_N \tag{1.17}$$

which leads to

$$S = \log N$$

Since

$$p_i' = \sum_j \eta_{ij} \quad for \quad i = 1, 2, \ldots, N$$

we have

$$S' = \sum_i \frac{\sum_j \eta_{ij}}{N} \log \frac{N}{\sum_j \eta_{ij}}$$

Hence, Eq. (1.16) leads to

$$\sum_i \frac{\sum_j \eta_{ij}}{N} \log \frac{N}{\sum_j \eta_{ij}} \geq \log N \tag{1.18}$$

Notice that, since we have assumed a lossless coupler, the other constraint is, from Eq. (1.12):

$$\sum_i \eta_{ij} = 1 \tag{1.19}$$

These expressions are indeed independent of the light waves. As an example, they can be applied to a 2×2 coupler. It is well known that a lossless 2×2 coupler should have a power coupling matrix of the form

$$H = \begin{pmatrix} 1-\eta & \eta \\ \eta & 1-\eta \end{pmatrix} \tag{1.20}$$

Obviously, Eq. (1.20) satisfies Eq. (1.18) and Eq. (1.19). It can be shown that the coupling matrix cannot be different from Expression (1.20). For instance, assume

$$H = \begin{pmatrix} 1-\eta_1 & \eta_2 \\ \eta_1 & 1-\eta_2 \end{pmatrix} \tag{1.21}$$

with $\eta_1 > \eta_2$, a device can be formed as shown in Fig. 1.7, with which a 2×1 coupler can be constructed with an efficiency of 100%. This is against the second law of thermodynamics. So it is only possible that $\eta_1 = \eta_2$.

So far, it has been assumed that the coupler is free from excess loss. The purpose is to make it easy to evaluate the system entropy. When excess loss is included, the coupling matrix can be written as

$$C = \begin{pmatrix} & \vdots & \\ \cdots & \alpha_{ij}\eta_{ij} & \cdots \\ & \vdots & \end{pmatrix} \tag{1.22}$$

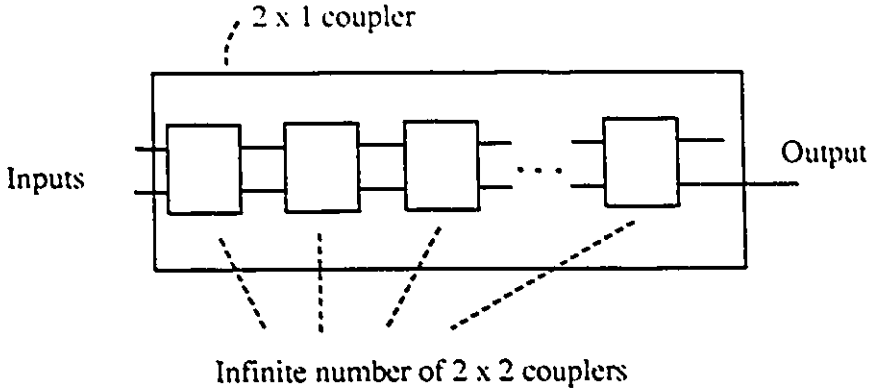

Figure 1.7: A false 2×1 coupler

where $0 \leq \alpha_{ij} \leq 1$, and may be called an excess loss factor. Notice that, η_{ij} is the matrix element of the loss-free coupler. When loss is introduced, an $N \times 1$ coupler can be realized. For example, starting from a perfect $N \times N$ star coupler:

$$H = \begin{pmatrix} \frac{1}{N} & \frac{1}{N} & \cdots & \frac{1}{N} \\ \frac{1}{N} & \frac{1}{N} & \cdots & \frac{1}{N} \\ \vdots & \vdots & \cdots & \vdots \\ \frac{1}{N} & \frac{1}{N} & \cdots & \frac{1}{N} \end{pmatrix} \tag{1.23}$$

We may let $\alpha_{ij} = 1$ for $j = 1$ and $\alpha_{ij} = 0$ for $j = 2, \ldots, N$. Hence:

$$C = \begin{pmatrix} \frac{1}{N} & \frac{1}{N} & \cdots & \frac{1}{N} \\ 0 & 0 & \cdots & 0 \\ \vdots & & & \\ 0 & 0 & \cdots & 0 \end{pmatrix} \tag{1.24}$$

Notice that the way to design the coupler connectivity is to design a loss-free coupler first. And we make sure that the connectivity satisfies Eq. (1.18) and Eq. (1.19) and then add loss to the matrix. In this way, unrealistic designs will not result.

We have so far assumed that all the light inputs have the same frequency. In a more general case, to describe a coupler fully, the wavelength has to be considered as a variable.

The loss-free matrix H can thus be generalized as:

$$H = \begin{pmatrix} \eta_{11}(\lambda_1) & \eta_{12}(\lambda_2) & \cdots & \eta_{1N}(\lambda_N) \\ \eta_{21}(\lambda_1) & \eta_{22}(\lambda_2) & \cdots & \eta_{2N}(\lambda_N) \\ \vdots & \vdots & & \vdots \\ \eta_{N1}(\lambda_1) & \eta_{N2}(\lambda_2) & \cdots & \eta_{NN}(\lambda_N) \end{pmatrix} \tag{1.25}$$

and matrix C as:

$$C = \begin{pmatrix} & \vdots & \\ \cdots & \alpha_{ij}(\lambda_j)\eta_{ij}(\lambda_j) & \cdots \\ & \vdots & \end{pmatrix} \tag{1.26}$$

Eq. (1.12) can be written as:

$$\sum_{i=1}^{N} c_{ij}(\lambda_j) \leq 1 \tag{1.27}$$

The equation for entropy can also be generalized. The way to do so is to consider different wavelengths in the same input or output fiber as different ports. The expression is however beyond the scope of this thesis.

In this chapter, we have conducted a general discussion about some important issues concerning optical communications and photonic networking. An important technique for photonic networking is the WDM/OFDM, which gives a practical way to use the vast bandwidth of a single mode fiber. For a photonic network, a pure optical medium has to be accessible for all the end users. Hence, passive coupling devices and their performance become vital to a photonic network. We have also discussed the two fundamental laws that govern the construction of the couplers. These laws are presented in a form that is easy to apply in design work.

In the next chapter, a number of novel techniques contributed by the author in his Ph.D. program will be presented. In the chapter, only the original ideals will be presented with some intuitive explanations. The theoretical analysis is provided in Chapter 3, where

a mathematical model will be given for the numerical analyses and simulations. Examples of numerical results will also be presented.

Chapter 2

Grating Degeneration and Sandwich Structure for Holographic Passive Fiber $N \times N$ Star Couplers

2.1 Introduction

As was discussed in the preceding chapter, an $N \times N$ passive star coupler is a key component in the application of optic fibers to photonic networks. The most commonly used fiber couplers so far have been fused fiber couplers, which are usually built in the form of 2×2 directional couplers. Such couplers are made by bringing the cores of two pieces of single-mode fiber sufficiently close to each other over an appropriate length. The coupling between the two fibers is achieved through the interaction of the evanescent parts of the guided fields. Various structures have been built using etching [24], fusion [25], or grinding and polishing [26], etc. It is evident that an ideal $N \times N$ coupler with N greater than 3 cannot be built by simply fusing N fibers together. This is illustrated in Fig. 2.1, where it can be seen from the geometry that if four fibers are fused together, the coupling coefficient between any two diagonally placed fibers (e.g., fiber 1 and 3) is very much likely to be different from that between two adjacent fibers (e.g., fiber 1 and 2). The structure of a

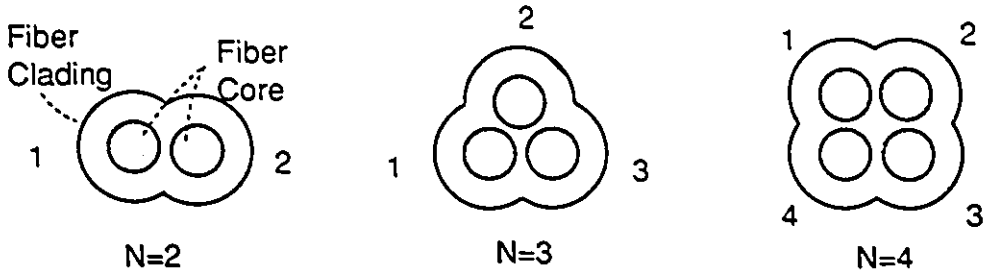

Figure 2.1: Cross-sections of fused fibers for $N = 2, 3$ and 4.

fused fiber star coupler requires a high degree of symmetry, i.e., there should not be a pair of fibers that have a relative geometrical relation different from other pairs. Evidently, when $N = 3$, the three fibers can be fused together with the desired symmetry, if satisfactory precision can be achieved in the fabrication. In the case of $N = 2$, the symmetry is not a concern, because each of the fibers has only one neighbouring fiber. This results in ease in fabrication, which in turn explains why 2×2 fused fiber couplers are so commonly used. Fortunately, these 2×2 couplers can be interconnected as building blocks for the construction of $N \times N$ star couplers. Fig. 1.3 shows how an 8×8 coupler is built out of 12 of these building blocks, arranged in three stages. Generally speaking, for an $N \times N$ coupler with $N = 2^n$, $n2^{n-1}$ such building blocks or more are needed depending on how the interconnection is made among them. Therefore, at least $N(n-1)$ interconnections are needed within the coupler and the complexity increases significantly with N. Usually the building blocks are arranged in $n = \log_2 N$ stages, which implies that the excess loss increases logrithmically with the number of ports N.

Because of the undesirable complexity associated with fused fiber couplers, the researchers have been searching for more straightforward and compact approaches for the realization of $N \times N$ fiber couplers. Novel designs have been proposed. One important design was proposed by C. Dragone [27, 28], in which the natural Fourier propagation of a fiber mode in a homogeneous medium or a planar waveguide is used to spread the power

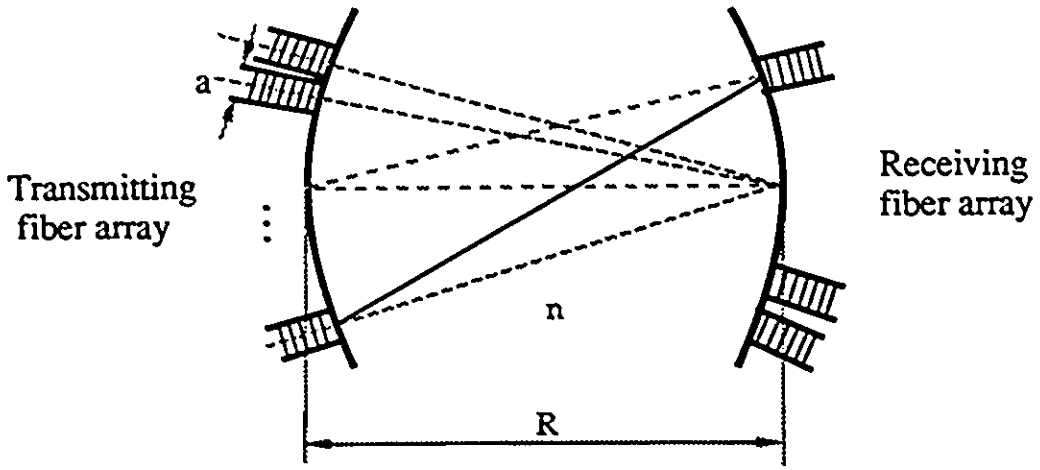

Figure 2.2: $N \times N$ coupler using Fourier propagation.

of any of the input lightwaves over the N output ports. The design of this approach is shown in Fig. 2.2. It is obviously compact and simple. However, the power efficiency is relatively low, being at most 35% at the edge and 55% at the center. A more elaborate analysis which takes the mutual coupling between the adjacent waveguides into account shows that for a particular 5×5 star coupler, an efficiency of 56 % is achievable [29]. The excess loss is due to the fact that no control can be exerted over the Fourier light propagation. For a coupler to have a high efficiency, two conditions must be satisfied. First, all the light from an input must be directed to the receiving aperture of the output fibers. Secondly, the light incident on the receiving apertures should match the transverse mode of the output fibers. With Fourier propagation, neither of the conditions can be satisfied. Some power will be lost because light can get away from the gaps between the receiving fiber ends or from the area outside the fiber array. Notice that, a fiber has a round aperture and a fiber array cannot have a receiving aperture covering the whole receiving surface. The rest of the power loss is caused by the mismatch between the received light and the fiber propagation mode. The mismatched portion will escape from the fiber after traveling a short distance, or will travel as cladding modes which should be removed before it reaches the detector.

Recently a more efficient approach was proposed by M. Tabiani and M. Kavehrad [30, 31]. In their proposal, a guided propagation is used instead of free Fourier propagation. The lightwave propagation is channelized by a medium which has a set of periodic structures called volume gratings. One property of this special medium is that the output beams only appear at a specific set of angles when the input beams are incident at the same set of angles. Therefore, compared with the transmission in homogeneous media, the light waves are more orderly when propagating through the index-varying medium, and thus a higher efficiency can be achieved. Since holography is one possible way of constructing the gratings, the coupler can properly be called a holographic star coupler. Though diffraction theory shows that such couplers can achieve an efficiency of 100% [31], a problem remains to be solved in practice, especially when the number of users N is large. According to [30], $\frac{N(N-1)}{2}$ gratings are needed for an $N \times N$ coupler, which means the number of gratings written in the recording material increases approximately as N^2. For example, a 3×3 coupler needs 3 overlapping gratings; while for a 10×10 coupler 45 gratings are needed. For a coupler with 16 input or outport ports, 120 different periodic structures must be constructed in one single dielectric slab. It is known that writing a large number of holograms in a single piece of recording material is a difficult task, especially when a good diffraction efficiency and a high signal-to-noise ratio are required. The main reason is that the dynamic range of a practical recording material is very limited. For example, DCG (dichromated gelatin)—a recording material with the highest modulation index in refractive index—has its maximum modulation index reported as 0.08 [32], which is probably too optimistic for this application because in the case of DCG, high modulation index and low noise can be two conflicting requirements. On the other hand, it can be shown that the dynamic range of the required refractive index for the slab increases with $N^{3/2}$.

Consider the case when $\Delta_i = \Delta$, from Eq. (23) of [31], we have:

$$\gamma = \frac{\omega\Delta}{2c}\sqrt{N-1} \tag{2.1}$$

where γ is a wave coupling factor defined in [31], N is the number of input/output ports

and Δ is the relative modulation index of each grating written in the dielectric slab. Since we want the power to be evenly distributed among all the diffraction orders including the zero-th order, Eq. (22) in [31] leads to

$$|\cos \gamma d| = |j\frac{\omega \Delta \sin \gamma d}{2c\gamma}|$$

where d is the thickness of the slab. The left side of this equation is the normalized amplitude of the zeroth order diffraction and the right side is that of the diffracted order. Substituting Eq. (2.1) for γ yields:

$$\sqrt{N-1} = |\tan(\frac{\omega \Delta d}{2c}\sqrt{N-1})|$$

When N is large enough, the solution to this equation is

$$\Delta \approx \frac{\pi c}{\omega d\sqrt{N-1}}$$

The dynamic range needed is thus:

$$\Delta_{max} = \frac{N(N-1)}{2}\Delta \approx \frac{\pi c}{2\omega d}N^{3/2} \tag{2.2}$$

It can therefore be concluded that the dynamic range is proportional to $N^{3/2}$. Also, it can be predicted that, when the number of ports increases, the sharply increasing number of gratings may quickly saturate any existing recording material, if the design in [30] or [31] is applied.

In this chapter, two new concepts are introduced to combat the dynamic range limitation problem. In the first technique which is called grating degeneration, more than one lightwave pair is allowed to share one common grating. The technique can significantly reduce the number of gratings, because it has been found that each grating in the slab can be made equivalent to at least a number of parallel 2×2 couplers. The second method uses a sandwich structure, by which a number of dielectric slabs is sandwiched together into one coupler with each slab containing smaller number of gratings. The two techniques can be either used individually or be combined to get a further reduction in the required number of gratings. Designs of a 4×4, an 8×8 and a 16×16 coupler will be

presented, as examples. It will be shown that with an additional technique called quasi-Bragg diffraction, a 16×16 coupler can be made from four sandwiched slabs, with each of the slabs bearing only two gratings. Furthermore, it will be shown in this chapter that the concept of grating degeneration is not limited to $N \times N$ star couplers. It can be applied also to volume-grating-based selective-broadcast or wavelength routing components.

The ideas of grating degeneration and sandwich structures have been published [33][34] before the completion of this thesis. Also, a patent application [35] about the techniques is pending.

2.2 Basic Concepts

In this section, basic ideas of grating degeneration and sandwich structures are presented. We will start with the schematic designs of the proposed couplers.

2.2.1 Schematic designs and mode matching for efficient coupling

Fig. 2.3 shows one schematic design proposed for a passive $N \times N$ star coupler. The fiber ends are mounted on the surfaces of the field lenses which have a focal length equal to the focal length of the collimating lenses. One dielectric slab or a few, bearing prearranged holographic gratings, are placed right between the two collimating lenses. Field lenses are used to ease the difficulty in mounting the fibers, otherwise the fibers have to be tilted towards the centers of the collimating lenses. Collimating lenses are used to convert spherical waves into plane waves so that a planar grating system can be used. One advantage of using planar gratings is that the gratings can be recorded at a wavelength (e.g., 0.5145 μm from a Ar^+ laser) different from the coupler working wavelength (probably 1.3 μm). A usable holographic recording material sensitive to infrared is not known yet. Should this material become available, we may remove the lenses and take full advantage of holographic techniques. It is known that the lenses can be integrated into the slab as

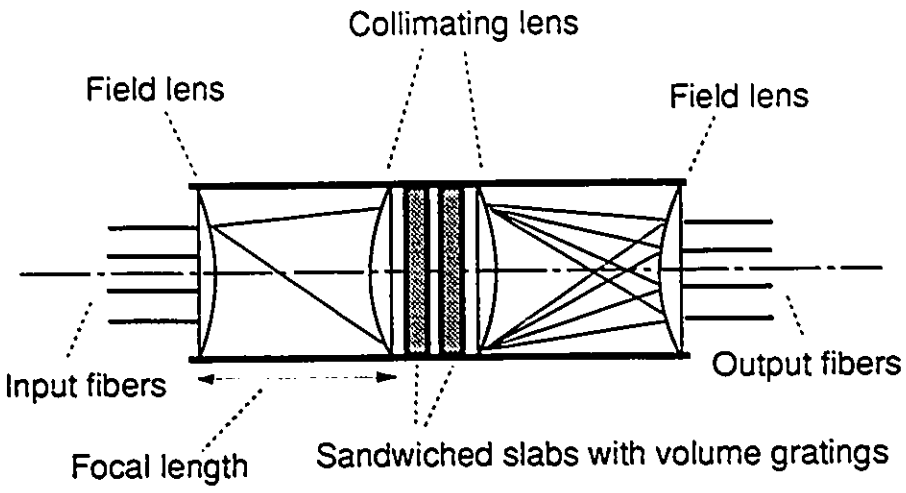

Figure 2.3: Schematic diagram of a $N \times N$ star coupler using volume gratings.

holographic lenses, or be combined with each of the gratings. More optical surfaces may be added in between the field lenses and the collimating lenses to correct the aberrations. However, more optical surfaces may cause more reflections, so high quality anti-reflection coatings must be applied on all optical surfaces.

From a practical point of view, the design presented in Fig. 2.3 may still be more a conceptual model than a practical implementation scheme. In practice, the problems with the design are that the coupler may be too bulky due to the use of conventional lenses, or that the optical surfaces may introduce too much unwanted reflection. These problems can be solved with simple modifications. Two examples of alternative designs are shown in Fig. 2.4 and Fig. 2.5. In Fig. 2.4, graded index (GRIN) rod lenses are used to replace the conventional lenses used in Fig. 2.3. The fibers can be directly mounted on the surfaces of the GRIN lenses. In Fig. 2.5, fiber tapers (fibers with a gradually expanding end, studied in great detail in [36] and [37]) are used for beam collimation, and the index matching is achieved by using two glass hemispheric blocks. This design closely resembles the design in [30, 31], which is depicted here in Fig. 2.6. However, it is actually different. In the design shown in Fig. 2.6, though fiber tapers are used for beam collimation, no index-matching blocks are used. The diffraction medium fills the entire

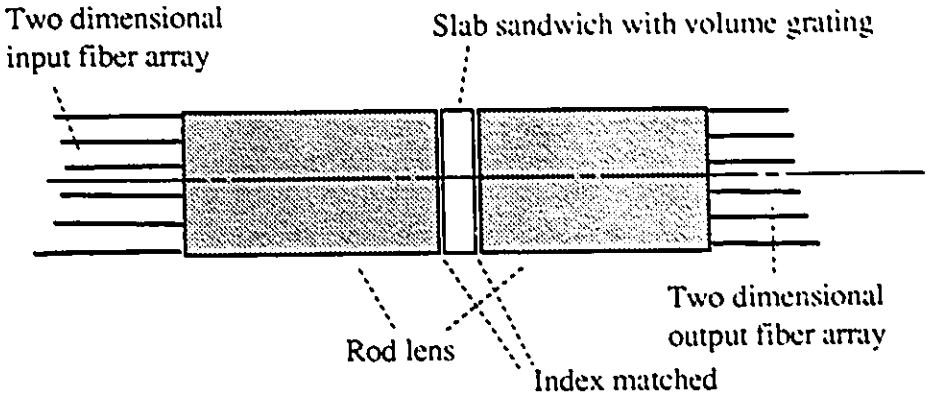

Figure 2.4: A modified coupler design using GRIN self-focus lenses.

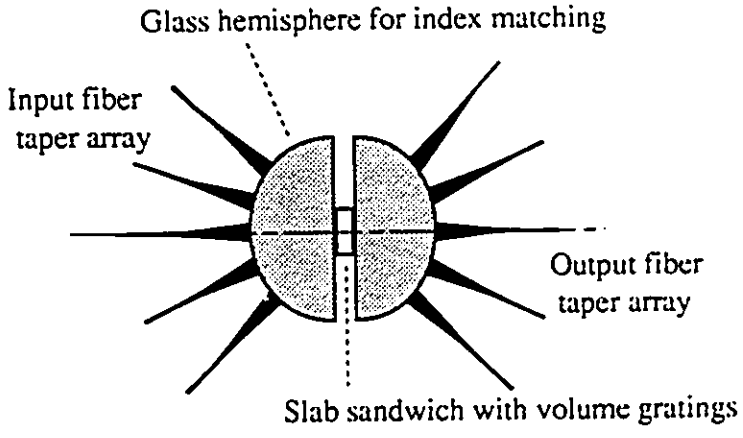

Figure 2.5: A modified coupler design using fiber tapers.

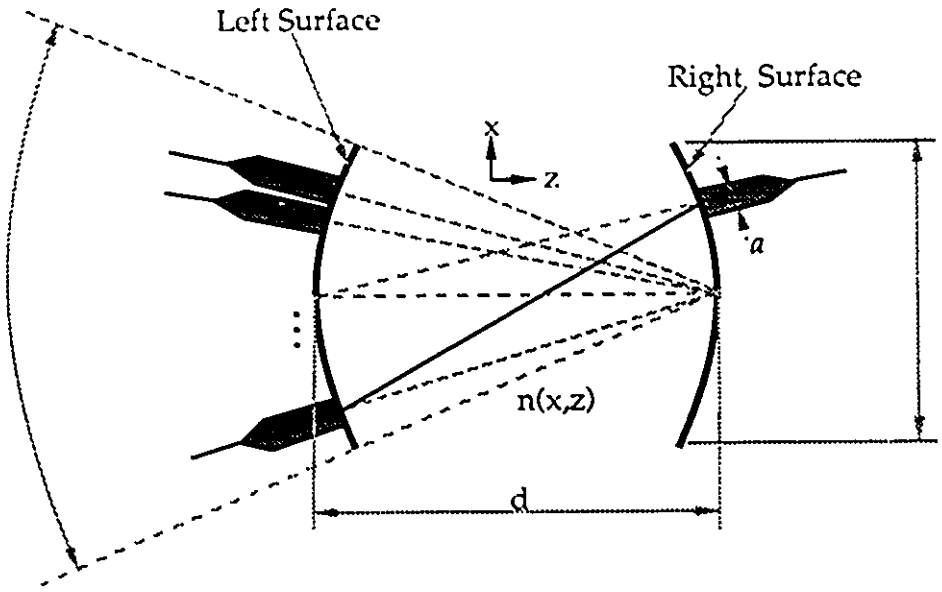

Figure 2.6: A coupler design shown in reference [31].

region in between the two taper arrays. This may cause the following problems:

1. The diameter a of the tapers used shown in Fig. 2.6 is smaller than the slab thickness d. Therefore, the alignment of the diffracted beams, whose diameter may become larger than that of the tapers, may be difficult. This is depicted in Fig. 2.7.

2. In most cases (except the zero-th diffraction orders), the light waves have to be received at an angle with the taper axis on the receiving side, as shown in Fig. 2.8. This contradicts the fact that a single mode fiber has a very small numerical aperture (NA). In other words, the coupler will have a mode-matching problem when the coupling between free-space and the fibers is considered. Actually, with a taper attached to the fiber end, the angular tolerance will be reduced even further [36]. This is because the second law of thermodynamics requires that when a receiving aperture is enlarged with passive means, its angle of reception will be reduced in such a way that the receiving area multiplied by the solid angle of reception remains a constant.

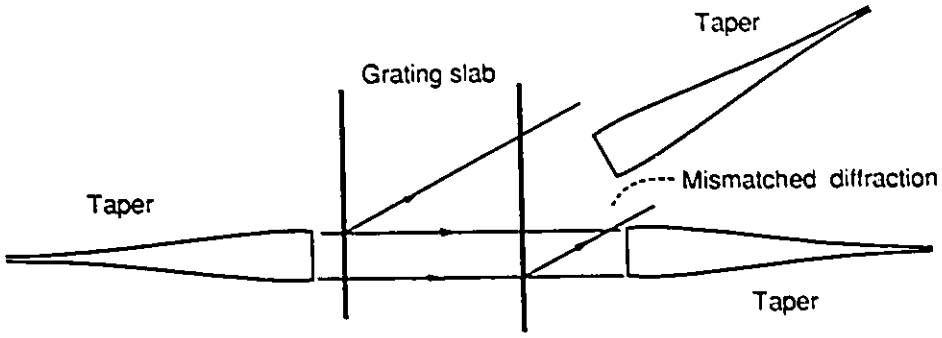

Figure 2.7: Change in diameter of a diffracted beam when the slab has a thickness much larger than the diameter of the taper.

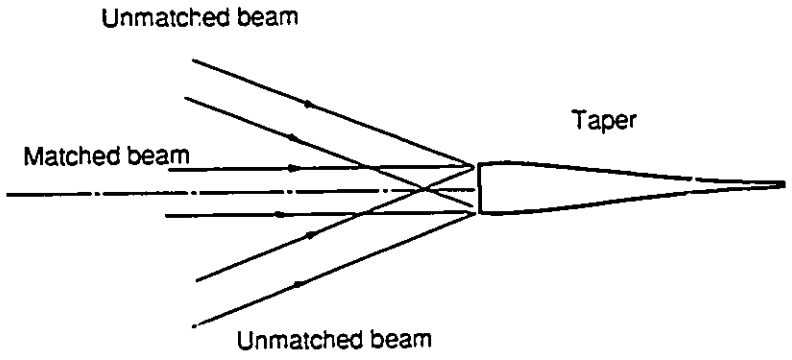

Figure 2.8: A receiving taper and the received beams in the design given in [30, 31]. The beams may be incident at an angle and mismatch the fiber mode.

The designs shown in Fig. 2.3, 2.4 and 2.5 do not have these problems, first, because the full aperture of the slab is used for each fiber. The aperture is much larger than the slab thickness, so there is a well defined plane of deflection and the change in the beam diameter can be neglected. This is especially important when fiber tapers are employed, as in the configuration shown in Fig. 2.5. Secondly, in the design shown in Fig. 2.3 each fiber only receives light waves normally incident on the fiber ends. It will be shown next that as long as the NA of the lenses is larger than that of the fibers, mode matching will not be a problem because the field pattern on the receiving side of the coupler is exactly the image of the field on the transmitting side. We will conduct the derivation under the Fresnel approximation and will adopt notations similar to those used in [38].

In Fig. 2.3, using a complex envelope, the light field on the output side of the left field lens can be expressed as:

$$E(x,y) = \sum_{i=1}^{N} A_i \psi(x - x_i, y - y_i) \tag{2.3}$$

where $\psi(x,y)$ stands for the dominant mode of a fiber, (x_i, y_i) stands for the lateral position of the i-th fiber end, and A_i represents the amplitude (a complex random process) of the field from the i-th fiber. After propagating through freespace and the first collimating lens, the light field at the output of the lens becomes:

$$\begin{aligned} E^{-}(x,y) &= \frac{e^{j\frac{2\pi}{\lambda}f}}{\lambda f} p(x,y) \mathcal{F}_{2D}\{E(x,y)\}|_{\xi=\frac{x}{\lambda f}, \eta=\frac{y}{\lambda f}} \\ &= \frac{e^{j\frac{2\pi}{\lambda}f}}{\lambda f} p(x,y) \sum_{i=1}^{N} A_i \Psi(\frac{x}{\lambda f}, \frac{y}{\lambda f}) e^{-j\frac{2\pi}{\lambda f}(x_i x + y_i y)} \end{aligned} \tag{2.4}$$

where f is the focal length of the lenses, $p(x,y)$ represents the aperture area of the slabsandwich, $\mathcal{F}_{2D}\{\cdot\}$ stands for the operation of two-dimensional Fourier transformation, ξ and η are components of the spatial frequencies corresponding to the directions of x and y, N is the number of input fibers and $\Psi(\xi,\eta)$ is defined as $\mathcal{F}_{2D}\{\psi(x,y)\}$. The aperture can be considered as a spatial low-pass filter and has a Fourier transform $P(\xi,\eta)$. Eq. (2.4) shows a summation of plane waves, which are the incident waves on the slab or slab sandwich.

On the output side of the slab sandwich, the field can be expressed as:

$$E^+(x,y) = \frac{e^{j\frac{2\pi}{\lambda}f}}{\lambda f} p(x,y) \sum_{i=1}^{N} A_i' \Psi(\frac{x}{\lambda f}, \frac{y}{\lambda f}) e^{-j\frac{2\pi}{\lambda f}(x_i x + y_i y)} \tag{2.5}$$

where

$$A_i' = \sum_{j=1}^{N} t_{ij} A_j \tag{2.6}$$

and t_{ij} is the amplitude transmission coupling coefficient between the i-th and the j-th waves. Notice that Eq. (2.6) is a mathematical expression that depicts the function of the core of the coupler—the grating-bearing dielectric slabs. Again the field is a summation of plane waves, which are in the same directions as those input plane waves shown in Eq. (2.4). However, according to (2.6), each output direction may carry signals from all the input waves.

Similarly, on the output surface of the right field lens, the field can be written as:

$$\begin{aligned} E'(x,y) &= \frac{e^{j\frac{2\pi}{\lambda}f}}{\lambda f} \mathcal{F}_{2D}\{E^+(x,y)\}|_{\xi=\frac{x}{\lambda f}, \eta=\frac{y}{\lambda f}} \\ &= e^{j\frac{4\pi}{\lambda}f} \sum_{i=1}^{N} A_i' \psi(x+x_i, y+y_i) * \frac{1}{(\lambda f)^2} P(\frac{x}{\lambda f}, \frac{x}{\lambda f}) \end{aligned} \tag{2.7}$$

where we have assumed the fiber transverse mode has the symmetry:

$$\psi(x,y) = \psi(-x,-y)$$

When the NA of the collimating lenses is much larger than that of the fibers, we have:

$$\frac{1}{(\lambda f)^2} P(\frac{x}{\lambda f}, \frac{y}{\lambda f}) \longrightarrow \delta(x,y)$$

and

$$E'(x,y) \longrightarrow e^{j\frac{4\pi}{\lambda}f} \sum_{i=1}^{N} A_i' \psi(x+x_i, y+y_i)$$

which holds the same mode pattern as that of $E(x,y)$.

It is evident that the above derivation can also be applied to the designs shown in Fig. 2.4. and Fig. 2.5 with slight modifications. In the former case, the GRIN self-focusing lenses simply take the place of both the field lenses and the collimating lenses, while in

the later case, each taper fulfils the function of the lenses. In short, the receiving fiber array is at the image plane of the transmitting fiber array in all the three designs.

In fact, whether lenses, self-focus lenses or tapers are used, the core of the coupler is the same pile of slabs, whose function is given by Eq. (2.6). The slabs receive only plane-wave inputs and give plane-wave outputs. Therefore, the lenses, the self-focus lenses or the tapers may just be considered as variations of the interfaces between the fibers and the grating slabs. A properly constructed interface ensures that the transverse mode of the fibers can be kept after the waves pass through the grating slabs. Nevertheless, the coupling is accomplished in the grating slabs. Next, we will discuss what happens at this core of the star couplers.

2.2.2 Grating degeneration

For simplicity, suppose there is only one volume grating written in a dielectric slab. It can be expressed, in terms of the slab refractive index, as:

$$n_(\vec{r}) = n_0(1 + \Delta \cos \vec{K} \cdot \vec{r}) \tag{2.8}$$

where n_0 is the average refractive index, or the DC component of the index, $\vec{K} = (K_x, K_y, K_z)$ is the grating vector with $|\vec{K}| = 2\pi/\Lambda$, Λ is the grating period, and the initial phase of the grating is assumed to be zero. Notice that, we will have the same grating if we change $\vec{K}$ to $-\vec{K}$, so in some of the figures in this chapter we will use vectors which have arrows at both ends to represent a grating vector. Suppose light waves may be incident on the grating slab in any or both of two predetermined directions. According to the diffraction theories of planar volume gratings such as [39], if the grating slab is sufficiently thick, the index modulation is weak and the two directions are arranged in such a way that Bragg condition is approximately satisfied, the field in the slab can be written as two plane waves:

$$E(\vec{r}) = a_1 e^{j\vec{k_1}\cdot\vec{r}} + a_2 e^{j\vec{k_2}\cdot\vec{r}} \tag{2.9}$$

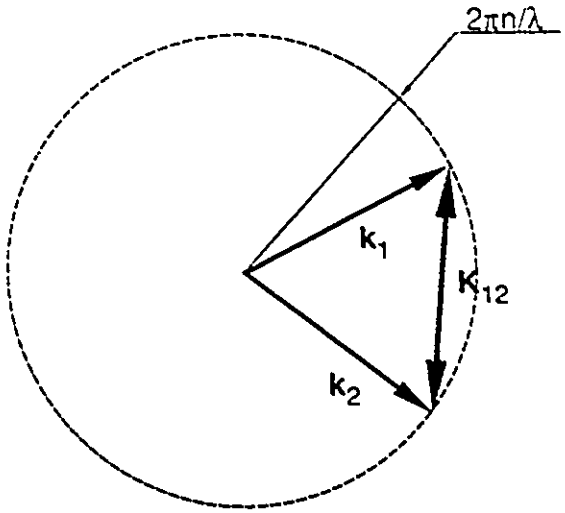

Note: **Bold face** letters stand for vectors.

Figure 2.9: The geometry of Bragg condition.

where

$$\begin{cases} \vec{k_i} = (k_{i,x}, k_{i,y}, k_{i,z}) & i = 1, 2 \\ \vec{r} = (x. y, z) \end{cases}$$

This is the so called two-wave approximation. Vector $\vec{k_i}$ $(i = 1, 2)$ is the wave vector of one of the two plane waves. Also, power may be exchanged between the two directions represented by the two wave vectors. In other words, the two waves are coupled. The strongest coupling happens when the Bragg condition is satisfied, i.e.,

$$\begin{cases} |\vec{k_1}| = |\vec{k_2}| = \frac{2\pi n_0}{\lambda} \\ \vec{k_1} - \vec{k_2} = \pm \vec{K} \end{cases} \tag{2.10}$$

where λ is the wavelength in free space. The geometry of this condition is shown in Fig. 2.9. Also notice that it is important to make sure that the grating is a volume grating or Bragg grating, which ensures that all the unwanted diffractions can be sufficiently suppressed. Hence, with the coupling between the two directions, whenever there is an input in either of the two directions, output waves in both directions can be found at the output side of the slab. This implies that a single volume grating is in fact a 2×2 coupler. With

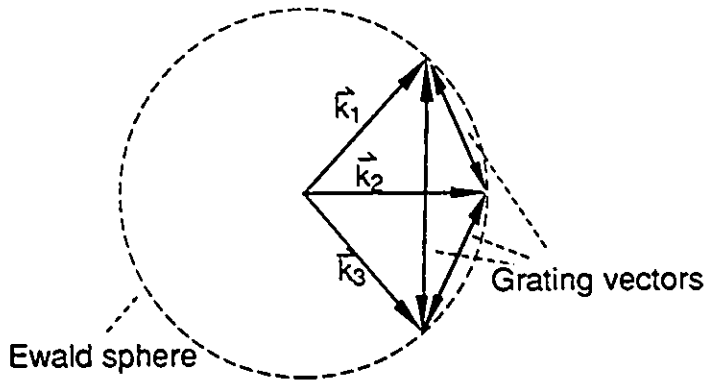

Figure 2.10: Grating vectors for a 3×3 star coupler. The Ewald sphere is the sphere in k-space with a radius of $2\pi n/\lambda$.

this idea in mind, the coupler proposed in [30, 31] can be actually considered as a series of 2×2 couplers superimposed in a single slab. In addition, there is in fact a 2×2 coupler for every combination of wave pairs, so the number of required gratings is just equal to the number of different ways of picking two waves out of the N waves. In the terminology of networking, a topology of complete mesh is built inside the slab from the above mentioned 2×2 single grating couplers. Though a complete mesh may not be the only topology for building the connection, it is perhaps the only topology that can offer the required symmetry which ensures that no input or output ports are "favoured" or distinct in the coupler. This issue was also discussed when the fused fiber coupler was investigated in the first section of this chapter. According to the scheme of [30, 31], a 3×3 coupler needs 3 gratings, and a 4×4 coupler needs 6 gratings. The gratings needed are depicted in Fig, 2.10 and Fig. 2.11. In [31], the grating patterns for 5×5 and 9×9 are given, and 10 or 36 gratings are required, respectively. The number of gratings does increase significantly when the number of ports increases. So the question to be answered next is whether this number can be reduced.

One way to reduce the number of gratings is to use the so called grating degeneration. The idea of grating degeneration is to properly arrange the directions of all the input light

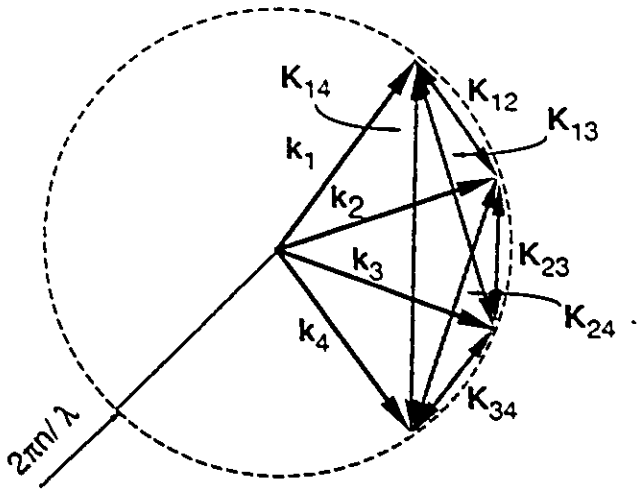

Figure 2.11: Grating vectors for a 4 × 4 star coupler.

waves in such a way that some of the originally different gratings become the same. In other words, some gratings degenerate into one grating. For convenience, consider the case of a 4 × 4 star coupler. Six different gratings are required in the slab when the configuration in [31] is used, see Fig. 2.11. The gratings are:

$$\pm\vec{K_{12}} = \vec{k_1} - \vec{k_2} \tag{2.11}$$

$$\pm\vec{K_{23}} = \vec{k_2} - \vec{k_3} \tag{2.12}$$

$$\pm\vec{K_{34}} = \vec{k_3} - \vec{k_4} \tag{2.13}$$

$$\pm\vec{K_{13}} = \vec{k_1} - \vec{k_3} \tag{2.14}$$

$$\pm\vec{K_{24}} = \vec{k_2} - \vec{k_4} \tag{2.15}$$

$$\pm\vec{K_{14}} = \vec{k_1} - \vec{k_4} \tag{2.16}$$

Remember, we can take either plus sign or minus sign in the above equations without changing the final result. Fig. 2.11 looks quite different compared to Fig. 5 of [31], but a closer examination of the directions of the vectors shows that they depict the same subject, namely, grating vector patterns. The only difference is that the starting points

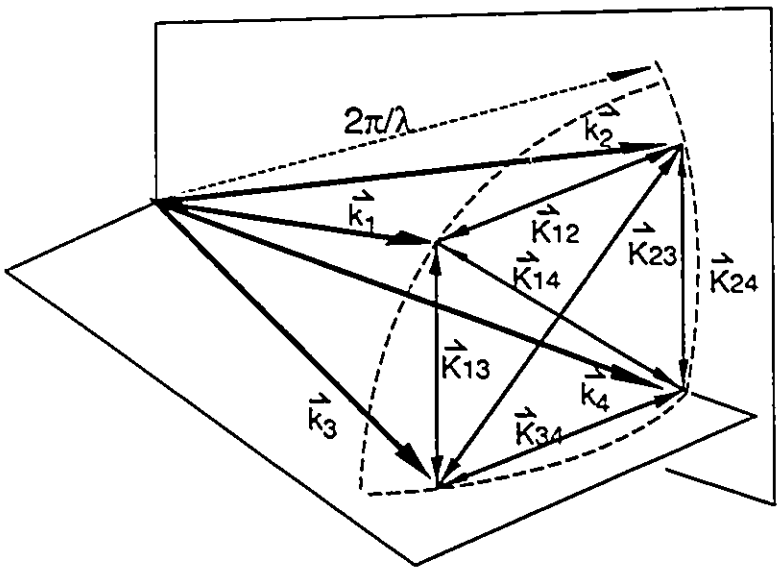

Figure 2.12: Arrangement of wave vectors for grating degeneration.

of the grating vectors are not placed at the same point in Fig. 2.11. The purpose of doing so is to emphasize the relation between wave vectors and grating vectors. Furthermore, in this chapter we will assume each grating has a sinusoidal waveform and a zero initial phase. Hence in this chapter, a grating vector plus a modulation index Δ will completely characterize a grating.

The directions of the wave vectors $\vec{k_i}$ can be arranged in the manner shown in Fig. 2.12, so that $\vec{K_{12}} = \vec{K_{34}}$, and $\vec{K_{13}} = \vec{K_{24}}$. In both cases, two originally different gratings degenerate into one. In this thesis, we refer to this kind of merge as grating degeneration. When degeneration happens, the number of needed gratings is obviously reduced. In the case of a 4×4 coupler, the best we can do is to have two degenerations as shown in Fig. 2.12 and the number of gratings can be reduced from 6 to 4. It is clear that two generalizations from the original configuration in [31] are required. First, the grating vector and the wave vectors of the waves should not be confined to the same plane. Secondly, the angular distribution of the wave vectors is not necessarily uniform.

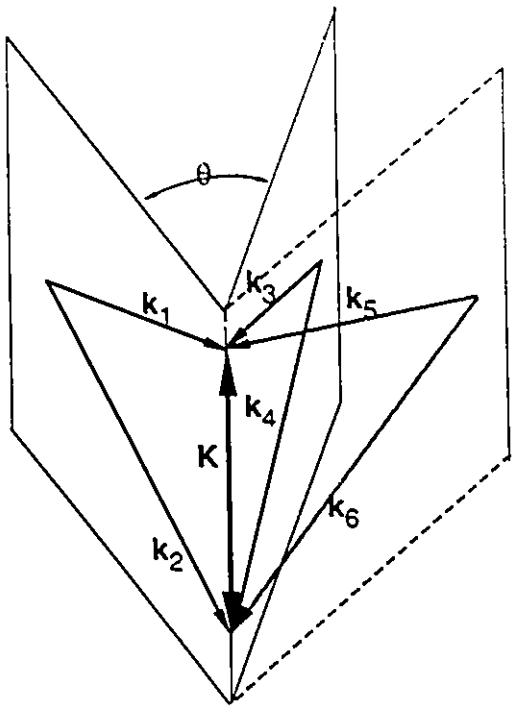

Note: **Bold face** symbols represent vectors.

Figure 2.13: A grating shared by different wave pairs.

As a consequence, the diffraction theories presented in [31] and [39] need be properly generalized. A generalized diffraction theory will be presented later in Chapter 3 of this thesis.

Another way of interpreting the grating degeneration is to examine the simple single-grating system shown in Fig. 2.13, where two wave pairs $\{\vec{k_1}, \vec{k_2}\}$ and $\{\vec{k_3}, \vec{k_4}\}$ are depicted. It is apparent that both pairs satisfy the Bragg condition and hence can be coupled by the same grating characterized by $\vec{K}$ (with no coupling between the two pairs). It is also apparent that the angle θ, between the two planes defined by the wave vector pairs can be arbitrary to a certain extent. Actually, as long as the angle is greater than the angular resolution of the lens system, the linearity of Maxwell's equations guarantees that no coupling will happen in between the two wave pairs. Generally, more than two wave pairs may be included. For instance, we can easily add one more wave pair $(\vec{k_5}, \vec{k_6})$ into the same single grating system, as it is shown in Fig. 2.13. It can thus be concluded that a single-grating system can be shared by a number of wave pairs. In other words, it is

equivalent to a number of 2×2 couplers in parallel. This is the very foundation on which the idea of grating degeneration is based.

A problem may arise when more than two wave pairs are coupled by one grating. Since the wave pairs cannot be arranged in a perfectly symmetrical way, different wave pairs may travel different lengths in the grating slab. The consequence is that different wave pairs may have a different coupling coefficient. This is not desirable, unless in a particular application, difference in coupling is required. In practice, two methods can be used to mitigate or eliminate this problem of unevenly distributed coupling. The first one is to make the angle between the planes of the wave pairs small, so that the difference in interaction length becomes insignificant. This method is basically limited by only the angular resolution of the lens system, which is determined by the relative aperture of the collimating lenses. The second method is to rearrange the positions of those pairs which have higher coefficients in such a way that they are slightly off the Bragg condition and the coupling is thus decreased to the same level as others. This method requires more delicate work to be done in design and implementation, and it can be combined with the first one.

2.2.3 Sandwiched structure

In this section, the same 4×4 coupler as shown in Fig. 2.11 will be used to help to explain the second technique of reducing the number of required gratings. Using grating degeneration, we have been able to reduce the number from 6 to 4. Now with the help of Fig. 2.14, it can be seen what happens if the slab is allowed to be split into two sandwiched slabs. Suppose we discard grating $\vec{K}_{14}$ and $\vec{K}_{23}$ and distribute the rest of the gratings among the two slabs. In the first slab, two gratings are recorded, namely, $\vec{K}_{12}$ and $\vec{K}_{34}$. After the four waves emerge from the first slab, the waves in the directions of $\vec{k}_1$ and $\vec{k}_2$ are coupled by the grating corresponding to $\vec{K}_{12}$, and the waves in the directions of $\vec{k}_3$ and $\vec{k}_4$ are coupled by the grating with grating vector $\vec{K}_{34}$,i.e.,

$$p_1^{(1)} = (1 - \eta_{12})p_1^{(0)} + \eta_{12}p_2^{(0)} \tag{2.17}$$

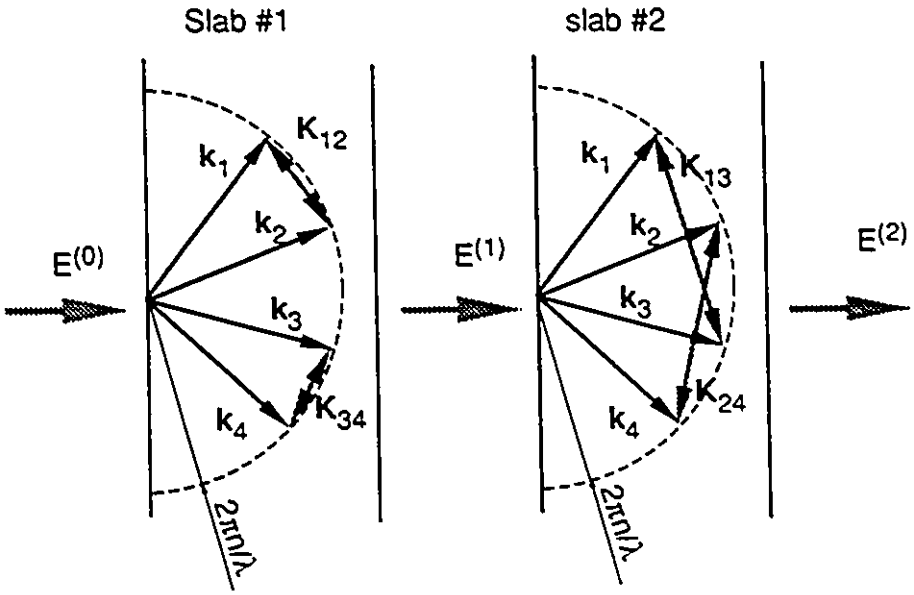

Note: **Bold face** symbols stand for vectors.

Figure 2.14: An illustration of a 4 × 4 star coupler with a sandwich structure.

$$p_2^{(1)} = \eta_{12} p_1^{(0)} + (1 - \eta_{12}) p_2^{(0)} \tag{2.18}$$

$$p_3^{(1)} = (1 - \eta_{34}) p_3^{(0)} + \eta_{34} p_4^{(0)} \tag{2.19}$$

$$p_4^{(1)} = \eta_{34} p_3^{(0)} + (1 - \eta_{34}) p_4^{(0)} \tag{2.20}$$

where $p_i^{(j)}$ $(i = 1, 2, 3, 4, j = 0, 1, 2)$ stands for a random process of the power of the i-th wave at the output of the j-th slab. Variable η_{kl} $(k, l = 1, 2, 3, 4)$ is the diffraction efficiency of the grating characterized by the vector $\vec{K}_{kl}$.

It can easily be shown that after the waves pass through the second slab which bears the grating $\vec{K}_{13}$ and $\vec{K}_{24}$, the four outputs can be expressed as

$$\begin{aligned} p_1^{(2)} &= (1 - \eta_{13})(1 - \eta_{12}) p_1^{(0)} + (1 - \eta_{13}) \eta_{12} p_2^{(0)} \\ &\quad + \eta_{13}(1 - \eta_{34}) p_3^{(0)} + \eta_{13} \eta_{34} p_4^{(0)} \end{aligned} \tag{2.21}$$

$$\begin{aligned} p_2^{(2)} &= (1 - \eta_{24}) \eta_{12} p_1^{(0)} + (1 - \eta_{24})(1 - \eta_{12}) p_2^{(0)} \\ &\quad + \eta_{24} \eta_{34} p_3^{(0)} + \eta_{24}(1 - \eta_{34}) p_4^{(0)} \end{aligned} \tag{2.22}$$

$$\begin{aligned} p_3^{(2)} &= \eta_{13}(1 - \eta_{12}) p_1^{(0)} + \eta_{13} \eta_{12} p_2^{(0)} \\ &\quad + (1 - \eta_{13})(1 - \eta_{34}) p_3^{(0)} + (1 - \eta_{13}) \eta_{34} p_4^{(0)} \end{aligned} \tag{2.23}$$

$$\begin{aligned} p_4^{(2)} &= \eta_{24} \eta_{12} p_1^{(0)} + \eta_{24}(1 - \eta_{12}) p_2^{(0)} \\ &\quad + (1 - \eta_{24}) \eta_{12} p_3^{(0)} + (1 - \eta_{24})(1 - \eta_{34}) p_4^{(0)} \end{aligned} \tag{2.24}$$

It can be seen that each output can receive parts of the signal power from all the input signals. In a special case, when $\eta_{ij} = 50\%$, each input wave will have its power evenly distributed among all four outputs. This means that even though we have discarded $\vec{K}_{14}$ and $\vec{K}_{23}$, the two layered sandwich structure is still a 4×4 coupler, with each slab bearing only two gratings. Obviously, using grating degeneration, we can further reduce the number of gratings to one per slab. The reduction in grating number is quite significant. According to the author's experience, constructing six different gratings in a single slab probably requires high standard facilities and good experimental skills, while recording one volume grating in a slab with a diffraction efficiency of 50% is a much easier task.

In the previous sections, we have shown that the basic element of a holographic star

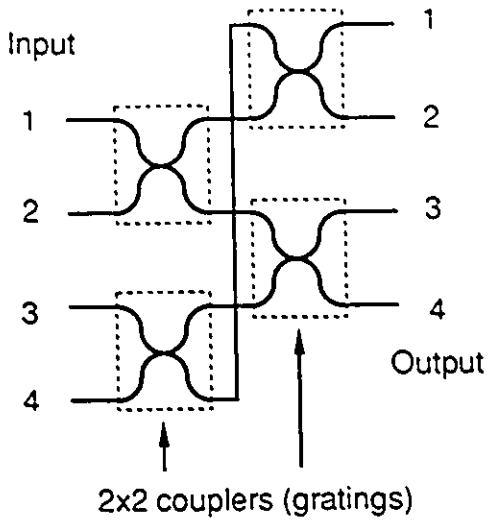

Figure 2.15: Logic connection for a 4×4 star coupler with a sandwich structure.

coupler is a volume grating which acts like a 2×2 star coupler. With this idea in mind, we find that from the point of view of topology, a sandwich structure is similar to a star coupler made from element 2×2 fiber couplers, as shown in Fig. 2.15. The number of slabs in the former case corresponds exactly to the number of stages in the later case. Therefore, the reasons why a sandwiched structure can reduce the required dynamic range are:

1. The gratings needed can be placed in separate slabs instead of one slab. The number of gratings in each slab is thus reduced.

2. The topology is different. Cascade connections, instead of complete mesh are used, so fewer gratings (2×2 couplers) are required.

The drawback of using cascade connections is the increased excess loss. The excess loss of sandwiched coupler is the sum of the excess loss introduced by each of the slabs in dB. In one extreme, if we use as many slabs as needed to minimize the number of gratings, the excess loss will be proportional to $\log_2 N$. This is similar to that of an $N \times N$ coupler constructed from 2×2 fiber couplers, because the logic element (2×2) and logic connections are the same. In conclusion, in designing a practical sandwich coupler, a trade-off needs

be done between the number of sandwiched slabs and the number of gratings in each slab, when N is given. The former is limited by the excess loss, the latter is bounded by the dynamic range of the recording material.

Compared with the sandwiched structure, the grating degeneration is a net winner. It does not introduce any extra excess loss, and hence can be used to the limit.

2.3 Design of a Grating System with Grating Degeneration and a Sandwich Structure

As mentioned in the preceding section, the grating-bearing slabs form the core of a holographic coupler. In this section, the principles of designing such slabs with the feature of using grating degeneration and sandwich structures will be discussed. The discussion will be constrained to the wave-vector arrangement required for grating degeneration and the topology for sandwich structures. It should be noticed that the discussion gives principles that are necessary but may not be sufficient. It is known that a wave vector cannot completely characterize a light wave. There are other physical quantities such as intensity, polarization and initial phase, which are needed to specify a wave. Similarly, a grating vector does not fully describe a grating. There are other features such as the modulation and the initial phase needed for a complete characterization of a grating. The complete picture of a grating system will be given in Chapter 3, where the Maxwell's equations are employed. Nevertheless, the content in this section is still important in the sense that it lays the foundation for more detailed designs.

Grating degeneration (or grating-sharing) is achieved by properly arranging the directions of the lightwaves and the orientation of grating vectors. The basic constraint for grating-sharing is the Bragg condition shown in Eq. (2.10) and Fig. 2.9. For a given grating, any wave pairs sharing the grating must satisfy the condition. If the wave vectors (or the components of the vectors) of a pair of waves are considered as variables (i.e., design

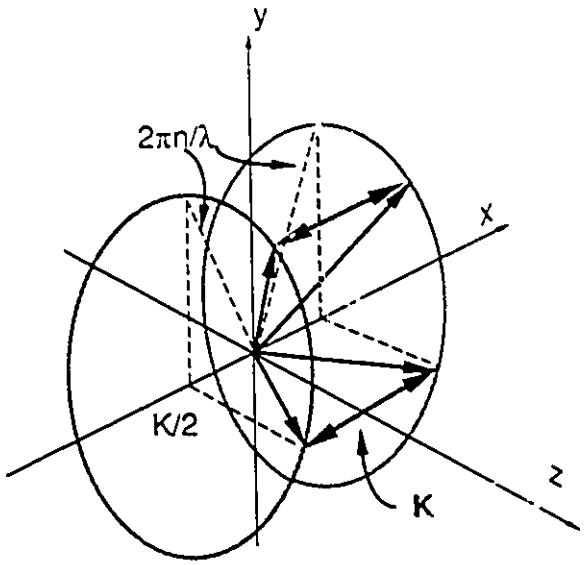

Note: **Bold face** symbols represent vectors

Figure 2.16: Wave vector tip-trajectories for grating degeneration.

parameters), they should satisfy the following expressions for a given grating vector $\vec{K}$:

$$\begin{cases} k_x^2 + k_y^2 + k_z^2 &= (\frac{2\pi n}{\lambda})^2 \\ k_x K_x + k_y K_y + k_z K_z &= \frac{K_x^2+K_y^2+K_z^2}{2} \\ \vec{k}' &= \vec{k} - \vec{K} \end{cases} \tag{2.25}$$

where $\vec{k}$ and $\vec{k}'$ are the wave vectors of the wave pair as variables. The first two equations represent a spherical surface and a plane surface. The intersection of these surfaces makes a circle in the k-space (spatial angular frequency space), which is the trajectory that the tip of the wave vector $\vec{k}$ should follow. The third line specifies the trajectory the second wave vector $\vec{k}'$ follows in terms of $\vec{k}$ and $\vec{K}$. The geometry of these equations is shown in Fig. 2.16. Any wave vector pairs $\{\vec{k}, \vec{k}'\}$ which have their vector tips placed on the trajectories can share the grating corresponding to the vector $\vec{K}$. However, Eq. (2.25) is still a bit overdone because three components are used to specify each of the wave vectors. It is known that out of the three components of any wave vector, e.g., $\vec{k}$, only two are independent. Without losing generality, if k_z represents the projection of $\vec{k}$ in the

direction perpendicular to the slab surfaces, we may simply choose the lateral components k_x and k_y as the independent variables. Cancelling all the k_z-components in Eq. (2.25) yields expressions for two-dimensional projections of the same trajectories:

$$\begin{cases} \frac{\{|k_x \cos\beta - k_y \sin\beta| - \frac{K_\rho}{2}\}^2}{[\frac{K_x}{K}]^2[(\frac{2\pi n}{\lambda})^2 - (\frac{K}{2})^2]} + \frac{[k_x \sin\beta + k_y \cos\beta]^2}{(\frac{2\pi n}{\lambda})^2 - (\frac{K}{2})^2} = 1 \\ \vec{k}'_\rho = \vec{k}_\rho - \vec{K}_\rho \end{cases} \tag{2.26}$$

where "ρ" indicates the transverse component versus "z" for longitudinal components, and

$$\begin{cases} \cos\beta = \frac{K_x}{K_\rho} \\ \sin\beta = \frac{K_y}{K_\rho} \\ K = \sqrt{K_\rho^2 + K_z^2} \\ K_\rho = \sqrt{K_x^2 + K_y^2} \end{cases} \tag{2.27}$$

The advantage of the use of Eq. (2.26) is its two-dimensional nature. It makes the design work easier, because a two dimensional trajectory can be easily depicted. A second advantage, which is more important, is that when the design shown in Fig. 2.3 or 2.4 is used, the two-dimensional trajectories are directly related to the positions of the fiber ends on the surfaces of the field lenses or that of the self-focusing lenses. The relation between the position of a fiber end (x, y) and the transverse component of the corresponding wave vector (k_x, k_y) is illustrated in Fig. 2.17, from which it can be shown that

$$(x, y) = -\frac{\lambda}{2\pi f}(k_x, k_y) \tag{2.28}$$

According to this relation, the trajectories of a pair of fiber ends that are coupled by the same grating are just a scaled version of Eq. (2.26). However, in this thesis, we will still stick to the k-space (spatial angular frequency domain) representation, even though the use of fiber positions could be more straightforward in many practical cases. The major concern of doing so is to keep the generality. The fiber end position representation depends on the particular schematic design of the coupler. For example, it cannot be used for the configuration depicted in Fig.2.5. Also, when the fiber is placed very far from the optical axis of the lenses, Eq. (2.28) may not be valid. These constraints do not hold if (k_x, k_y)

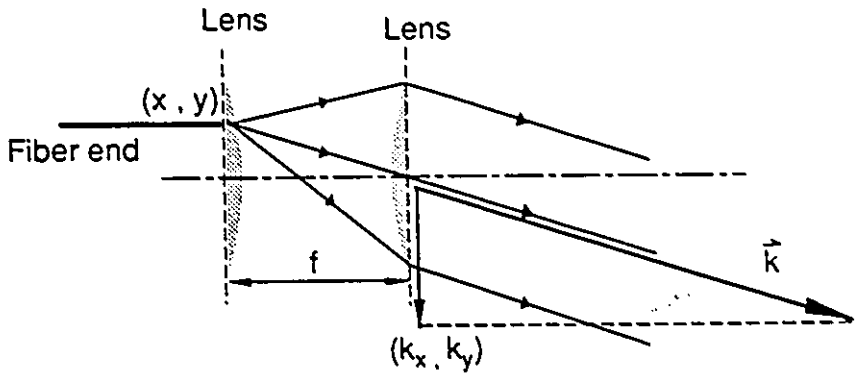

Figure 2.17: Relation between the fiber end position and the wave vector tip position in k-space.

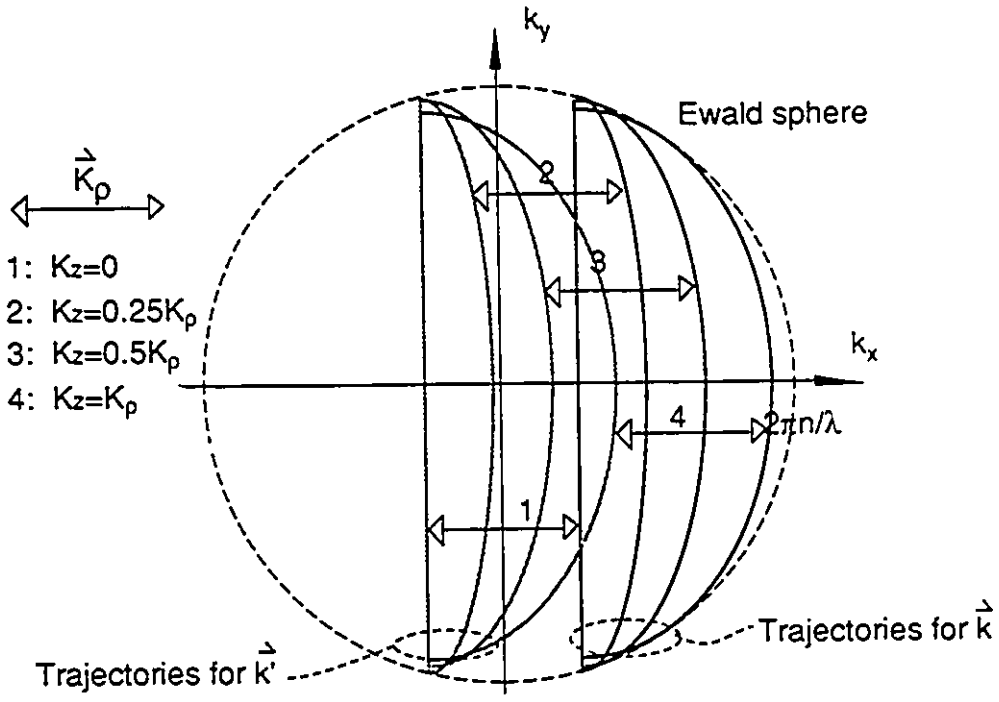

Figure 2.18: 2-dimensional trajectories for grating degeneration.

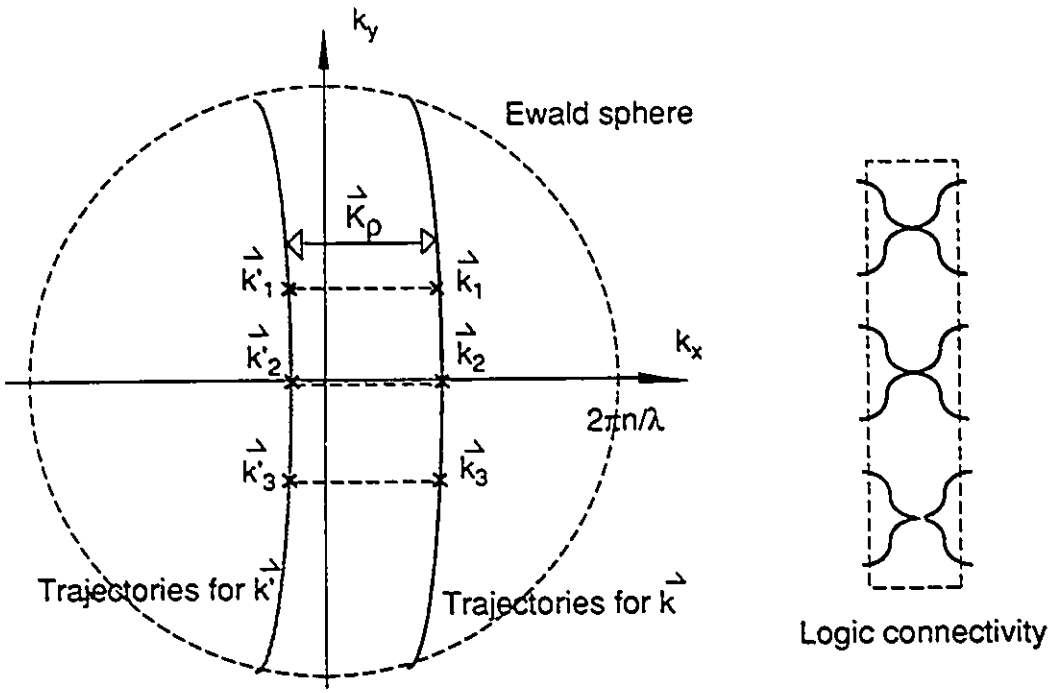

Figure 2.19: A 2-dimensional wave vector tip-diagram.

is used to specify a grating slab design. Fig.2.18 shows a set of trajectories for given $\vec{K}$s. The transverse components are kept constant with the longitudinal components set to a set of values. In a general case, a trajectory pair is a pair of ellipses with one being the shifted version of the other. The direction and the amount of shift is determined by the transverse grating vector. In the special case that $K_z = 0$, the ellipses become parallel straight lines. Fig. 2.19 shows a design with three wave pairs sharing the same grating. In the rest of the thesis, all the designs of grating degenerations will be presented in the form given in Fig. 2.19, namely, a pattern of the lateral projections of the wave vector tips.

Apart from grating degeneration, the principles governing the design of sandwich structures should also be investigated. The most important issue is the topology. As mentioned in the previous section, every single grating component can be considered as a

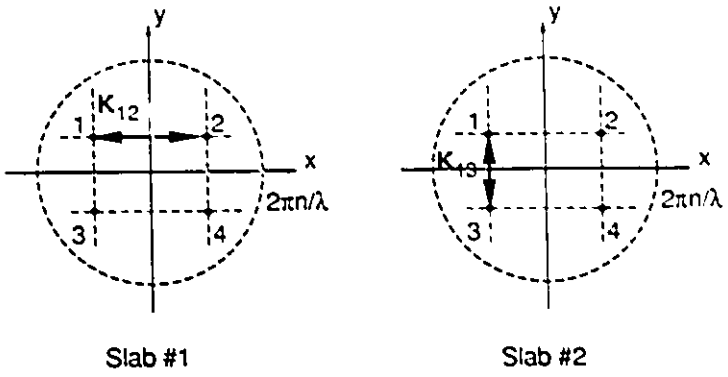

Figure 2.20: Tip-pattern design for 4×4 couplers.

2×2 coupler, which is actually a bidirectional link between two pairs of input and output ports; or a number of such couplers or links in parallel when grating degeneration can be achieved. When a topology with multiple stages is applied, the number of slabs is just equal to the number of stages in the topology. Obviously, the topology used for fused fiber $N \times N$ couplers, such as those depicted in Fig. 1.3 and Fig. 2.15 can be used. In this case, n slabs are needed, if $N = 2^n$. Therefore, in designing the grating system of a coupler, first, we use as many gratings as required to couple or interconnect all the plane waves according to the predetermined topology and then try to change the directions of the waves. To be more specific, we change the wave vector tip positions on the plane of $k_x O k_y$, to fit as many wave pairs into as few set of trajectories as possible so as to minimize the number of required gratings.

Three design examples, i.e., designs for 4×4, 8×8 and 16×16 couplers are shown in Fig. 2.20 through Fig. 2.22. Though it may not be easy to work out a general optimum design for a coupler of arbitrary N, the optimum design or at least an acceptable design can be obvious when N is small. In this case, we do not have to be worried about excess loss due to slab cascading. From an experience with DCG (dichromated gelatin), it is quite conservative to expect the excess loss of each slab to be below 0.1 dB. Therefore, the excess loss of, e.g., 10 layers can easily be kept below 1 dB. It can easily be verified that

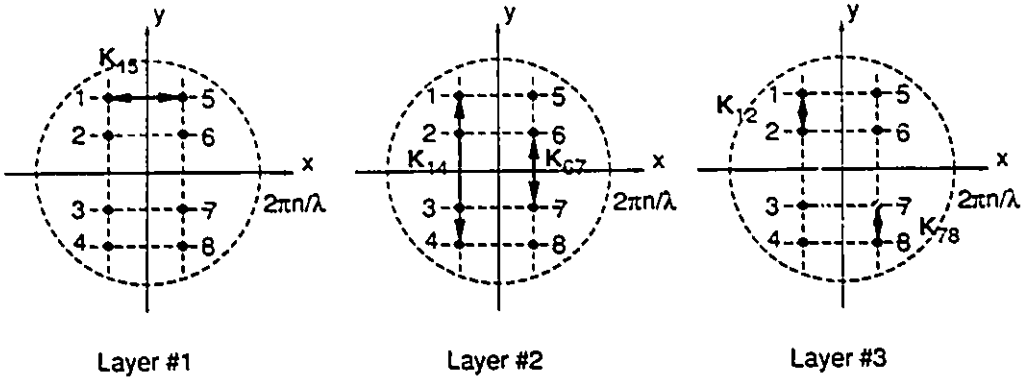

Figure 2.21: Tip-pattern design for 8 × 8 couplers.

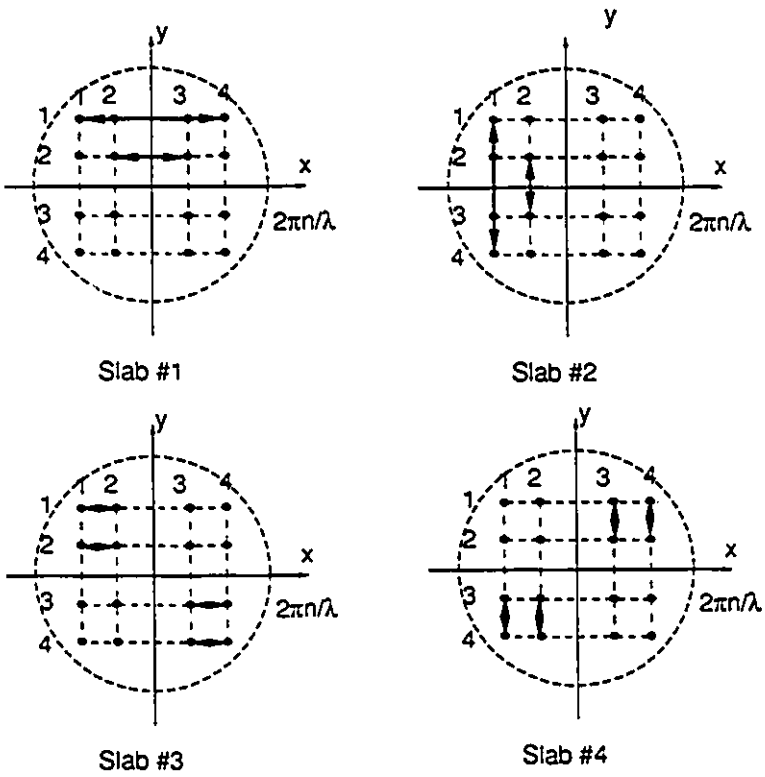

Figure 2.22: Tip-pattern design for a 16 × 16 coupler.

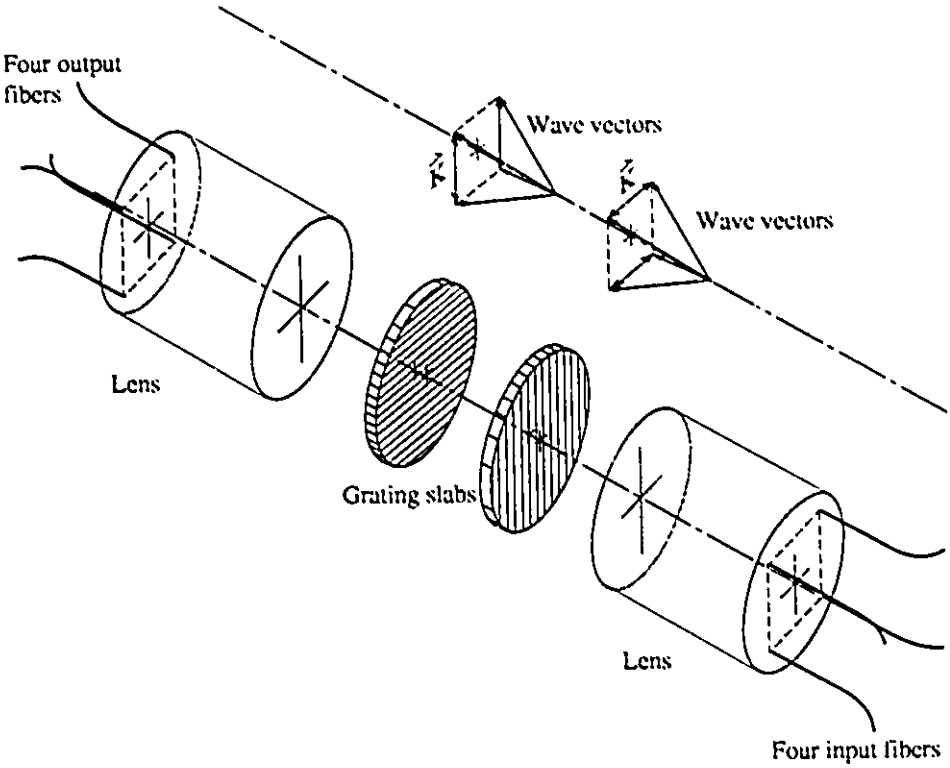

Figure 2.23: An illustration of a 4 × 4 holographic coupler with grating degeneration and sandwich structure.

the designs shown in Fig. 2.20 to 2.22 satisfy Eq. (2.26). For a 4 × 4 coupler, two slabs are needed and there is only one grating written in each slab. Fig. 2.23 gives a more detailed depiction of the 4 × 4 design. It can be seen that the grating in the first slab provides a "horizontal" coupling among the four directions or waves; while the second grating slab provides a "vertical" coupling among the four directions. The cascading of the two slabs provides the coupling for all the four directions or waves. For an 8 × 8 coupler, three slabs are needed. At most two gratings have to be written on each of the slabs. For the 16 × 16 coupler, 4 slabs are required, and at most 4 different gratings are needed in each slab. We can compare this design with that in [31]. With a single-slab-no-degeneration configuration, 120 different gratings are needed in one slab. The improvement is apparent.

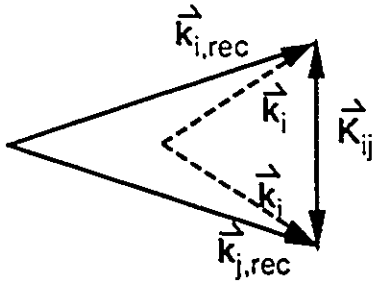

Figure 2.24: Geometrical relation between wave vectors $\vec{k}_{i,rec}$, $\vec{k}_{j,rec}$ and $\vec{k}_i$, $\vec{k}_j$.

For implementation, a conventional holographic technique is needed. The basic idea is to let two light waves interfere with each other and then record the interference pattern in a slab of photosensitive material whose refractive index, after a certain processing procedure, is directly proportional to the intensity of the interference field. Since we have suggested the use of planar systems (Fig. 2.3, 2.4 and 2.5), a different wavelength can be used for the grating construction. An important relation for the grating recording is

$$\vec{k}_{j,rec} - \vec{k}_{i,rec} = \vec{K}_{ij} \tag{2.29}$$

where $\vec{k}_{j,rec}$, $\vec{k}_{i,rec}$ are the wave vectors of the two waves used in constructing grating $\vec{K}_{ij}$. Eq. (2.29) is very similar to the second line of Eq. (2.10) in appearance. Combining these two equations yields

$$\vec{k}_{j,rec} - \vec{k}_{i,rec} = \vec{k}_j - \vec{k}_i \tag{2.30}$$

The geometric interpretation is shown in Fig. 2.24. Note that, $|\vec{k}_{i,rec}| = |\vec{k}_{j,rec}| = \frac{2\pi n}{\lambda_{rec}}$, where λ_{rec} is the wavelength used in construction, which is probably 0.514 μm when DCG is used.

Fig. 2.25 shows a schematic diagram of a possible set-up for grating construction. For mass production purpose, the grating construction set-up can be scaled up by a certain factor, so that larger pieces of grating slabs can be made. The large pieces can then be cut into smaller pieces to multiply the quantity. This is another advantage we can take from using a planar grating configuration.

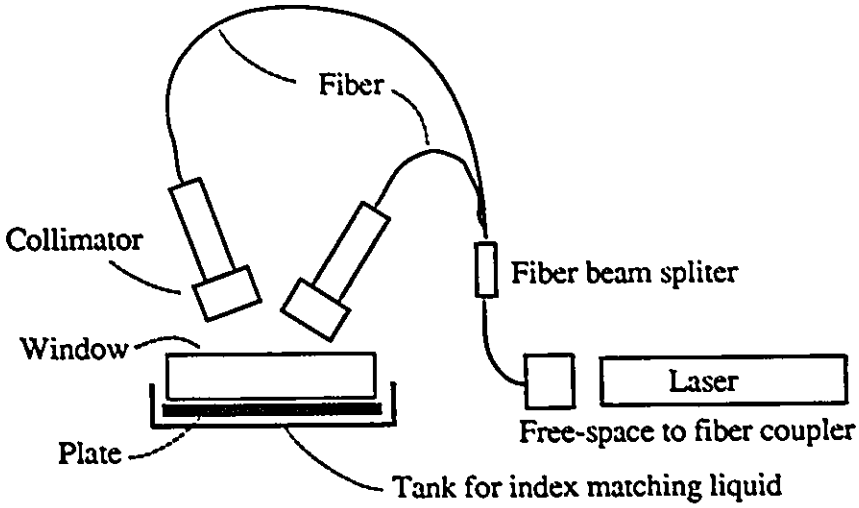

Figure 2.25: Schematic diagram of an experimental set-up for constructing volume gratings.

2.4 Experiment

In this section, to support the concepts and the designs proposed in the preceding sections, some of the experimental work will be presented. The work was mainly conducted by Dr. E. Simova, and the author assisted the work with his knowledge and experience in hologram fabrication.

Dr. Simova has been working for some time on the fabrication of star couplers of various sizes, using different recording materials and configurations. One of these couplers was fabricated according to a design shown in this thesis. In grating construction, silver halide sensitized gelatin (SHSG) was used as recording material. SHSG turned out to be remarkably satisfactory in terms of sensitivity, modulation index and signal-to-noise ratio due to its silver-halide-based sensitization and its pure-gelatin nature. The recording set-up was a very conventional one. A laser beam from a He-Ne laser was split into two beams with a beam splitter. The beams were filtered with pinholes, expanded and then collimated. Both beams were then directed to the holographic plate with mirrors.

The coupler fabricated in the experiment is based on the design of a 4×4 coupler

shown in Fig. 2.20. Two identical volume gratings were constructed. Both have a diffraction efficiency of about 50 %. The gratings were then sandwiched together with one of them being rotated 90° around its axis. The performance of this sandwich was tested with 1300 nm laser light. The results are shown in the following table:

	Power transmittance					
	Output direction					
Input direction	1	2	3	4	Loss	Homogeneity
1	0.142	0.194	0.191	0.146	32.7%	27%
2	0.191	0.160	0.151	0.187	31.1%	21%
3	0.208	0.143	0.153	0.205	29.1%	32%
4	0.142	0.188	0.205	0.169	29.6%	31%

It can be seen that the performance of this sandwich is promising. Obviously, it does function as a 4 × 4 coupler. For each input direction, the input light is split up by the sandwich into four beams in four different output directions. The excess loss was measured to be about 30 % including the loss (about 20 %) caused by the Fresnel reflections at the surfaces of the two substrates. This part of the loss can be reduced with index matching techniques. The rest of the loss is caused by scattering and absorption of the gelatin. This part can be reduced by optimizing the processing procedures. Evidently, the results offer a strong support to the concepts of grating degeneration and sandwich structure presented in this chapter. It also proves that the design given in Fig. 2.20 is correct.

2.5 Quasi-Bragg Diffraction for 16 × 16 Holographic Couplers

So far, it has been assumed in this chapter that the Bragg condition is perfectly satisfied in all the grating-bearing slab designs. In this section, as the title suggests, we will stray

from this practice. A new technique using off-Bragg diffractions will be introduced. It can further simplify the design of 16×16 couplers. Though the technique, termed here as quasi-Bragg diffraction, is particularly tailored for a 16×16 coupler, the principles can be applied to grating slab designs with N other than 16.

Before the technique is presented, it is necessary to investigate the reason why Bragg gratings are used in the holographic couplers. Generally, holographic gratings can be classified as thick (or volume, or Bragg) gratings and thin gratings. The major advantage of a thick grating over a thin grating is that it has the so called volume effect. This makes it selective to the incident angle and wavelength. Also, the volume effect may be used to enhance the wanted diffraction orders and suppress the unwanted, so that a more efficient coupler can be constructed. This volume effect is always associated with three-dimensional diffraction structures. In the particular subject of interest in this thesis, the effect is directly related to the thickness of the grating slabs. However, whether a grating can be considered as thick or thin does not only depend on the absolute physical thickness of a grating slab. When gelatin-based recording material is used, the thickness of a grating slab, not including the substrate, ranges from a few microns to about one hundred microns. However, thick gratings, as well as thin gratings, can be written in slabs of all possible thickness. The parameter for distinguishing thick from thin gratings can be found in [39]. Notice that, the discovery of the relation should not be credited to [39], because it had been widely used in the study of acoustic diffraction gratings. The parameter is rewritten here as:

$$Q = 2\pi \frac{(\lambda/n)}{\Lambda} \frac{d}{\Lambda} \tag{2.31}$$

Usually, a grating is considered as thick when $Q \geq 10$. As shown in Eq. (2.31), Q is the product of two factors. One is the "relative wavelength"—the ratio of the wavelength in medium n to the grating period. The other is the relative thickness which is defined as the thickness with respect to the grating constant (or period) Λ. For example, in Fig. 2.26, slab A and B have the same thickness d, but if slab A is considered thick for a given wavelength, slab B may probably be considered thin. The major difference between the

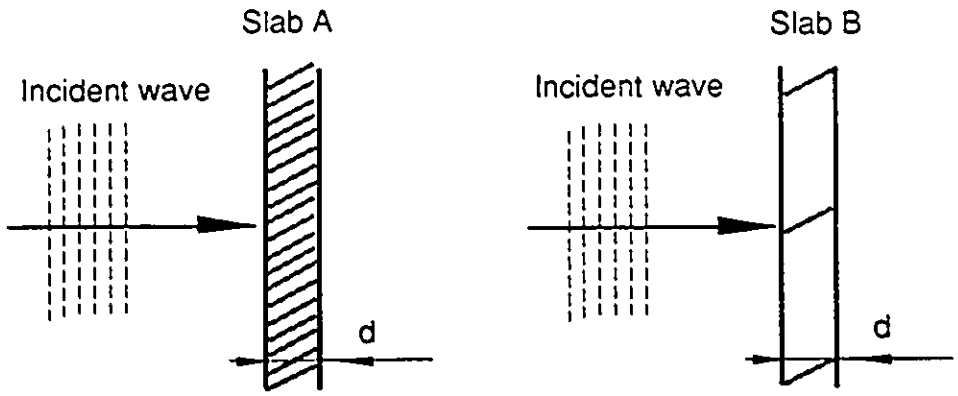

Figure 2.26: A thick grating and a thin grating of the same thickness.

two grating slabs is that slab A has a set of fringe planes whose period is comparable or less than the thickness; while the grating period of grating B is much larger than the thickness. Apparently, because of the large period of slab B, even though it possesses 3-dimensional features like thickness, fringe planes (instead of fringes) which have even a slant angle (determined by the longitudinal component of the grating vector), etc., it can be simply considered as a thin transparency which does not have these features. A thin grating transparency can be characterized by merely a transverse grating vector $\vec{K}_\rho$ and the phase modulation to a passing light wave. Notice that we do not consider amplitude-modulating materials in this thesis.

When a lightwave is incident on a perfectly thin grating, the diffraction pattern is shown in Fig. 2.27, which has usually a number of diffraction orders. The directions of these diffraction orders are determined by the so called grating equation:

$$\vec{k}_{m,\rho} = \vec{k}_{0,\rho} + m\vec{K}_\rho \quad for \;\; m = 0, \pm 1, \pm 2, \cdots \tag{2.32}$$

where the subscript ρ indicates the transverse component vectors. Obviously, in the case of thin gratings, the grating vector has only a transverse component. The grating equation only gives the relation among the transverse component vectors of the grating vectors and that of the wave vectors. However, it is sufficient to determine the deflection directions of all the diffraction orders. It is known that in a homogeneous medium, the magnitude of a

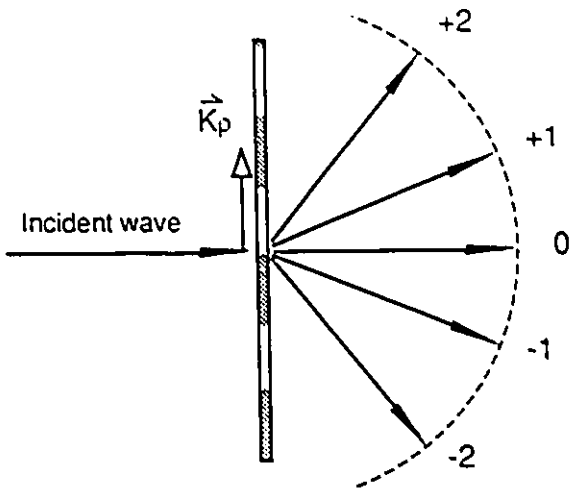

Figure 2.27: The diffraction orders of a thin grating.

wave vector is $\frac{2\pi n}{\lambda}$ with n being the refractive index. When both the transverse component and the magnitude are known, the direction of the wave can obviously be determined. The geometry is shown in Fig. 2.28.

Actually, the grating equation is not only applied to a thin grating, but also to thick gratings. When the directions of the diffraction orders are to be determined, the longitudinal component of the grating vector, together with all the features of 3-dimensional nature can be just neglected. The real difference between thick and thin gratings is in the power distribution among the diffraction orders, especially when the direction of the incidence changes. It turns out that a thick grating has an angular or wavelength selectivity due to the volume effect, while a thin grating does not. The volume effect results from the fact that an extra dimension in the grating structure introduces extra constraints to the wave propagation. In a volume grating, the structural field pattern of a incident light has to be in harmony with a three-dimensional grating structure instead of a two dimensional one as in the case of thin gratings in order to obtain the strongest diffraction. However, with a perfectly thin grating, no matter how the incident direction changes, the intensities of the output orders will not change. In addition, the power distributions between

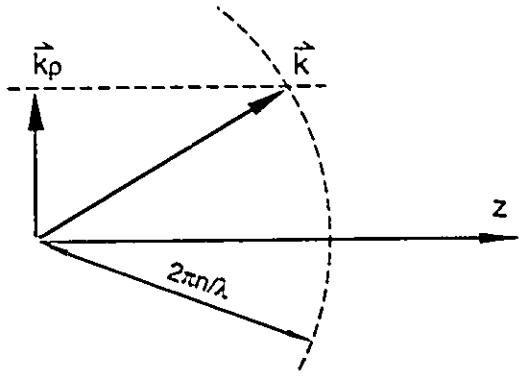

Figure 2.28: The wave vector of a diffraction order can be easily found from its transverse component.

the positive diffraction orders and the negative orders are basically even. When a thick grating is used, the picture is different. Though the directions of the diffraction orders are still determined by the grating equation, their intensities will be dependent on those features related to the third dimension. One diffraction order may become dominantly strong when the incident light is in such a direction that the Bragg condition is satisfied for that particular order. Actually, the diffraction can be so strong that all the incident power goes to this particular order (This corresponds to a diffraction efficiency of 100%), and only one diffraction order can be observed. In a more general case, two diffraction orders can be observed: one is the pass-through order (or the order $m = 0$); the other is the diffracted one (may be the order $m = +1$ or $m = -1$). The rest of the orders are suppressed by the volume effect, or in other words, by the selectivity. The selectivity is a very important property when a coupler is to be made. If a thin grating were used, first, unwanted diffraction orders would appear, as it is shown in Fig. 2.29. Two unwanted waves are depicted in the figure: the wave corresponding to $\vec{k}_2$ and the wave labeled as -1, though the number may not be limited to two in practice. The former is the order $m = +1$ diffraction when the light is incident from the direction of $\vec{k}_1$ or the order $m = +2$ diffraction of the wave $\vec{k}_0$; the latter is the order $m = -1$ diffraction when

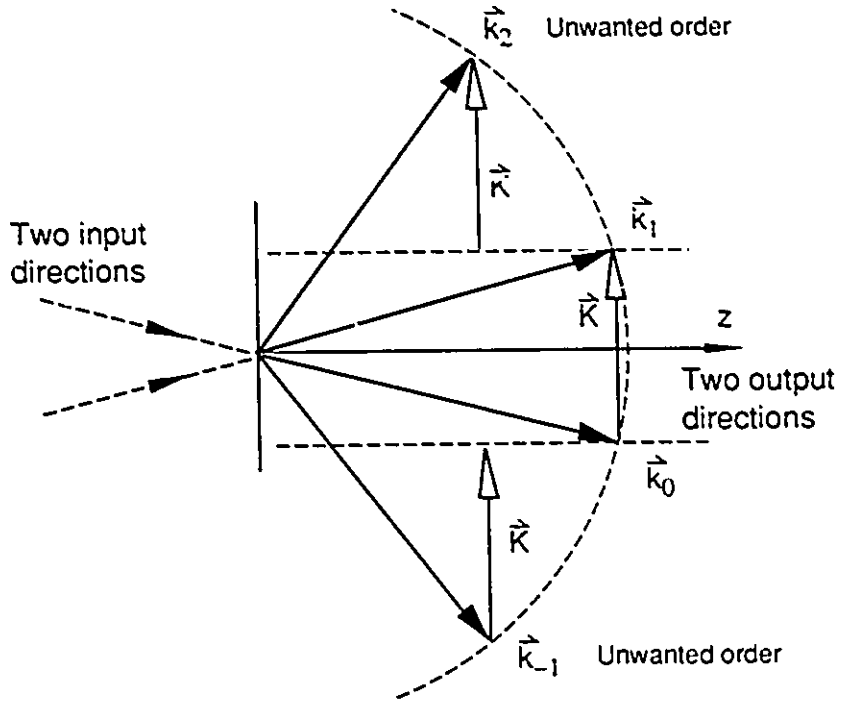

Figure 2.29: A 2×2 coupler made from a thin grating. The unwanted orders may appear due to the lack of selectivity.

the light is incident in the direction of $\vec{k}_0$ or the order $m = -2$ diffraction of the wave $\vec{k}_1$. Apparently, these unwanted orders introduce excess loss to the coupler, because they are not to be coupled into any of the fiber ends. In comparison, all the unwanted orders can be eliminated in a thick grating, if the vector $\vec{k}_0$ and $\vec{k}_1$ are arranged to satisfy the Bragg condition and if the Q of the grating is sufficiently high. This means a higher efficiency. In addition, since the diffraction efficiency of a thick grating can be as high as 100%, we may get theoretically any amount of coupling between the two wanted waves ranging from 0 to 1. It can be shown that this range is not achievable with a thin grating, because the highest diffraction efficiency is about 40.4% [40].

So far we have been discussing the disadvantages of using thin gratings. However, it should be noticed that apart from the disadvantages, a thin grating actually has its advantages. In Section 2.2, we have introduced the technique of grating degeneration, in which two or more pairs of light waves can share one grating. Actually, if the grating is a thin grating, this kind of grating merge (or degeneration) is much easier, because the grating is not under the constraint of Bragg condition any more. With a thick grating, a two-dimensional arrangement of the waves is needed to satisfy Bragg condition, while a thin grating can be shared with or without a two dimensional arrangement. The only thing that has to be satisfied is that the originally different gratings to be merged should have the same transverse component vector, after the directions of the waves are rearranged. An example is shown in Fig. 2.30(a), and Fig. 2.30(b) shows that a grating can be shared with the wave vectors arranged in the same plane. It can be seen that without the restriction of Bragg condition, the grating system of a coupler can be further simplified. This is exactly what will be done with the new technique. The problem is how to avoid the excess loss introduced by the unwanted diffraction orders, and the solution is to maintain only the right amount of selectivity.

In practice, it is not possible to draw a line between thick and thin gratings. Though a grating can usually be considered as thick if the parameter Q is larger than 10, a more rigorous way is to generally consider the gratings as a three-dimensional structure without

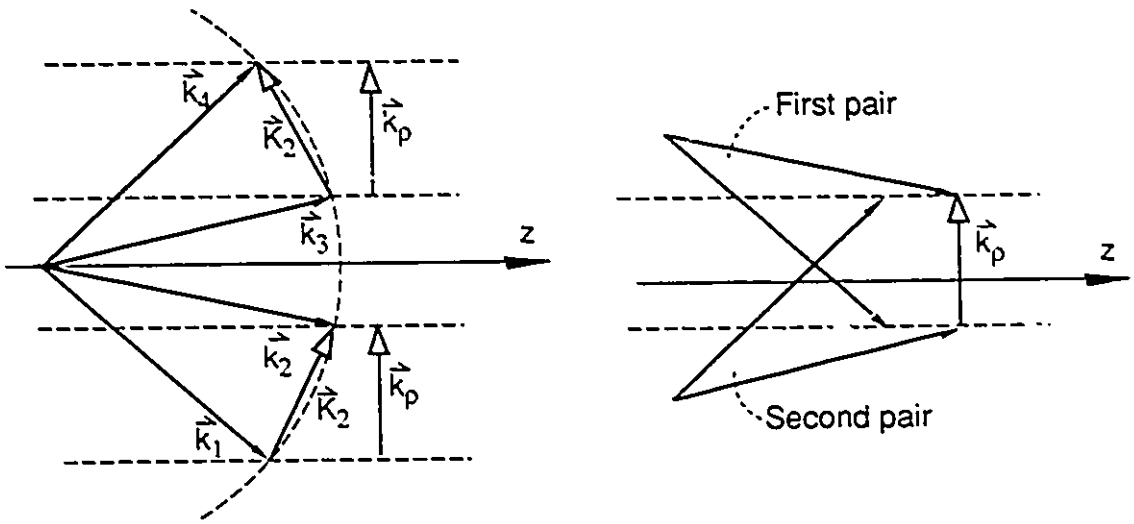

Figure 2.30: When thin gratings are used, (a) gratings of the same transverse component can be considered as the same, or in other words, (b) two pairs of light waves can share one grating, even though Bragg condition is not satisfied.

assuming any value for Q when the power distribution of the diffraction orders is a concern; while neglecting the thickness when only the directions are considered. A thin grating can be considered as a special case when volume effect is extremely weak ($Q \rightarrow 0$). It is known that the higher the Q is, the more selective the grating is, in terms of the ability to suppress the unwanted orders. The question is how much selectivity can be considered as sufficient. Apparently, $Q \geq 10$ is not necessarily a suitable criterion, because it was introduced for simplifying the mathematics of diffraction theory [39], which is obviously not the purpose of this section. In fact, even in the designs presented in the previous sections, where thick gratings are used and Bragg conditions are satisfied, the Q has to be controlled in practice in such a way that:

1. all the unwanted orders are sufficiently suppressed,
2. the volume effect is strong enough to keep the desired level of coupling, which is probably 50% in diffraction efficiency, and
3. the selectivity is not too strong, so that there can be a sufficient tolerance for ease in alignment.

Now consider the design shown in Fig. 2.22, the third and the fourth slab have four gratings. They are apparently the most complicated and the most difficult ones to build. Since slab 3 is actually a rotated version of slab 4, we may just concentrate on the last slab and see what can be done. It is evident that any technique applicable to slab 4 can be applied to slab 3. In slab 4, the four gratings evidently have the same transverse grating vector. According to the grating equation, the four gratings are the same in terms of deflecting light from one direction to another. This means that if the gratings can be made thin, all the four gratings may be merged into one grating. However, to avoid the excess loss introduced by the unwanted diffraction orders, thick gratings are used and the longitudinal components of the four gratings are not the same. This ensures that the volume effect can make the coupling level between wanted waves high and the unwanted waves low. The price of the achievement is the complexity—four gratings are

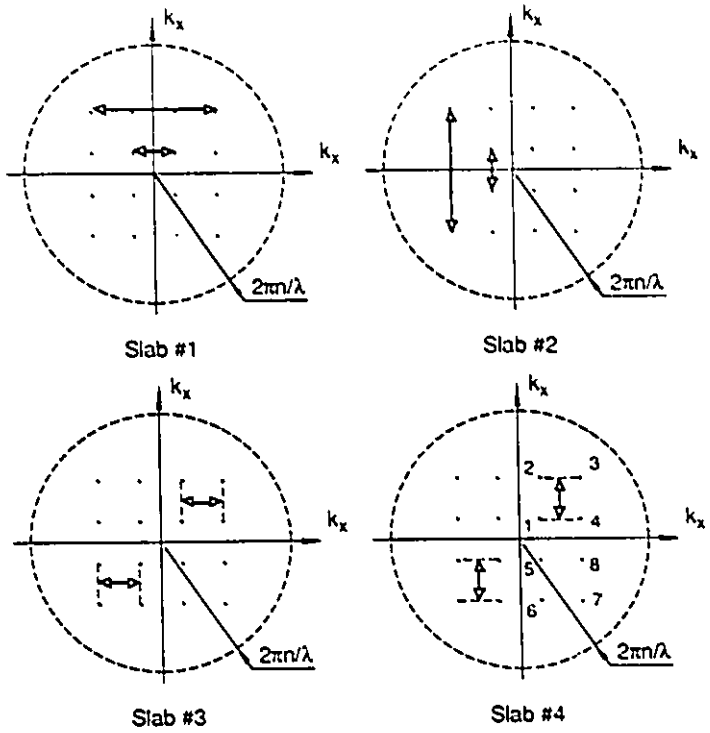

Figure 2.31: A new design for a 16×16 star couplers. Only two grating are needed in the third and fourth slab, because the Bragg condition is relaxed by using a less selective grating. The suppression of unwanted diffraction orders is ensured by properly arranging the wave vectors.

used. This complexity is obviously not desirable. The question is whether the price can be reduced while keeping what is desired. The proposed technique is shown in Fig. 2.31. Based on the observation that the grating vector $\vec{K}_{12}$ and $\vec{K}_{34}$ are not much different in the longitudinal direction, the two originally different gratings are replaced by a single grating placed about half way in between the two original gratings. A similar practice can be done to $\vec{K}_{56}$ and $\vec{K}_{78}$. We will concentrate on the former.

Obviously, with the new design, the number of gratings in slab 3 or 4 is reduced. Instead of four gratings, two gratings are used in each slab. However on the other hand, we do not replace all the four gratings by one in the new design, as we could have done, if the use of thin gratings were assumed. This gives a chance to avoid the unwanted orders by using a controlled level of selectivity. One consequence of the merge of gratings is

that the Bragg condition cannot be satisfied If the gratings have a high Q, the coupling between the wanted waves will also be reduced due to the volume effect. Therefore, a logical solution is to use a grating with a lower Q, which implies the use of "thinner" gratings. A thinner grating has a better tolerance to the violation of Bragg condition, so a sufficient coupling may still be obtained if the violation is not too severe. It is true that the maximum achievable diffraction efficiency of the gratings is lower, too, but in this particular star coupler application, the grating diffraction efficiency does not have to be very high. In most cases 50% can be considered sufficient. This is much easier to achieve compared with many other holographic element applications. Furthermore, the reduction in diffraction efficiency may also be partly compensated by other means such as increasing the modulation index.

In short, we have proposed to trade the maximum diffraction efficiency for a large tolerance, so that a grating can be shared by more light waves. This is particularly suitable to star coupler applications because a diffraction efficiency higher than 50 % is not necessary. The most important aspect of the technique is the control of the Q parameter and the arrangement of the directions of the waves for eliminating the unwanted wave. The key to the solution is that the violation of the Bragg condition by the unwanted waves must be much worse than by the wanted ones, so that they can be easily discriminated by the already weakened volume effect.

In order to evaluate the degree of the violations, a crude intuitive measurement is illustrated in Fig. 2.32, where the degree of violation is defined as:

$$\begin{aligned} \delta &= |\vec{k}_0 + \vec{K} - \vec{k}_1| \\ &= |k_{z,0} + K_z - k_{z,1}| \end{aligned} \tag{2.33}$$

The distance δ is in k-space (or spatial frequency domain) and in the direction of the normal line of the slab surface. When Bragg condition is satisfied, $\delta = 0$. In Fig. 2.33, an example is illustrated, where a single grating is used for a 2×2 coupler. It is so arranged that the wanted waves, which are the waves corresponding to $\vec{k}_0$ and $\vec{k}_1$, satisfy the Bragg condition. A relatively strong coupling may occur between the two waves. $\vec{k}_2$ and $\vec{k}_{-1}$

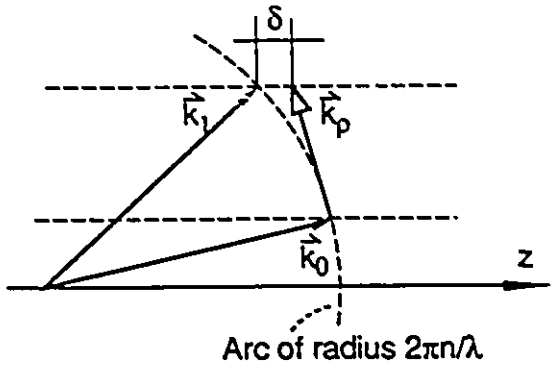

Figure 2.32: An intuitive measurement of the degree of violation from Bragg condition.

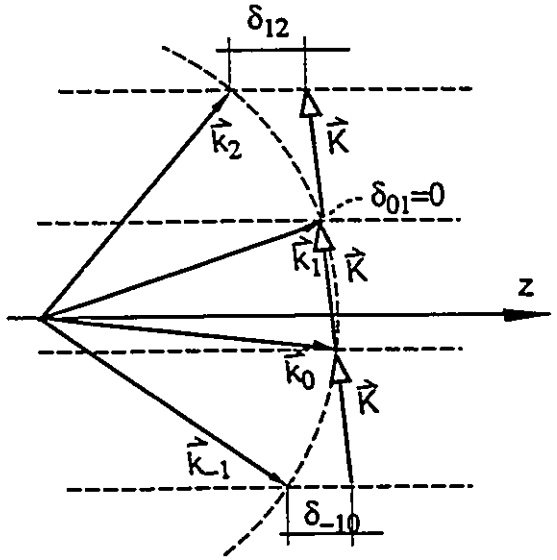

Figure 2.33: The wanted and the unwanted waves in a 2×2 coupler whose design follows Bragg condition.

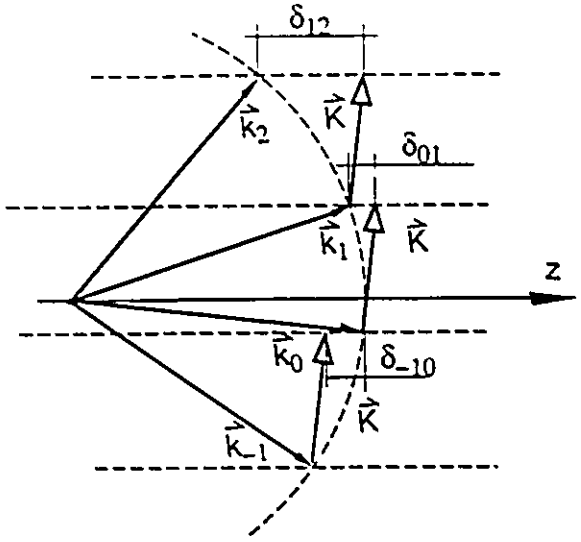

Figure 2.34: The wanted and the unwanted waves in a 2 × 2 coupler which does not exactly follow the Bragg condition. The unwanted orders can be discriminated, because they have a larger δ measure than the wanted ones.

are wave vectors for the two most probable unwanted waves. As it is shown in the figure, the distance δ_{12} and δ_{-10} are not zero. If the Q of the grating is sufficiently high , the unwanted orders can be suppressed. Fig. 2.34 shows a similar case, where quasi-Bragg diffraction is used. In the case, a more tolerant (less selective) grating must be used to maintain the coupling between the wanted waves whose wave vectors are $\vec{k}_0$ and $\vec{k}_1$, respectively. However, the selectivity must be just high enough to basically eliminate the unwanted waves with wave vector $\vec{k}_2$ and $\vec{k}_{-1}$. A necessary condition for this elimination can be expressed as:

$$\delta_{12} \gg \delta_{01} \quad and \quad \delta_{-10} \gg \delta_{01} \tag{2.34}$$

With small variation, this condition can be applied to the design shown in Fig. 2.31. We will first present a geometric approach shown in Fig. 2.35. Because of the symmetry, we will only consider the four waves in the first quadrant of the two-dimensional vector-tip diagram. For the same reason, we will only consider $\vec{k}_1$ and $\vec{k}_2$. The strongest unwanted diffractions which may be excited from the two wanted waves are shown in terms of

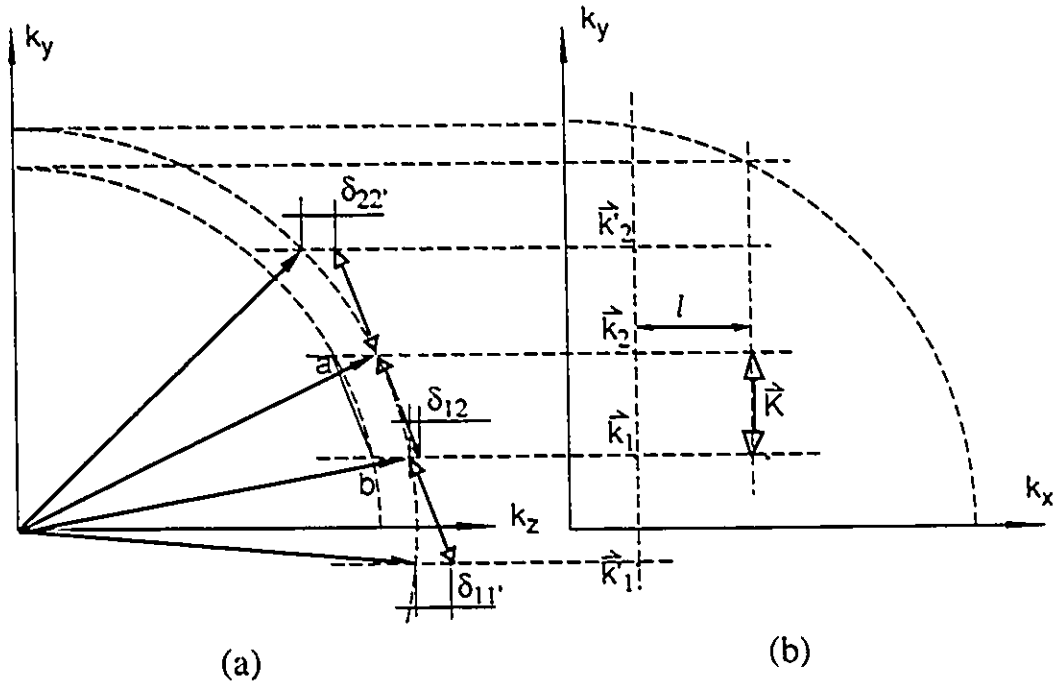

Figure 2.35: A geometric presentation of the new technique. (a) the design viewed from the direction perpendicular to the plane k_yOk_z. (b) the design viewed from the direction perpendicular to the plane k_xOk_y

$\vec{k}_1'$ and $\vec{k}_2'$. Part (b) of the figure shows the tip-pattern of the four wave vectors under consideration. Part (a) shows the same vectors viewed from a different angle. Since the violation δ is always in the longitudinal direction, they can be easily found from the geometry shown in part (a) of the figure. The grating vector can be found by linking the point a and b in part (a). The violation by the two wanted waves is represented by δ_{12}, and the violations for the two unwanted waves are represented by $\delta_{11'}$ and $\delta_{22'}$, respectively. For a practical design, the position of $\vec{k}_1$ and $\vec{k}_2$, the distance l between $\vec{k}_1 - \vec{k}_2$ and $\vec{K}$ must be placed in such a way that

$$\delta_{11'} \gg \delta_{12} \quad and \quad \delta_{22'} \gg \delta_{12} \tag{2.35}$$

It is evident that this is achievable. The violation measure can also be calculated with the following mathematical formulae:

$$\delta_{ij} = |\sqrt{(\frac{2\pi n}{\lambda})^2 - |\vec{k}_{i,\rho}|^2} - \sqrt{(\frac{2\pi n}{\lambda})^2 - |\vec{k}_{j,\rho}|^2} + K_{ij,z}| \tag{2.36}$$

where

$$\vec{k}_{i,\rho} - \vec{k}_{j,\rho} + \vec{K}_{ij,\rho} = 0 \tag{2.37}$$

and $i, j = 1, 2, \ldots$ or $1', 2', \ldots$.

In summary, it has been shown that it is possible to reduce the number of gratings from four to two per slab for the third and fourth slab of a 16 × 16 coupler. The new design is shown in Fig. 2.31. In the design, the Bragg condition is not exactly satisfied, so the selectivity of the Bragg grating has to be moderate to keep a sufficient coupling. At the same time, the violation of the Bragg condition by the waves to be coupled must be far less than that by the unwanted diffraction orders. Also, the selectivity of the Bragg grating should be just high enough to distinguish the difference between the wanted and the unwanted, so that the unwanted can be sufficiently suppressed. Here, the technique of reducing the number of gratings is called quasi-Bragg diffraction. Even though we do not generalize the technique to couplers other than 16 × 16, it can certainly be applied to designs with N larger than 16. In addition, only the original idea and a general guide for

using this technique is presented in this chapter. More sophisticated tools have to be used to do a practical, yet detailed analysis or design. These tools will be given in Chapter 3.

2.6 Application of Grating Degeneration to Self-Routing Couplers

Though the focus of this thesis has been placed on star couplers, the techniques introduced so far, such as grating degeneration, can be applied to other devices made from holographic gratings. One example is the so called wavelength division multiplexed self-routing coupler proposed in [41, 42]. The coupler is based on a grating-bearing dielectric slab which fulfils the function of wavelength routing according to a perfect shuffle topology. It is believed that besides the star-type photonic network, the use of shufflenet is another efficient way to break the electronic bottleneck [9].

Compared with the use of star coupler, the major advantage of using a routing coupler in a shufflenet is the elimination of the power division problem. Instead of being split into N parts, each input signal in a shufflenet can only take one of two (or a few) possible routes according to the wavelength of the input. This means that the coupler is free from splitting loss and its insertion loss is pure excess loss. In fact, the absence of the splitting loss may also make the shuffle network tolerant to higher excess loss, because firstly, the power budget is not so stringent due to not splitting the power and secondly, the signal can be regenerated in between the hops. Nevertheless, one disadvantage of the shuffle network is the higher traffic flow through the nodes, which is the price paid for the more simplified coupler structure.

The working mechanism of the routing coupler is shown in Fig. 2.36. Two Bragg gratings are recorded in a dielectric slab for an input beam. Because of the volume effect, an input light beam at one of the two predetermined wavelengths is diffracted by only one of the two gratings, and thus is routed to one of the predetermined output directions. When N input ports are required for a routing coupler, and when m routes leading to a

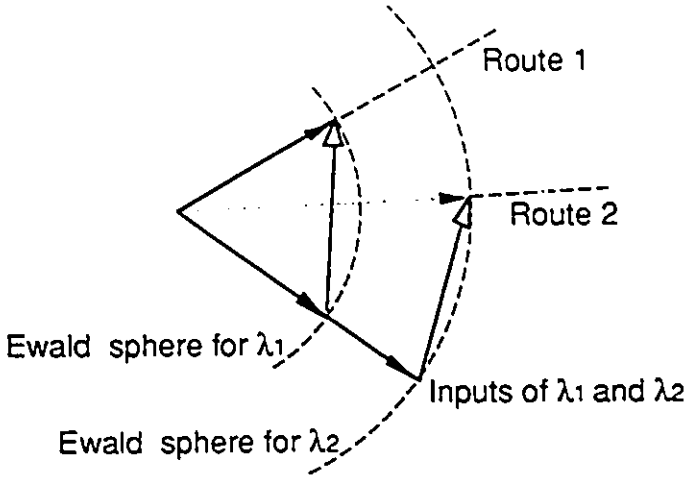

Figure 2.36: Wavelength routing with Bragg gratings.

certain collections of N output ports are provided to each input, generally mN gratings, with $1 < m \leq N$, have to be constructed in the slab. All the gratings can be superimposed in one single slab. This can be expressed, as it is shown in [42], in terms of the refractive index of the slab:

$$n(\vec{r}) = n_0\{1 + \sum_{i=1}^{N}\sum_{j=1}^{N} \Delta_{ij} \cos(\vec{K}_{ij} \cdot \vec{r})\} \tag{2.38}$$

where it is assumed that at most N^2 gratings ($m = N$) may be used to facilitate the interconnections between any input and output port. Notice that, a minor modification has been made in Eq. (2.38), compared with Eq. (13) in [42]. A routing matrix can be formed based on the modulation indices Δ_{ij}:

$$\Delta = \begin{pmatrix} & \vdots & \\ \cdots & \Delta_{ij} & \cdots \\ & \vdots & \end{pmatrix} \tag{2.39}$$

when perfect shuffle connectivity is used, only a few of the N^2 gratings are needed. This is termed as selective-broadcast mode in [41, 42]. For example, when the number of input

or output ports is $N = 8$, [42] gives a routing matrix shown as:

$$\Delta = \begin{pmatrix} 0 & 0 & 0 & 0 & \Delta & \Delta & 0 & 0 \\ 0 & 0 & 0 & 0 & 0 & 0 & \Delta & \Delta \\ 0 & 0 & 0 & 0 & \Delta & \Delta & 0 & 0 \\ 0 & 0 & 0 & 0 & 0 & 0 & \Delta & \Delta \\ \Delta & \Delta & 0 & 0 & 0 & 0 & 0 & 0 \\ 0 & 0 & \Delta & \Delta & 0 & 0 & 0 & 0 \\ \Delta & \Delta & 0 & 0 & 0 & 0 & 0 & 0 \\ 0 & 0 & \Delta & \Delta & 0 & 0 & 0 & 0 \end{pmatrix} \tag{2.40}$$

where sixteen gratings are used.

It is actually more natural to use gratings for routing than for power division. Gratings are inherently wavelength sensitive. When used in star couplers, they can only work essentially at one wavelength due to the dispersion associated with any kind of grating. In addition, in the case of holographic gratings, the volume effect adds more constraints to wavelength variations. The collective effect of dispersion and the volume effect on the bandwidth of a coupler can generally be expressed as:

$$H(\lambda) = H_d(\lambda) H_B(\lambda) \tag{2.41}$$

where $H(\lambda)$ is the transfer function between a pair of input and output ports of the coupler, $H_d(\lambda)$ is the transfer function when only the dispersion is considered, and $H_B(\lambda)$ is the transfer function showing only the effect of Bragg condition. Generally speaking, both dispersion and volume effect contribute to the narrow bandwidth (still hundreds of GHz) of a star coupler. Nevertheless, when gratings are used in wavelength routing couplers, this narrow bandwidth or wavelength selectivity is just what is desired.

A similar device is the well-known WDM multiplexer/demultiplexer [43] using a blazed grating [44]. Blazing a grating has quite the same effect as the use of a thick holographic grating. Both practices add a third dimension to the grating structure and make the grating selective (to wavelength and angle). The selectivity again is used to

suppress unwanted diffraction orders and to enhance the wanted diffractions. However, holographic volume gratings have one edge over blazed gratings, i.e., a number of gratings can be integrated on a single slab. The same advantage is shown when a star coupler is made from holographic gratings. Though a grating is not much different in function from an ordinary beam splitter when used in a star coupler, many such splitters can be superimposed in one planar slab in order to form a compact device. The similarity can also be found with holographic optical elements (HOEs). HOEs are usually thin and flat in comparison to conventional elements, and they suffer the same bandwidth problem due to their nature as a diffraction device.

Though it is assumed in [41, 42] that the same grating system as the one used for a star coupler can be used for routing if the system is constructed in a selective-broadcasting mode, it should be noticed that there exists one significant difference between the two types of grating systems. In the star coupler presented in [30, 31], all the zero-th order diffractions (or the direct-pass-through beams) are utilized while in a self-routing coupler [41], the opposite is the case. It is known that the zeroth orders of a grating are wavelength insensitive when dispersion is considered. They become wavelength sensitive only when the volume effect is considered. However, the zeroth order has a totally different type of wavelength dependence, compared with the non-zero-th orders. Instead of a narrow passband, they have a narrow stopband, as it is shown in Fig. 2.37. This is obviously not suitable for wavelength routing purpose. The difference in the use of zero-th orders leads to significant differences in coupler construction. For example, consider the simplest case, when an 2×2 star coupler is compared with a 2×2 routing coupler in Fig. 2.38. In both of the grating systems, there are two input waves and two output waves. However, in the star configuration, the two input waves are aligned with the two output waves so that the zero-th orders can be used. In this case, only two different directions or two waves have to be considered. In contrast, in a routing coupler, all four waves must be arranged in distinctively different directions, so as to avoid the use of wavelength-insensitive directly-pass-through beams, and the coupling among the four waves has to be

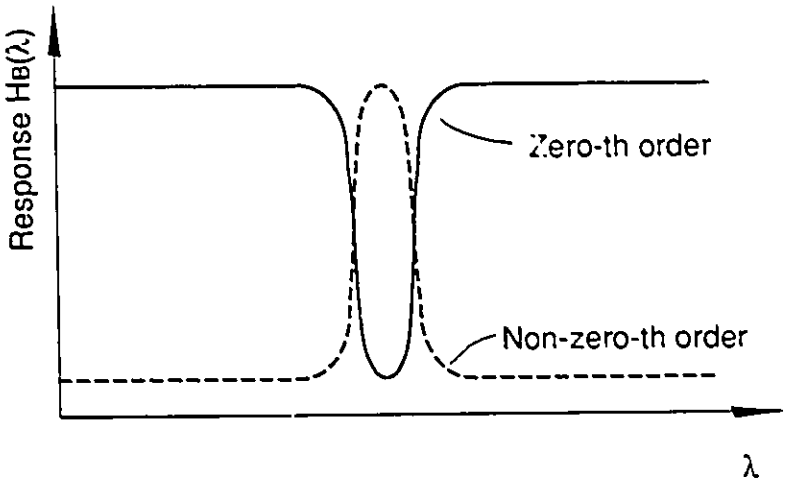

Figure 2.37: Typical frequency response of a zero-th order diffraction in comparison with a non-zero-th order, when volume effect is considered.

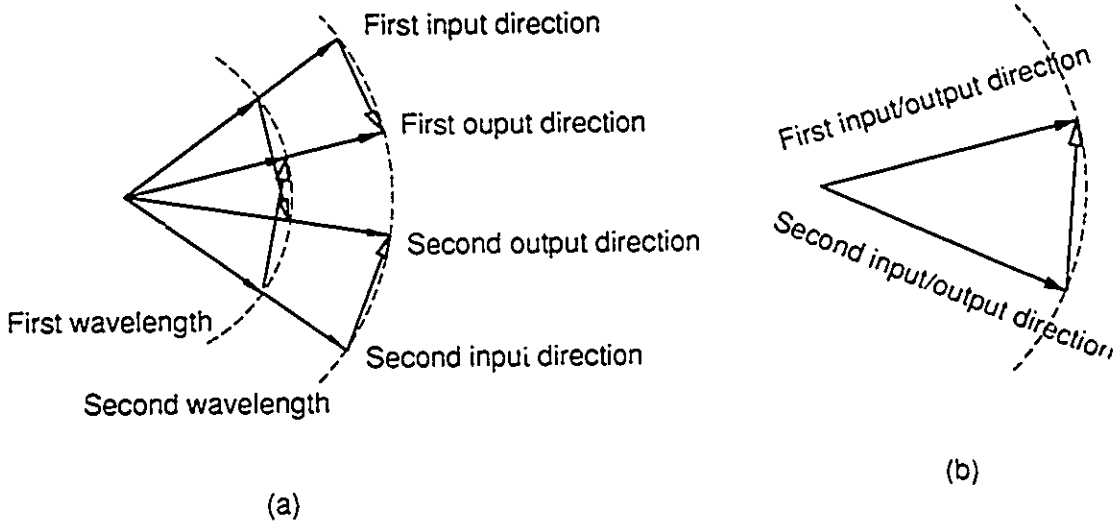

Figure 2.38: Comparison between a star coupler and a routing coupler. Grating systems of (a) a 2 × 2 star coupler, and (b) a 2 × 2 routing coupler.

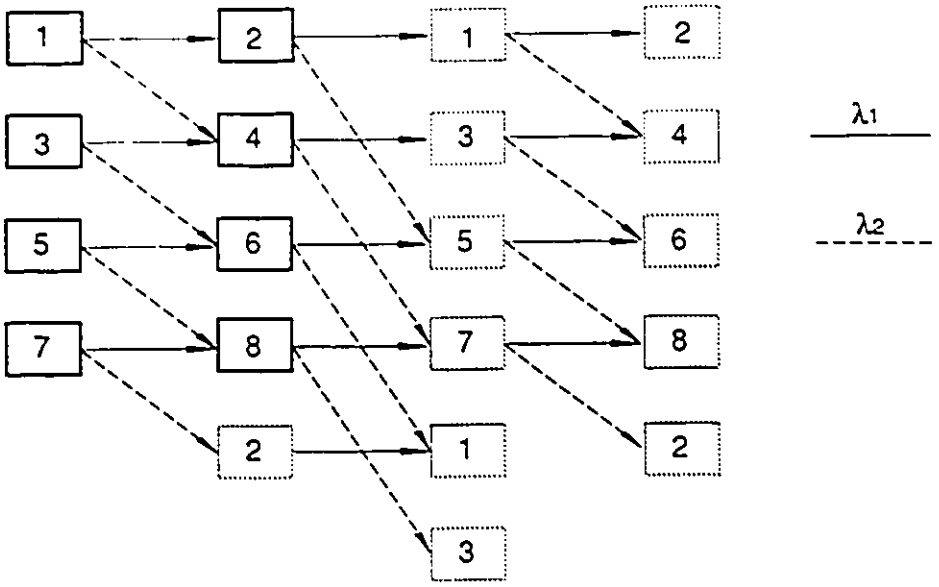

Figure 2.39: Connectivity of an 8×8 shufflenet.

managed. Additionally, multiple wavelengths have to be incorporated in the design of a routing coupler. For example, in Fig. 2.38(a), two wavelengths are used. This is indicated by the two Ewald spheres of different radii. Another difference in the designs of the two systems is the different requirements for the diffraction efficiency. In a wavelength routing design, 100% efficiency is always desired because any leftover in zero-th orders means excess loss. However, a considerable deviation from the desired value can be tolerated, because a shufflenet structure can tolerate higher excess loss due to the absence of the power division. Nevertheless, this is not true with star couplers. The diffraction efficiency has to be accurately controlled for uniformly splitting the light, though the efficiency is not desired to be 100 % due to the use of directly-pass-through orders.

Despite the differences, the concepts introduced for $N \times N$ star couplers in the previous sections can still be applied to the design of a routing coupler. In this section, an 8×8 routing coupler will be used as an example. Using perfect shuffle, the connectivity of an 8×8 routing coupler is shown in Fig. 2.39. It is assumed that each user can switch its transmitter between two wavelengths: λ_1 and λ_2. It is evident that no more than

three hops are required for a packet to be delivered from one node to any of the others. The 16 gratings required to realize the connectivity are depicted in Fig. 2.40, where the 16 directions are represented by 16 radially oriented straight lines, the gratings required are specified by their transverse component vectors. It is assumed in Fig. 2.40 that the 16 waves (or directions, 8 inputs and 8 outputs) are uniformly distributed, though not necessarily so. It is also assumed that the 16 wave vectors and the grating vectors are arranged in a three-dimensional manner, just as for grating degeneration in the previous sections. It can be seen that to each input direction, labeled as $n = 1, 2, \ldots, 8$, two gratings are attached which couple the input waves into two other directions at different wavelengths. For example, input direction 1 is coupled to output $2'$ at wavelength λ_1 and to output $4'$ at wavelength λ_2. On the other hand, every output direction, labeled as n', is also attached to two gratings at different wavelengths. For example, output $1'$ can receive light from 2 at λ_1, and from 6 at λ_2. Right away from Fig. 2.40, we can tell that the gratings can be merged. For example, $\vec{K}_{12'}$, $\vec{K}_{83'}$, $\vec{K}_{47'}$ and $\vec{K}_{56'}$ are actually the same grating, and $\vec{K}_{21'}$ can be merged with $\vec{K}_{65'}$, etc. Therefore, instead of sixteen gratings as suggested in [41], only six are required. This apparently reduces significantly the difficulty in the fabrication of the grating slabs. Furthermore, if we use the technique of sandwich structure, these gratings can be constructed in different slabs. The author believes that, even though this will not further reduce the number of gratings as in the case of star coupler, it can still be easier sometimes to make more slabs bearing fewer gratings than more gratings on fewer slabs.

The wavelengths in the design must be carefully chosen. The relation between λ_1 and λ_2, according to the geometry shown in Fig. 2.40, can be written as:

$$\frac{\lambda_1}{\lambda_2} = \frac{\sin\frac{\pi}{16}}{\sin\frac{5\pi}{16}} = 0.566 \tag{2.42}$$

So if λ_1 is chosen to be 0.85 μm, λ_2 should be 1.5 μm. When Eq. (2.42) is not satisfied, the number of achievable degenerations will decrease, and two more gratings would be required.

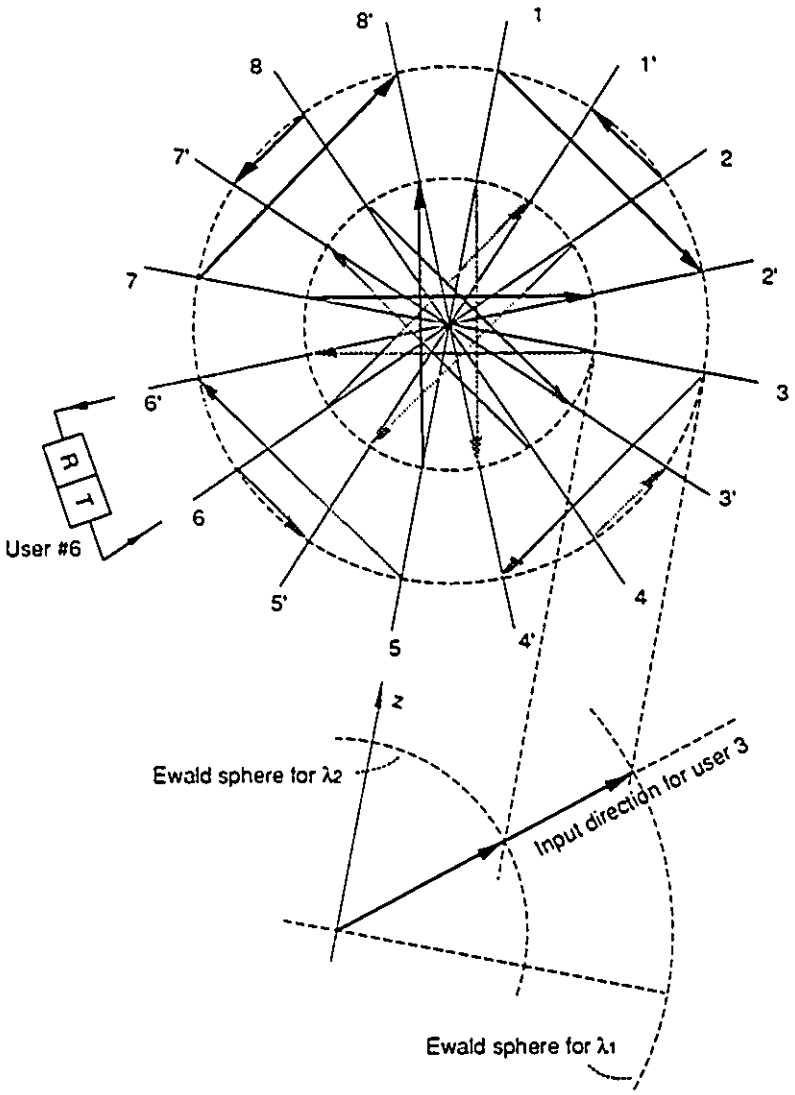

Figure 2.40: A design of an 8×8 routing coupler using two wavelengths.

In this section, by using a specific example, namely, an 8×8 shufflenet routing coupler, we have shown that the concept of grating degeneration, introduced originally for star couplers, can also be applied to shufflenet construction. The benefit is the simplification of the required grating system. However, since we have only presented a specific design example, it is important to be aware of the fundamental principles for the design of a more general routing coupler. The law to be obeyed is again, as in the case of star coupler, the Bragg condition, and the following generalizations from the given 8×8 design can be made according to the specific application:

1. A shuffle topology of a larger number N, than the one shown in Fig. 2.39, may be incorporated in self-routing coupler. Generally, two parameters are required to specify a shufflenet. One is the degree of the graph p, the other is the number of columns, I. The number N can be found as $N = Ip^p$.

2. The number of wavelengths may be more than two according to the particular topology. However, the number should not be less than p.

3. The constellations (a pattern of the wave vector tips in k-space) may not necessarily be arranged in circles, as it is shown in Fig. 2.40, nor should they necessarily be distributed uniformly. However, when a pattern of higher degree of symmetry is used, there is generally a better chance to obtain more degeneracy. Also, it should be noticed that some constellations are not independent. For example, those from the same fiber but with different wavelengths have definite relative positions.

2.7 Summary

In this chapter, we have shown that with two novel techniques, i.e., grating degeneration and sandwich structures, the grating system used in a $N \times N$ star couplers can be significantly simplified. The concept of grating degeneration is based on the fact that every single volume grating can be used as a number of parallel 2×2 couplers if the propaga-

tion directions are properly arranged; while the sandwich structure employs a multi-stage topology which requires a smaller number of 2×2 building blocks. It turns out that two slabs, each bearing one single grating, are required for a 4×4 coupler; a 16×16 coupler needs four slabs, each bearing no more than four gratings. This is in comparison with six gratings for 4×4 and 120 gratings for 16×16 in a single slab with the original design presented in [30]. It has also been found that if slightly-off-Bragg diffraction is allowed, the number of required gratings can be further reduced. The key is to make the amount of violation of the Bragg condition much smaller for the desired diffraction orders than for the undesired orders. It has been shown that for a 16×16 star coupler, the number of gratings can be reduced to two per slab. We refer to this technique as quasi-Bragg diffraction. Though the focus is placed on the design of broadcasting star couplers, all the three techniques have the potential to be applied to other holographic-grating-based devices. An example of applying grating degeneration to the design of an 8×8 wavelength self-routing coupler has been presented. Out of the 16 gratings originally required, 10 are degenerate and thus only six gratings need be constructed. Besides, it has been pointed out that there is a substantial difference between the grating system of a star coupler and that of a routing coupler in the use of the zeroth order diffractions. In a star coupler, the waves are arranged in N distinct directions, while in a routing coupler, $2N$ directions should be considered because the input and output waves must be deliberately misaligned to avoid using zeroth orders. It should be pointed out that all the designs and discussions given so far are conceptual, because we have been only considering the Bragg condition, which is not sufficient to describe the diffraction process in the slab. To fully characterize a coupler, we have to refer to the Maxwell's equations which govern the behaviour of electromagnetic field in all frequency ranges. This is what will be done in the next chapter.

Chapter 3

Numerical Analysis of Holographic Fiber Star Couplers

3.1 Introduction

In Chapter 2, three novel techniques for holographic $N \times N$ star couplers have been introduced. It has been shown that the concepts can also be applied to holographic wavelength-sensitive routing couplers. However, all the three techniques have been developed on the basis of two fundamental equations. One is the grating equation, which determines the directions of the diffracted lightwaves; the other is the Bragg condition, which guarantees maximum coupling between waves of different directions. These two equations are obviously not adequate for a full description of the lightwave diffraction process, inside the grating slabs of a coupler. First of all, no information about the intensities of the diffraction orders can be obtained, though such information is vital to coupler design because: 1) a coupler has to split the power of an incoming wave precisely into a number of fractions according to the predetermined coupler connectivity, 2) all the undesired diffraction orders which satisfy the grating equation have to be low in intensity for the coupler to have a low excess loss. Secondly, the polarization of a lightwave is another unneglectable quantity whenever any lightwave device is considered. The above

mentioned two equations do not provide any information about the effect of the couplers on this aspect of a lightwave. Furthermore, it is not adequate to specify a grating by only giving its grating vector, as has been done throughout Chapter 2. The modulation index and the initial phase are equally important to the performance of the grating. It is clear that for the purpose of implementing a coupler, a much more advanced tool is needed to depict the propagation of light waves in great detail. The objective of this chapter is therefore to provide such a tool, namely, a rigorous theory of holographic grating diffraction, strictly based on the fundamental Maxwell's equations.

Holographic gratings are also frequently referred to as planar gratings, because the interference pattern of the two beams in construction forms a series of planar fringe planes in the recording medium. Planar grating diffraction is an old topic. It is claimed in [45] in 1982 that there had been more than 400 relevant papers on this topic since 1930. In recent years, a considerable number of papers are being published in this field. The most significant work, in the author's opinion, is the coupled wave theory put forward by Kogelnik [39] in 1969. The theory is still widely used for estimating the performance of holograms and gratings. The major assumptions of the theory are 1) neglecting all the diffraction orders but two—the zero-th and the first orders, 2) neglecting the second derivatives, assuming that the coupling is low and that the coupling length is long, 3) assuming that the Bragg condition is approximately satisfied. It turns out that these assumptions are true in most practical cases, and more importantly, the theory explains almost all the important characteristics observed with a thick Bragg grating. After Kogelnik's work, people had been trying to generalize the theory by making fewer or different assumptions. One example is the so-called "two-wave second-order coupled-wave theory [45]", which keeps the second derivatives. Another example is the first-order "multiwave coupled-wave theory", which includes high order diffractions [46]. When the dephasing, or the off-Bragg-condition cases are neglected, the theory degenerates into Raman-Nath theory [45]. For the incident-wave-dominated case, there are various scattering theories, but due to the assumed low diffraction efficiency, the theories do not have a high practical

value. Later, rigorous diffraction theories appeared. They are basically in two different forms. One is called coupled-wave theory; the other is termed modal theory. The major difference between the two forms is in the field representation. The former represents the field in terms of "order", which is defined according to the transverse frequency components of the field, while the latter uses modes – the elementary solutions to the Maxwell's equations– to represent the field. The two forms are actually equivalent, because they are both rigorous solutions to the scalar Helmholtz equation (only the TE waves were considered). However, the scalar Helmholtz equation by itself is not rigorous for describing light. Rigorous theories did not appear until the introduction of the three-dimensional (or vector field) theories [47] [50]. The main features are the use of the vector field representation and an arbitrary incident direction. In [48], a single grating of anisotropic material is analyzed. In [49], the theory was extended to cover cascaded gratings, and in [50], superimposed gratings.

The theory presented in this chapter can be categorized as rigorous vector-field diffraction theory. The differences between this theory and the existing theories are as follows:

1. The theory is tailored for the application of couplers made from holographic gratings, the emphasis is put on the superimposed grating systems. Though such grating systems have been covered in [50], the details of the treatment is not fully discussed. In this chapter, the harmonics of a component grating are considered as different superimposed gratings. This, the author believes, simplifies the theory compared with Equation 80 of [50], where only two gratings are considered together with their harmonics.

2. The theory is configured in such a way that the incident waves impinge on the slab from a set of directions. This again suits the need of analyzing $N \times N$ star couplers. It is known that in a $N \times N$ coupler, there is an input direction corresponding to each of the output directions.

3. Instead of coupled-wave differential equations, the theory employs a set of algebraic mode equations which are actually more straightforward. Besides, the mode equations are the equations of the E-field only, which is another distinct feature of the theory. The number of equations for each order is four instead of six. This makes the computer algorithm straightforward.

4. The theory includes the phases of the gratings as parameters, which is important for the generality of the theory when the number of gratings is larger than 3.

5. The theory employs Jones matrices to characterize the response of a grating system to the polarization of an input signal. This turns out to be efficient.

6. The theory uses a set of natural coordinate reference systems, which simplifies the mode equations and is believed to be convenient for practical purposes.

In the next section, some fundamental issues will be discussed as the starting point of the theory. Then mode-equations will be derived from the Maxwell's equations. The boundary equations are also derived to obtain a unique set of Jones matrices. In Section 3.3, grating equations are discussed. In Section 3.4, a simplified treatment for cascade slabs are given based on the Jones matrix representation. Examples of computer simulations are presented in Section 3.5, and Section 3.6 concludes the chapter.

3.2 Modelling a Multi-Planar-Grating System

As mentioned in the preceding chapter, a grating-bearing dielectric slab or a slab sandwich is the core of a holographic coupler. In this section, a model for numerically analyzing the performance of a single slab grating system composed of a number of superimposed planar gratings is presented. A computer algorithm is derived to simulate light wave diffraction by the grating-bearing slab shown in Fig. 3.1. In the figure, all the gratings are written in region G, which is a dielectric slab with a space-varying refractive index. The slab is assumed to have an infinite size but a finite thickness d. It is buried in two homogeneous

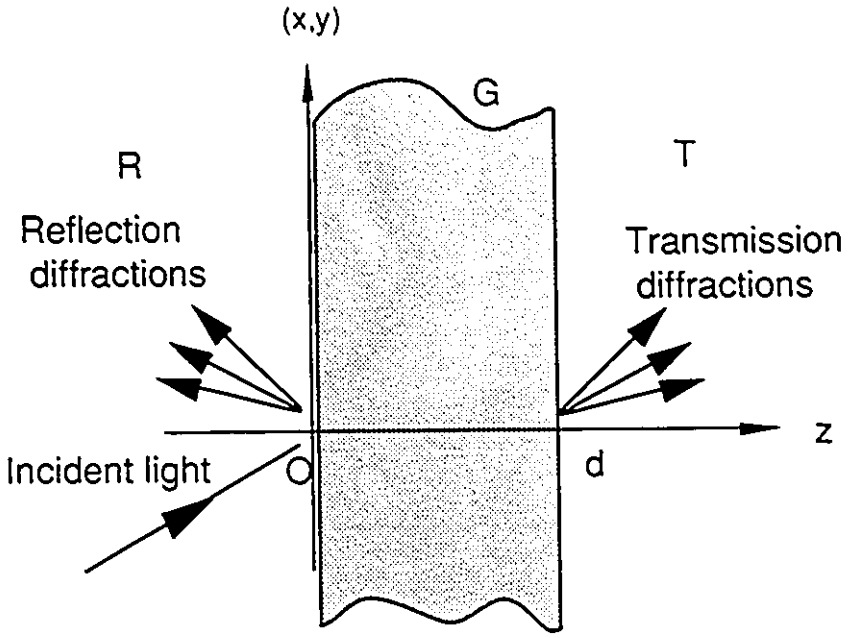

Figure 3.1: A single dielectric slab and an incident wave.

media R (indicating reflection region) and T (indicating transmission region), which have refractive indices of n_R and n_T, respectively. A light beam, assumed to be a plane wave, of an arbitrary polarization and from an arbitrary direction, is incident on the left surface of the slab. A Cartesian coordinate system is employed with the z-axis placed in the direction of the normal line of the surfaces and the origin fixed on the surface of incidence (the left surface). The model to be presented in the following sections can be used as a tool to simulate how the incident light is diffracted, i.e., how the light beam is split into orders of reflected and transmitted beams, how the power is distributed and what polarization each diffracted order has, etc.

3.2.1 Foundation of the theory

The light field is an electromagnetic field of a certain frequency range, the behaviour of light, to be more specific here, the diffraction of an incident light by the grating-bearing slab, is completely governed by Maxwell's equations:

$$\begin{cases} \nabla \cdot \epsilon(\vec{r})\epsilon_0 \vec{E} &= 0 \\ \nabla \cdot \mu\mu_0 \vec{H} &= 0 \\ \nabla \times \vec{E} &= -\mu_0\mu \frac{\partial \vec{H}}{\partial t} \\ \nabla \times \vec{H} &= \epsilon_0\epsilon \frac{\partial \vec{E}}{\partial t} \end{cases} \tag{3.1}$$

where ϵ_0 and μ_0 are the permittivity and the permeability in vacuum, μ and ϵ are the relative permeability and the dielectric constant, and $\vec{E}$, $\vec{H}$ are the electric field (E-field) and the magnetic field (H-field), respectively. At a surface of discontinuity between two continuous media, e.g., medium 1 and 2, the equations can be written in the form of boundary conditions:

$$\begin{cases} \hat{n} \cdot (\varepsilon_2 \vec{E}_2 - \varepsilon_1 \vec{E}_1) &= 0 \\ \hat{n} \times (\vec{E}_2 - \vec{E}_1) &= 0 \\ \hat{n} \cdot (\mu_2 \vec{H}_2 - \mu_1 \vec{H}_1) &= 0 \\ \hat{n} \times (\vec{H}_2 - \vec{H}_1) &= 0 \end{cases} \tag{3.2}$$

where $\hat{n}$ is the normal vector of the surface, which has unity length. Notice that, throughout this chapter the hat " $\hat{}$ " is used to indicate a vector with length.

Consider a single frequency (or single wavelength) light field with an E-field $\vec{E}(\vec{r};t) = \vec{E}(\vec{r})\exp(-j\omega t)$, where $\vec{E}(\vec{r})$ is the space-varying complex envelope, and $\exp(-j\omega t)$ is the time-varying factor of the field. Maxwell's equations (3.1) and the boundary conditions degenerate to

$$\begin{cases} \nabla \times \vec{E} &= j\omega\mu\mu_0\vec{H} \\ \nabla \times \vec{H} &= -j\omega\varepsilon\varepsilon_0\vec{E} \end{cases} \tag{3.3}$$

and

$$\begin{cases} \hat{n} \times (\vec{E}_2 - \vec{E}_2) &= 0 \\ \hat{n} \times (\vec{H}_2 - \vec{H}_2) &= 0 \end{cases} \tag{3.4}$$

Canceling $\vec{H}$ leads to an equation about the E-field $\vec{E}(\vec{r})$, which can be considered as a generalized wave equation:

$$\nabla^2\vec{E}(\vec{r}) - \nabla[\nabla \cdot \vec{E}(\vec{r})] + k^2\mu\varepsilon(\vec{r})\vec{E}(\vec{r}) = 0 \tag{3.5}$$

where $k = 2\pi/\lambda = \omega/c$, with λ being the wave length in vacuum, and c being the speed of light. It is assumed that the permeability is a constant. This is true for most dielectric materials. Once E-field is determined, H-field can be determined with the relation:

$$\vec{H}(\vec{r}) = \frac{-j}{\omega\mu_0\mu}\nabla \times \vec{E}(\vec{r}), \tag{3.6}$$

since the H-field can be uniquely determined by the E-field to an additive constant. It is reasonable that only the E-field is considered in the model. Similarly, from Eq. (3.4), at the surfaces of discontinuity, the E-field has to follow:

$$\begin{cases} \hat{n} \times (\vec{E}_2(\vec{r}) - \vec{E}_1(\vec{r})) &= 0 \\ \hat{n} \times [\frac{1}{\mu_2}\nabla \times \vec{E}_2(\vec{r}) - \frac{1}{\mu_1}\nabla \times \vec{E}_1(\vec{r})] &= 0 \end{cases} \tag{3.7}$$

Eq. (3.5) and Eq. (3.7) form the foundation of the the algorithm. They uniquely determine the light field inside and outside the slab, thus all the features of the diffraction orders such as the directions of propagation, power densities and states of polarization.

3.2.2 Gratings in the slab

In the grating slab, it is assumed that M planar volume gratings are written. They are of arbitrary orientation, period, modulation and initial phases. It is assumed that the product of relative permittivity and permeability of the slab medium G can be written as

$$\mu\varepsilon(\vec{r}) = n_0^2[1 + \sum_{i=1}^{M} 2\Delta_i \cos(\vec{K}_i \cdot \vec{r} + \phi_i)] \qquad 0 \le z \le d \tag{3.8}$$

where $\vec{r}$ is the position vector (x, y, z), d is the thickness of the slab, ϕ_i, Δ_i and $\vec{K}_i$ are the initial phase, the relative modulation index and the grating vector of the i-th grating. The grating vector is defined as $\frac{2\pi}{\Lambda_i}\hat{n}$ with Λ_i being the spacing between any two fringe planes and with $\hat{n}$ being the normal vector of the fringe planes. Notice that, by planar gratings, we do not refer to planar slabs but to gratings with planar fringe planes. In Eq. (3.8), the crest fringe planes of the i-th grating may be defined as:

$$\vec{K}_i \cdot \vec{r} + \phi_i = 2\pi l \qquad l = 0, \pm 1, \pm 2, \cdots \tag{3.9}$$

Obviously, these are a set of planes in the slab, which indicate the crests of the dielectric constant. Though planar gratings are 3-dimensional gratings, there are gratings which are not planar but 3-dimensional. For example, the gratings shown in Fig. 3.2 cannot be analyzed with the model given in this chapter. It is a grating made by etching multi-level grooves on a substrate (called surface relief grating).

When the relative modulation index Δ_i's are sufficiently low, the refractive index of the slab can be written as:

$$n(\vec{r}) = \sqrt{\mu\varepsilon(\vec{r})} \approx n_0[1 + \sum_{i=1}^{M} \Delta_i \cos(\vec{K}_i \cdot \vec{r} + \phi_i)] \tag{3.10}$$

which shows that n_0 can be interpreted as the average refractive index or the DC component of the index. The AC components of different spatial frequencies (represented by grating vectors) are the element gratings with a relative strength or amplitude Δ_i with respect to the DC component.

Many diffraction theories of planar gratings neglect the initial phase of a grating by setting it to zero. In the case of a single grating, this conduct does not cause any loss

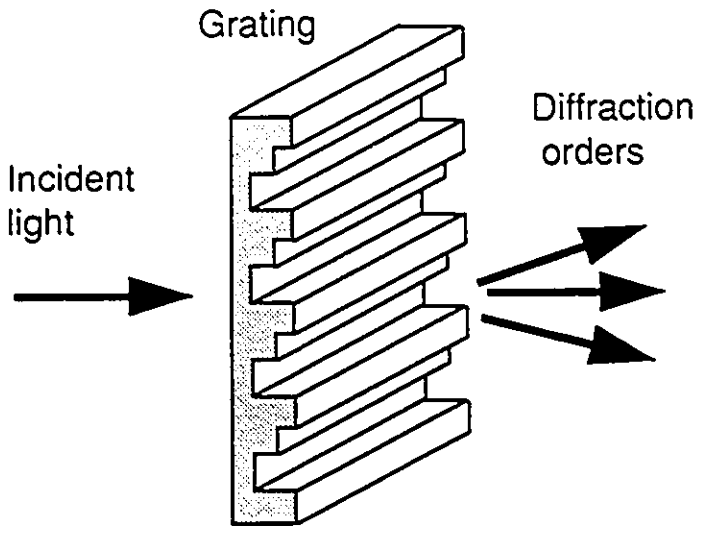

Figure 3.2: An example of non-planar 3-dimensional grating.

of generality, provided that the grating is not a "pure reflection" type [51, 52]. A pure reflection grating is defined as a grating whose fringe planes are parallel to the surfaces of the slab. Evidently, if the grating is not of pure reflection type, we may shift the origin of the Cartesian coordinate system along the left surface of the slab by a fraction of the grating period Λ_p, so that a fringe, defined as a line of equal phase on the slab surface, coincides with the origin of the coordinate system. This is shown in Fig. 3.3. Since the grating slab is assumed to have an infinite size, which means it has no periphery, the shifting of the origin should not make any difference to the final results. Therefore, setting the initial phase to zero does not cause any lose of generality. In the case of pure reflection grating, there is obviously no way to set the initial phase to zero by shifting the origin in the transverse direction, because no fringes can be seen on the surface. Shifting the origin in the longitudinal direction will at the same time move the position of the boundaries due to the slab's finite thickness. Actually, it is the relative position of the fringes to the slab surfaces that matters. Hence, to change this relative position, an initial phase has to be used to characterize a pure reflection grating. In practice, especially when a holographic technique is applied, it is not likely that there is any absolutely pure reflection grating,

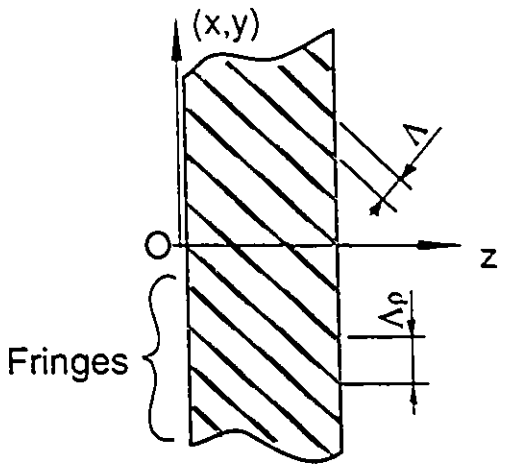

Figure 3.3: The origin is placed on a fringe to set the initial phase zero.

and the size of a real grating slab cannot be infinitely large. However, we may count the number of fringes across the slab surface. If the number is large, we may consider the grating a non-pure-reflection grating and set the initial phase to zero. When the number is very small, we may consider the grating a pure reflection type and keep the initial phase as a variable. An extreme example of pure reflection gratings is the multilayer dielectric filter, e.g., an anti-reflection coating. It can be considered as a grating in a general sense. It has layers of materials of different index parallel to the substrate. No fringes can be counted across the slab surface, and the initial phase, to be more exactly, the thickness of the first layer of material plays a very important role in the performance of the coating.

When a two-grating system is considered, the same reasoning can be applied except that the relative positions of the two sets of grating fringes need to be considered. If there is an angle between the two fringe sets, we can always find one of the intersections of the fringes. The intersection can be chosen to be the origin of the Cartesian coordinate system. In this way, we can set the initial phases of both gratings to zero. This is illustrated in Fig. 3.4.

However, if the two sets of grating fringes are parallel to each other, there may not be an intersection to be used as the origin. So in the case of a two-grating system, at

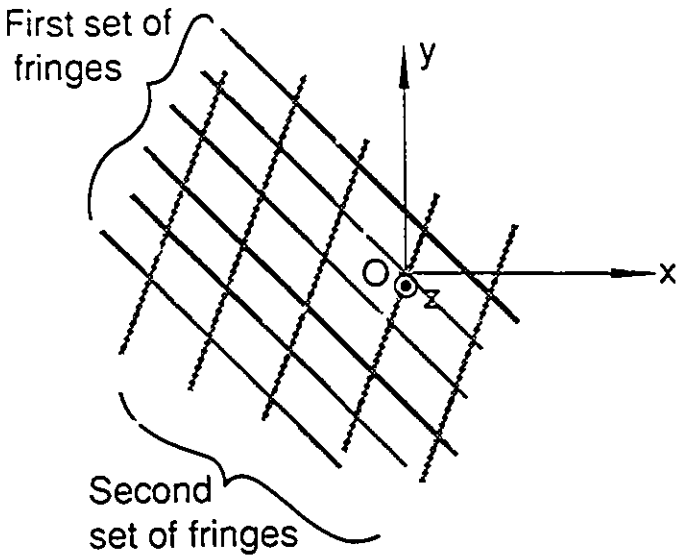

Figure 3.4: The origin is placed on an intersection of the two sets of fringes to set both the initial phases to zero.

least, one of the initial phases is needed to maintain the generality. When the number of gratings is three or larger, even if the gratings are not reflection type, the initial phases of the gratings must be considered as a general case. When we draw three lines on a paper randomly, there is little chance that they intersect at the same point (see Fig. 3.5). Therefore, when three or more than three sets of fringes are written in the slab, it is a rare case when all initial phases can be set to zero. Therefore, we may conclude that for the purpose of not losing the generality, initial phases of the grating components must be included in expression (3.8). This ensures a proper analysis for a multi-grating system. Also, the model can always be used for pure reflection type gratings.

3.2.3 Field in the slab

Substituting Eq. (3.8) for $\mu\varepsilon(\vec{r})$ in Eq. (3.5) yields a partial differential equation which must be satisfied by the E-field inside the slab. It is assumed that the E-field takes the

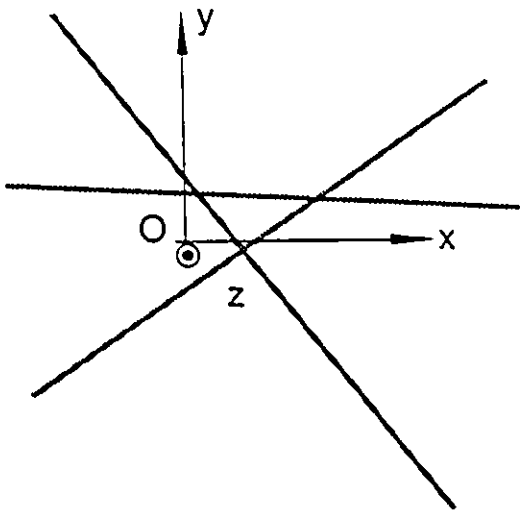

Figure 3.5: Three randomly drawn lines may not happen to intersect at the same point.

form:

$$\vec{E}(\vec{r}) = \sum_{m_1} \sum_{m_2} \cdots \sum_{m_M} \vec{a}(\mathrm{m}) e^{j\vec{k}(\mathrm{m})\cdot\vec{r}} \tag{3.11}$$

which is composed of a set of plane wave components (which may be called plane-wavelets) with complex amplitude vector $\vec{a}(\mathrm{m})$ and wave vector $\vec{k}(\mathrm{m})$. In Eq. (3.11), m is an M-dimensional vector index, i.e.,

$$\mathrm{m} = (m_1, m_2, ..., m_M) \tag{3.12}$$

where $m_i = 0, \pm 1, \pm 2, \cdots$, with $i = 1, 2, \cdots, M$. The M-dimensional index m may be called the "order" of the corresponding plane wave component. It is a natural extension from the diffraction orders of a single grating. In the case of a single grating, one integer is usually used to indicate different diffraction orders. It is reasonable that when the diffraction of M gratings is modeled, M integers have to be used to indicate a diffraction order. However, the experience shows that using an M-dimensional vector index is not an easy operation when a computer simulation is considered. In order to make the operation easier, a serial number J is introduced to indicate the diffraction orders. It is defined that J is a non-negative integer and that each diffraction order is assigned a distinct serial

number J as its label. Besides, the mapping from $\mathbf{m}$ to J can be arbitrary provided that it is unique. For example, in a two-grating system, if the 4 diffraction orders of interest are $\mathbf{m} = (0,0), (-1,0), (0,-1)$, and $(-1,-1)$, respectively, we may randomly assign a serial number to every order and thus establish a mapping table as follows:

m=	(0,0)	(-1, 0)	(-1,-1)	(0, -1)
J=	0	1	2	3

Actually, it can be seen that, in addition to a single integer index, another advantage of introducing the serial number J is that we can easily pick up only those orders which are significant. This makes the computation much easier. This issue will be discussed later in Section 3.5.

With the help of serial number J, Eq. (3.11) can be rewritten as:

$$\vec{E}(\vec{r}) = \sum_{J=0}^{\infty} \vec{a}(J) e^{j\vec{k}(J)\cdot\vec{r}} \tag{3.13}$$

where the wave vector $\vec{k}(J)$ is defined as:

$$\begin{aligned} \vec{k}(J) &= \vec{k}_\rho(J) + \hat{z}k_z(J) && (3.14) \\ &= \vec{k}(0) + \sum_{i=1}^{M} m_i(J)\vec{K}_i \\ &= \vec{k}(0) + \mathbf{m}(J)\vec{\mathbf{K}}^T && (3.15) \end{aligned}$$

where $\vec{k}_\rho(J)$ is the transverse component vector, and $k_z(J)$ is the longitudinal component. Notice that $\mathbf{m}(J)$ is a vector of dimension M, previously written as $\mathbf{m}$ in Eq. (3.11). The vector $\vec{\mathbf{K}}^T$ is defined as a column vector of size M:

$$\vec{\mathbf{K}}^T = \begin{pmatrix} \vec{K}_1 \\ \vec{K}_2 \\ \vdots \\ \vec{K}_M \end{pmatrix} \tag{3.16}$$

where $\vec{K}_i$ is the grating vector of the i-th grating. Eq. (3.15) provides the relation between wave vectors of different orders. Once any of the vectors is known, all other vectors can be found from the equation. Usually, the direction of the incident wave is given. Assume that the incident wave has a transverse wave vector $\vec{k}'_\rho$, then one of the wave vectors can have a known transverse component, because there must exist an integer J', such that

$$\vec{k}_\rho(J') = \vec{k}'_\rho \tag{3.17}$$

This will be further discussed in Section 3.3. Obviously, if Eq. (3.17) holds, all the transverse components of the wave vectors can be found. From Eq. (3.15), expressions can be found for $\vec{k}_\rho(J)$ and $\vec{k}_\rho(J')$. Canceling $\vec{k}_\rho(0)$ and substituting Eq. (3.17) for $\vec{k}_\rho(J')$, we have:

$$\vec{k}_\rho(J) = \vec{k}'_\rho + [\mathrm{m}(J) - \mathrm{m}(J')]\vec{\mathbf{K}}_\rho^T \qquad J = 0, 1, 2, \ldots \tag{3.18}$$

The computation of the longitudinal components is not so straightforward. In a special case when all the Δ_i's are zero, i.e., when there are actually no gratings written in the slab, we have, not surprisingly:

$$k_z(J) = \sqrt{k^2 n_0^2 - k_\rho^2(J)} \tag{3.19}$$

which can only be used for homogeneous slabs. However, for an inhomogeneous grating slab, we have to go back to Eq. (3.5) for a solution. For convenience, it is assumed that $q = k_z(0)/kn_0$. It will be shown that $k_z(0)$ or equivalently q can be found from a set of linear equations derived from Eq. (3.5). Once q is found, all the other longitudinal components can be found, just as in the case of transverse components. From (3.15), we have:

$$k_z(J) = kn_0 q + \mathbf{m}(J)\mathbf{K}_z^T \tag{3.20}$$

where q will be obtained in the next section. Before we go on to the next subject, let us consider the validity of Eq. (3.13). Since it is now merely an assumption, one may wonder whether or not the assumption is true. At this point of the chapter, this question can not be answered yet. However, we may apply the uniqueness theorem [22], which

states that there is one and only one solution to a properly specified problem. If we assume the problem is specified by Eq. (3.5) and Eq. (3.7), and the assumption turns out to be a solution, it is the solution and the only solution of the system. The insight of the uniqueness theorem is obvious. Since Maxwell's equations and the corresponding boundary conditions are all the rules a light field follows and the field must be physically realistic, there can be only one solution to the equations and the conditions. In the following sections, we will show that Eq. (3.13) can satisfy both Eq. (3.5) and Eq. (3.7) and is thus a unique solution to the problem.

3.2.4 Mode and mode equations

In this section, a group of equations will be derived from Eq. (3.5). From these equations, a set of vectors $\vec{a}(J)$ and the corresponding longitudinal component $k_z(0)$ (or q) will be found. They form a set of possible vector field solutions to Eq. (3.5) and each of the solutions is called a mode.

Substituting Eq. (3.13) into Eq. (3.5) yields:

$$[(kn_0)^2 - k^2(J)]\vec{a}(J) + \vec{k}(J)[\vec{k}(J)\cdot\vec{a}(J)] + (kn_0)^2 \sum_{s=-,+}\sum_{i=1}^{M} \Delta_i e^{-sj\phi_i}\vec{a}(J_i^s) = 0 \qquad (3.21)$$

$$for \quad J = 0, 1, 2, \cdots, \infty$$

where J_i^- is the serial number for the order $\mathbf{m}(J) - \mathbf{u}_i$ with $\mathbf{u}_i$ being an M-dimensional vector index whose j-th element can be found as $u_{i,j} = \delta_{ij}$. Similarly, J_i^+ is the serial number for the order $\mathbf{m}(J) + \mathbf{u}_i$. J_i^- and J_i^+ stands for the "adjacent" diffraction orders of the order J in the direction of $-\vec{K}_i$ and $\vec{K}_i$, respectively, see Fig. 3.6. Eq. (3.21) is the mode equation in vector form. In other words, a q and a set of $\vec{a}(J)$, which defind a mode of the field, are to be found to satisfy this equation. For computation, Eq. (3.21), which is in a vector form, has to be converted to scalar form. Theoretically, Eq. (3.21) can be dot-multiplied by unit vectors $\hat{x}$, $\hat{y}$ and $\hat{z}$, respectively, and each of the equations in (3.21) is then split into three scalar-form equations. However, for convenience, a slightly different approach is used here. First of all, new sets of orthogonal unit vectors are defined

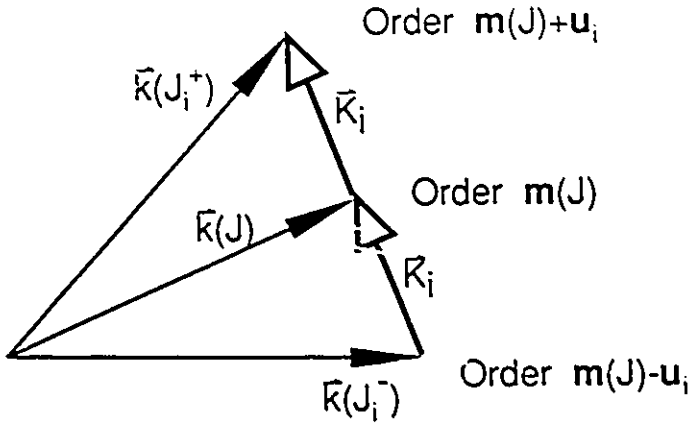

Figure 3.6: Adjacent diffraction orders of the order $\mathrm{m}(J)$.

as:

$$\begin{cases} \hat{\rho}(J) &= \frac{\vec{k}_\rho(J)}{|\vec{k}_\rho(J)|} \\ \hat{\tau}(J) &= \hat{\rho}(J) \times \hat{z} \\ \hat{z}(J) &= \hat{z} \end{cases} \tag{3.22}$$

which form the basis of a set of natural Cartesian coordinate system, see Fig. 3.7. Notice that, for each diffraction order m (or J), there is a preferred basis which has a unit vector $\hat{\rho}(J)$ parallel to the plane of diffraction of the order. Here, the plane of diffraction of a certain order refers to the plane defined by the normal line of the slab surface $\hat{z}$ and the wave vector of the diffraction order $\vec{k}(J)$, or more practically, $\vec{k}_\rho(J)$.

For each J, dot-multiplying Eq. (3.21) with $\hat{\tau}(J)$, $\hat{\rho}(J)$ and $\hat{z}$, respectively, results in three desired scalar equations. Defining $a_\delta(J) = qa_\tau(J)$, after some manipulation, yields the following linear equations, which are referred to here as mode equations:

$$\begin{aligned} qa_\delta(J) &= -2V_z(J)a_\delta(J) + [1 - V_\rho^2(J) - V_z^2(J)]a_\tau(J) \\ &\quad + \sum_{s=-,+}\sum_{i=1}^{M}\{\Delta_i e^{-sj\phi_i}\cos\alpha_i^s(J)a_\tau(J_i^s) - \Delta_i e^{-sj\phi_i}\sin\alpha_i^s(J)a_\rho(J_i^s)\} \quad (3.23) \\ qa_\tau(J) &= a_\delta(J) \quad (3.24) \\ qa_\rho(J) &= -V_z(J)a_\rho(J) + [V_\rho(J) - \frac{1}{V_\rho(J)}]a_z(J) \end{aligned}$$

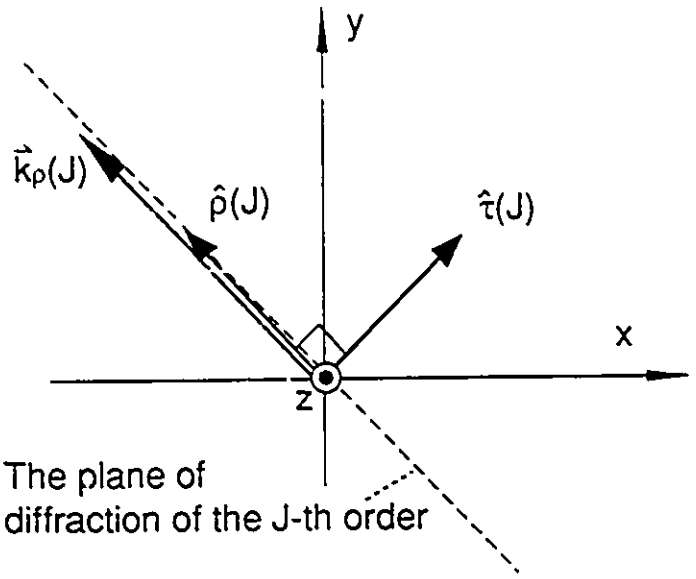

Figure 3.7: The basis for the J-th order diffraction. Scalar form mode equations are obtained by dot-multiplying $\hat{\rho}(J)$, $\hat{\tau}(J)$ and $\hat{z}(J)$ with the vector form mode equation.

$$-\frac{1}{V_\rho(J)}\sum_{s=-,+}\sum_{i=1}^{M}\Delta_i e^{-sj\phi_i}a_z(J_i^s) \tag{3.25}$$

$$\begin{aligned} q\{a_z(J)+\sum_{s=-,+}\sum_{i=1}^{M}\Delta_i e^{-sj\phi_i}a_z(J_i^s)\} = \\ -V_\rho(J)a_\rho(J)-V_z(J)a_z(J)-V_z(J)\sum_{s=-,+}\sum_{i=1}^{M}\Delta_i e^{-sj\phi_i}a_z(J_i^s) \\ -V_\rho(J)\sum_{s=-,+}\sum_{i=1}^{M}\Delta_i e^{-sj\phi_i}[\sin\alpha_i^s(J)a_\tau(J_i^s)+\cos\alpha_i^s(J)a_\rho(J_i^s)] \end{aligned} \tag{3.26}$$

where $q = k_z(0)/kn_0$, $\alpha_i^-(J)$ is the angle between the plane of diffraction of the J-th order and the diffraction plane of its adjacent order J_i^-. Similarly, $\alpha_i^+(J)$ is the angle between the two planes of diffraction of the orders J and its neighbour J_i^+. We have also defined:

$$\vec{V}(J) = \frac{\vec{k}(J)}{kn_0} - q\hat{z}$$

and used the relations:

$$\begin{cases} a(\vec{J}_i^{\pm}) \cdot \hat{\tau}(J) &= a_\tau(J_i^{\pm}) \cos\alpha^{\pm}(J) - a_\rho(J_i^{\pm}) \sin\alpha^{\pm}(J) \\ a(\vec{J}_i^{\pm}) \cdot \hat{\rho}(J) &= a_\tau(J_i^{\pm}) \sin\alpha^{\pm}(J) + a_\rho(J_i^{\pm}) \cos\alpha^{\pm}(J) \end{cases} \tag{3.27}$$

The above mode equations form a typical generalized eigensystem in the form:

$$\mathbf{Aa} = q\mathbf{Ba} \tag{3.28}$$

where a is a column vector of infinite size:

$$\mathbf{a} = \begin{pmatrix} a_z(0) \\ \vec{a}(0) \\ a_z(1) \\ \vec{a}(1) \\ \vdots \\ a_z(J) \\ \vec{a}(J) \\ \vdots \end{pmatrix} \tag{3.29}$$

with $\vec{a}(J)$ being a column vector of size 3:

$$\vec{a}(J) = \begin{pmatrix} a_\tau \\ a_\rho \\ a_z \end{pmatrix} \tag{3.30}$$

A and **B** are two dimensional arrays of infinite size. Their array elements are determined by the equations from (3.23) through (3.26).

In practice, **A**, **B** and **a** cannot have an infinite size. They must be truncated to a finite size, say L. L should be large enough for a sufficient precision. $L/4$ is the number of significant diffraction orders under consideration. It is important to include all the significant orders in the $L/4$ diffraction orders. This issue will be discussed later in this chapter.

The eigensystem of Eq. (3.28) yields L eigenvalues and L corresponding vectors. According to Eq. (3.13), each eigenvalue and its eigenvector can be used to form a mode

which is a solution to Eq. (3.5). Since Eq. (3.5) is a linear equation, any linear combinations are also its solutions. Therefore, generally speaking, the E-field inside the slab takes the form:

$$\vec{E}(\vec{r}) = \sum_{l=1}^{L} C_l \sum_{J=0}^{L/4-1} \vec{a}_l(J) e^{j\vec{k}_l(J)\cdot\vec{r}} \tag{3.31}$$

where from Eq. (3.15), we have

$$\vec{k}_l = \vec{k}_\rho(0) + \hat{z}kn_0 q_l + \mathbf{m}(J)\vec{\mathbf{K}}^T \tag{3.32}$$

where q_l and $\vec{a}_l(J)$ are the l-th eigenvalue and the corresponding eigenvector of Eq. (3.28). The coefficients $C_l (l = 1, 2, ...L)$ are complex constants which are to be determined by the boundary conditions. If a unique set of C_l can be found to make Eq. (3.31) satisfy Eq. (3.7), we can declare that the whole grating diffraction problem is successfully solved.

3.2.5 Field outside the slab and the boundary conditions

From the boundary condition (3.7), a set of equations can be found. They can be used to determine the unique set of coefficients C_l. At the same time, all the diffracted light waves outside the slab, including both the reflected orders and the transmitted orders, will also be determined. Actually, knowledge on the outside light waves are of more practical value, and these waves are determined by C_l.

The field outside the slab for $z \leq 0$ is assumed to be

$$\begin{aligned} E(\vec{r}) &= \vec{I} e^{j[\vec{k}_\rho(J')\cdot\vec{\rho} + z\sqrt{k^2 n_R^2 - k_\rho^2(J')}]} \\ &\quad + \sum_{J=0}^{L/4-1} \vec{R}(J) e^{j[\vec{k}_\rho(J)\cdot\vec{\rho} - z\sqrt{k^2 n_R - k_\rho^2(J)}]} \end{aligned} \tag{3.33}$$

where $\vec{\rho} = (x, y, 0)$, which is the transverse component of the vector $\vec{r}$. In the region T, i.e., for $z \geq d$, the field is assumed to be:

$$E(\vec{r}) = \sum_{J=0}^{L/4-1} \vec{T}(J) e^{j[\vec{k}_\rho(J)\cdot\vec{\rho} + z\sqrt{k^2 n_T - k_\rho^2(J)}]} \tag{3.34}$$

In both the regions R and T, it is assumed that, the field is composed of a bunch of plane waves which have complex vector-amplitudes $\vec{R}(J)$ or $\vec{T}(J)$ and transverse wave

vectors $\vec{k}_\rho(J)$. The z-component of a wave vector of a reflected beam in region R is always negative, indicating that the wave travels from right to left, but positive z-components are found for wave vectors in region T because the waves travel from left to right. In addition, the incident wave has an amplitude $\vec{I}$ and a transverse wave vector $\vec{k}_\rho(J')$ combined with a positive longitudinal component indicating that the wave travels from left to right. Again, whether the assumptions (3.33) and (3.34) are true or not depends on the uniqueness theorem or in other words, on if any solutions can be found for Eq. (3.5) and (3.7). Obviously, the field outside the slab must also satisfy the Maxwell's equations (3.1). It can be shown that the equations are satisfied if the plane waves satisfy the following two conditions. First, the waves must be transverse waves (notice that, the media outside the slab is homogeneous). This means the amplitude vectors must be perpendicular to its wave vectors. The second condition requires that all the wave vectors in the region R have a magnitude kn_R, and all the wave vectors in region T have a magnitude of kn_T. The second condition is already satisfied in Eq. (3.33), and Eq. (3.34), whereas the first condition can be satisfied when :

$$\begin{cases} \vec{I} = \begin{pmatrix} I_\perp \\ I_\parallel \end{pmatrix} &= I_\perp \hat{\tau} + I_\parallel \cos\theta_R(J')\hat{\rho}(J') - I_\parallel \sin\theta_R(J')\hat{z} \\ \vec{R} = \begin{pmatrix} R_\perp \\ R_\parallel \end{pmatrix} &= R_\perp \hat{\tau}(J) - R_\parallel(J)\cos\theta_R(J)\hat{\rho}(J) - R_\parallel(J)\sin\theta_R(J)\hat{z} \\ \vec{T} = \begin{pmatrix} T_\perp \\ T_\parallel \end{pmatrix} &= T_\perp \hat{\tau}(J) + T_\parallel(J)\cos\theta_T(J)\hat{\rho}(J) - T_\parallel(J)\sin\theta_T(J)\hat{z} \end{cases} \tag{3.35}$$

Notice that, the polarization state of an incident wave, or a reflected diffraction order or a transmitted diffraction order is dependent on the complex amplitude component perpendicular to the corresponding plane of diffraction and that parallel to the plane. Hence, the column vector $\begin{pmatrix} I_\perp \\ I_\parallel \end{pmatrix}$ gives us the polarization of the incident light as well as its intensity. Similarly, $\begin{pmatrix} R_\perp \\ R_\parallel \end{pmatrix}$ or $\begin{pmatrix} T_\perp \\ T_\parallel \end{pmatrix}$ shows the polarization and the strength of

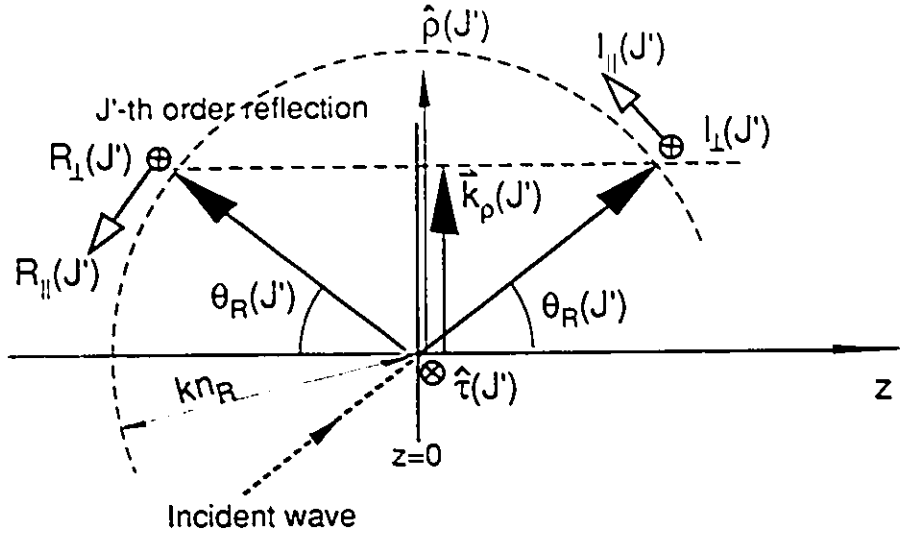

Figure 3.8: Components of the amplitude vectors $\vec{I}(J')$ and $\vec{R}(J')$.

the J-th diffraction order in region R or T, respectively. Fig. 3.8 and Fig. 3.9 show how $I_\perp$, $I_\parallel$, $R_\perp(J)$, $R_\parallel(J)$, $T_\perp(J)$ and $T_\parallel(J)$ are defined.

Applying Eq. (3.7) at the boundaries $z = 0$ and $z = d$, using expressions (3.31), (3.33), (3.34) and (3.35) yields two groups of equations. The first group of equations is:

$$\sum_{l=1}^{L} C_l\{\cos\theta_R(J) + \frac{n_0}{n_R}[V_z(J) + q_l]\}a_{l,\tau}(J) = 2I_\perp \cos\theta_R(J')\delta_{JJ'} \quad (3.36)$$

$$\sum_{l=1}^{L} C_l\{-\cos\theta_T(J) + \frac{n_0}{n_T}[V_z(J) + q_l]\}a_{l,\tau}(J)\cdot \cdot\exp(jq_l n_0 kd) = 0 \quad (3.37)$$

$$\sum_{l=1}^{L} C_l\{[1 + \frac{n_0}{n_R}[V_z(J) + q_l]\cos\theta_R(J)]a_{l,\rho}(J) - - \sin\theta_R(J)\cos\theta_R(J)a_{l,z}(J)\} = 2\cos\theta_R(J')I_\parallel\delta_{JJ'} \quad (3.38)$$

$$\sum_{l=1}^{L} C_l\{[-1 + \frac{n_0}{n_T}[V_z(J) + q_l]\cos\theta_T(J)]a_{l,\rho}(J) - - \sin\theta_T(J)\cos\theta_T(J)a_{l,z}(J)\}\exp(jq_l n_0 kd) = 0 \quad (3.39)$$

$$for \quad J, J' = 0, 1, 2, \cdots$$

with which, a unique set of coefficients C_l can be determined (therefore, the specified

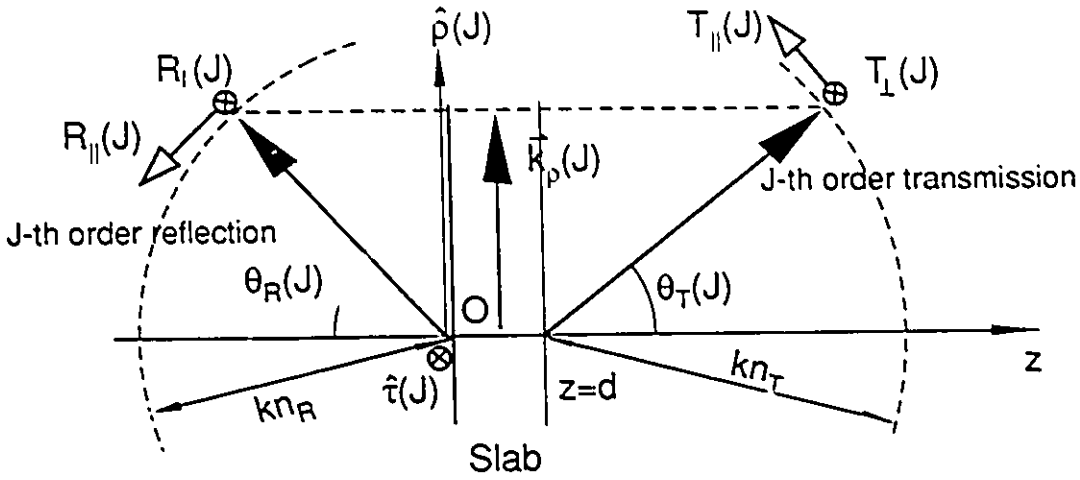

Figure 3.9: Components of the amplitude vectors $\vec{R}(J)$and $\vec{T}(J)$.

problem is solved). The second group of equations can be used to determine the amplitude of the diffraction orders:

$$R_{\perp}(J) = \sum_{l=1}^{L} C_l a_{l,\tau}(J) - I_{\perp}\delta_{JJ'} \tag{3.40}$$

$$R_{\parallel}(J) = -\frac{1}{\cos\theta_R(J)} \sum_{l=1}^{L} C_l a_{l,\rho}(J) + I_{\parallel}\delta_{JJ'} \tag{3.41}$$

$$T'_{\perp}(J) = \sum_{l=1}^{L} C_l a_{l,\tau}(J) \exp(jq_l n_0 kd) \tag{3.42}$$

$$T'_{\parallel}(J) = \frac{1}{\cos\theta_T(J)} \sum_{l=1}^{L} C_l a_{l,\rho}(J) \exp(jq_l n_0 kd) \tag{3.43}$$

where

$$T'_{\perp} = T_{\perp} e^{jkn_T \cos\theta_T(J)d - jkn_0 V_Z(J)d} \tag{3.44}$$

$$T'_{\parallel} = T_{\parallel} e^{jkn_T \cos\theta_T(J)d - jkn_0 V_Z(J)d} \tag{3.45}$$

In most practical cases, the phase factor $e^{jkn_T \cos\theta_T(J)d - jkn_0 V_Z(J)d}$ can be neglected, because it is just a constant phase for both of the polarizations. Also, it cannot change the polarization of the diffraction order. Eq. (3.41) and (3.43) can also be written equivalently

as:

$$R_{\parallel}(J) = \sum_{l} C_l[\frac{n_0}{n_R}(V_z(J) + q_l)a_{l,\rho}(J) - \sin\theta_R(J)a_{l,z}(J)] - I_{\parallel}\delta_{JJ'} \tag{3.46}$$

$$T_{\parallel}(J) = \sum_{l} C_l[\frac{n_0}{n_T}(V_z(J) + q_l)a_{l,\rho}(J) - \sin\theta_T(J)a_{l,z}(J)]e^{jq_l k n_0 d} \tag{3.47}$$

The two equations are better in the sense that there are no division operations compared with Eq. (3.41) and (3.43).

At last, up to this point of the chapter, the multi-grating diffraction problem is completely solved. For a given multi-planar-grating slab and a given incident light beam of an arbitrary direction and polarization, a solution, i.e., the diffracted waves inside and outside the slab can be found by following the procedures listed below:

1. Find the matrices **A** and **B** in Eq. (3.28) from Eq. (3.23) to (3.26).
2. Find the eigenvalues and eigenvectors of the eigensystem (3.28).
3. Solve the linear equations (3.36) through (3.39).
4. Determine the complex amplitude vectors of all the diffraction orders under consideration with Eq. (3.40) to (3.43).

According to the law of uniqueness, the solution found is unique and thus all the assumptions about the field structures, e.g., Eq. (3.13), (3.31), (3.33), etc., are true.

3.2.6 Jones matrix

When the polarization of the incident wave changes, the output of a grating system change, too. Theoretically, for an input of different polarization, the algorithm described in the preceding subsections has to be run again to obtain the outputs with the right polarizations and intensities. However, there is an easy treatment, by which the algorithm does not have to be run for a polarization change. The treatment is based on the linearity of the Maxwell's equations and the boundary conditions. The linearity shows that the

response of a linear system to a linear combination of two inputs is the same linear combination of the corresponding outputs. Therefore, if the input of the grating slab is

$$\vec{I}(J') = \begin{pmatrix} I_{\perp}(J') \\ I_{\parallel}(J') \end{pmatrix}$$

which can be written as a combination of two inputs:

$$\vec{I}(J') = I_{\perp}(J') \begin{pmatrix} 1 \\ 0 \end{pmatrix} + I_{\parallel}(J') \begin{pmatrix} 0 \\ 1 \end{pmatrix} \tag{3.48}$$

the output, taking the J-th transmission order as an example, is

$$\begin{aligned} \vec{T}(J,J') &= \begin{pmatrix} T_{\perp}(J,J') \\ T_{\parallel}(J,J') \end{pmatrix} \\ &= I_{\perp}(J') \begin{pmatrix} t_{\perp\perp}(J,J') \\ t_{\parallel\perp}(J,J') \end{pmatrix} + I_{\parallel}(J') \begin{pmatrix} t_{\perp\parallel}(J,J') \\ t_{\parallel\parallel}(J,J') \end{pmatrix} \end{aligned} \tag{3.49}$$

where $\begin{pmatrix} t_{\perp\perp}(J,J') \\ t_{\parallel\perp}(J,J') \end{pmatrix}$ is the response to $\begin{pmatrix} 1 \\ 0 \end{pmatrix}$ and $\begin{pmatrix} t_{\perp\parallel}(J,J') \\ t_{\parallel\parallel}(J,J') \end{pmatrix}$ is the response to $\begin{pmatrix} 0 \\ 1 \end{pmatrix}$. Hence, we may have

$$\begin{aligned} \vec{T}(J,J') &= \begin{pmatrix} t_{\perp\perp}(J,J') & t_{\perp\parallel}(J,J') \\ t_{\parallel\perp}(J,J') & t_{\parallel\parallel}(J,J') \end{pmatrix} \begin{pmatrix} I_{\perp}(J') \\ I_{\parallel}(J') \end{pmatrix} \\ &= M_T(J,J') \begin{pmatrix} I_{\perp}(J') \\ I_{\parallel}(J') \end{pmatrix} \quad for \quad J,J' = 0,1,\cdots \end{aligned} \tag{3.50}$$

where $M_T(J,J')$ may be called Jones Matrix of the J-th transmission order. Similarly, we may have one for the J-th reflection order

$$M_R(J,J') = \begin{pmatrix} r_{\perp\perp}(J,J') & r_{\perp\parallel}(J,J') \\ r_{\parallel\perp}(J,J') & r_{\parallel\parallel}(J,J') \end{pmatrix} \quad for \quad J,J' = 0,1,2,\cdots \tag{3.51}$$

For Jones matrices, the algorithm is run twice (Once for input $\begin{pmatrix} 1 \\ 0 \end{pmatrix}$ and once for $\begin{pmatrix} 0 \\ 1 \end{pmatrix}$, actually only the boundary conditions of the algorithm are repeated), for a given grating slab and an incident wave of particular direction. The resulting Jones matrices completely characterize the response of the grating system to any change in the input polarization.

Apart from the Jones matrix, we may also have a set of power coupling coefficients which are defined as:

$$c_T(J,J') = \frac{P_T(J)}{P_I(J')} = \frac{\cos\theta_T(J)}{\cos\theta_R(J')}\frac{|\vec{T}(J)|^2}{|\vec{I}(J')|^2} \tag{3.52}$$

$$c_R(J,J') = \frac{P_R(J)}{P_I(J')} = \frac{\cos\theta_R(J)}{\cos\theta_R(J')}\frac{|\vec{R}(J)|^2}{|\vec{I}(J')|^2} \tag{3.53}$$

$$for\ J,J' = 0,1,2,\cdots$$

These coefficients are the ratio of the output power $P_T(J,J')$ or $P_R(J,J')$ to the input power $P_I(J')$. From Eq. (3.50) and (3.52), we may have:

$$c_T(J,J') = \frac{\cos\theta_T(J)}{\cos\theta_R(J')}\frac{(I_\perp^*(J') \quad I_\parallel^*(J'))M_T^\dagger(J,J')M_T(J,J')\begin{pmatrix} I_\perp(J') \\ I_\parallel(J') \end{pmatrix}}{(I_\perp^*(J') \quad I_\parallel^*(J'))\begin{pmatrix} I_\perp(J') \\ I_\parallel(J') \end{pmatrix}}$$

$$= \frac{\vec{I}^\dagger(J')\Phi_T(J,J')\vec{I}(J')}{|I_\perp(J')|^2 + |I_\parallel(J')|^2} \tag{3.54}$$

$$= \frac{\vec{I}^\dagger(J')\Phi_T(J,J')\vec{I}(J')}{|\vec{I}(J')|^2} \tag{3.55}$$

where

$$\Phi_T(J,J') = \frac{\cos\theta_T(J)}{\cos\theta_R(J')}M_T^\dagger(J,J')M_T(J,J') \tag{3.56}$$

Similarly, we may have:

$$c_R(J,J') = \frac{\vec{I}^\dagger(J')\Phi_R(J,J')\vec{I}(J')}{|\vec{I}(J')|^2} \tag{3.57}$$

where

$$\Phi_R(J,J') = \frac{\cos\theta_R(J)}{\cos\theta_R(J')}M_R^\dagger(J,J')M_R(J,J') \tag{3.58}$$

$\Phi_T(J, J')$ and $\Phi_R(J, J')$ may be called diffraction efficiency matrices. Notice that, power coupling coefficients are dependent on both the grating slab and the input polarization, while the diffraction efficiency matrices are independent of the input polarization. They characterize the grating slab only, just as the Jones matrices.

For a given set of inputs $\begin{pmatrix} I_\perp(J') \\ I_\parallel(J') \end{pmatrix}$, $c_T(J, J')$ and $c_R(J, J')$ can form coupling matrices:

$$C_T = \begin{pmatrix} & \vdots & \\ \cdots & c_T(J, J') & \cdots \\ & \vdots & \end{pmatrix} \tag{3.59}$$

and

$$C_R = \begin{pmatrix} & \vdots & \\ \cdots & c_R(J, J') & \cdots \\ & \vdots & \end{pmatrix} \tag{3.60}$$

which give the functionality or the connectivity of the grating slab. Recall that, we have generally discussed some fundamental issues about the power coupling matrices in Chapter 1.

3.3 Grating Equation

The grating equation is first used in Eq. (3.18) of Section 2.3 without any interpretation. Eq. (3.18) is rewritten here with integer $J' = 0$ for convenience as:

$$\vec{k}_\rho(J) = \vec{k}_\rho(0) + \sum_{i=1}^{M} m_i(J)\vec{K}_{i,\rho} \tag{3.61}$$

where $\vec{K}_{i,\rho}$ is the transverse component vector of the i-th grating vector $\vec{K}_i$. Notice that,

$$\vec{K}_i = \vec{K}_{i,\rho} + \hat{z}K_{i,z} = K_{i,x}\hat{x} + K_{i,y}\hat{y} + K_{i,z}\hat{z}$$

so

$$\vec{K}_{i,\rho} = K_{i,x}\hat{x} + K_{i,y}\hat{y}$$

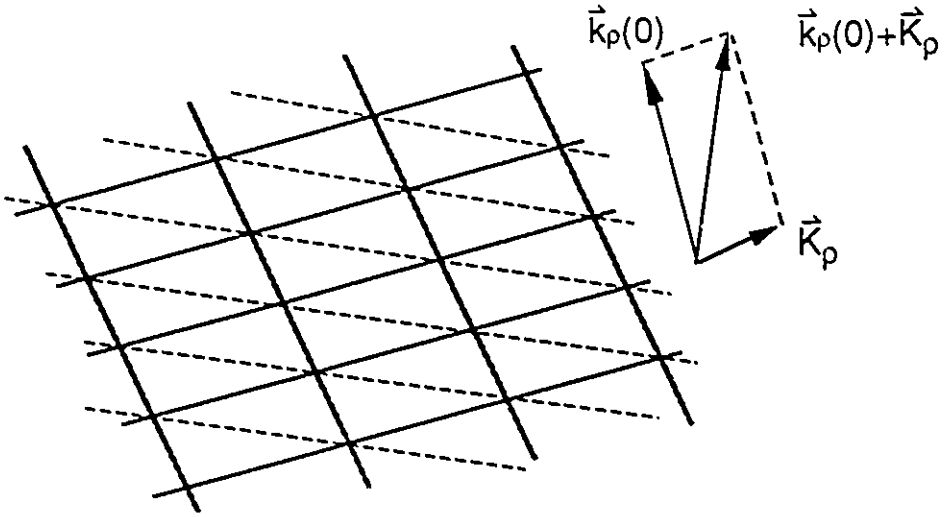

Figure 3.10: The fringes seen on the surface of a grating slab.

One important feature of the grating equation is that it gives only the relation between the transverse structures of the gratings, the incident wave and the diffracted waves. However, the grating equation is sufficient for determining the directions of all the possible diffracted light beams. Actually, the propagation direction of the light waves has nothing to do with the longitudinal structure of the gratings. This implies that, even though only a planar-fringe grating system is considered in this thesis, the equation can be applied to a much more generalized collection of gratings including, e.g., surface relief gratings.

Let us consider a single grating with a lateral periodic structure represented by $\vec{K}_\rho$. This structure is represented by the thick grid in Fig. 3.10. Suppose a light wave is incident on the structure. It is evident that the wave is also a periodic structure which is characterized by $k_\rho(0)$ as shown in Fig. 3.10. Apparently, the diffracted waves are results of interaction between the two periodic structures. It is reasonable that the stimulated diffraction order forms a periodic structure which is in harmony with $\vec{K}_\rho$ and $\vec{k}_\rho(0)$. This structure turns out to be $\vec{k}_\rho(0) + \vec{K}_\rho$. Similarly, $\vec{k}_\rho(0) - \vec{K}_\rho$ is also a structure which is in harmony with both $\vec{K}_\rho$ and $\vec{k}_\rho(0)$. We have used a rather vague expression "in harmony" without defining it. In fact, in Fig. 3.10, we can see that the grid $\vec{k}_\rho(0)+\vec{K}_\rho$ does not break

either of the two original periodic structures. It has the same period in the direction of $\vec{K}_\rho$ as that of $\vec{K}_\rho$ and the same period in the direction of $\vec{k}_\rho(0)$ as that of $\vec{k}_\rho(0)$. Apparently, $\vec{k}_\rho(0) - \vec{K}_\rho$ has the same property. These two stimulated periodic structures are in fact the $+1$ and -1 order diffractions. It is true that these stimulated waves can interact with $\vec{K}_\rho$, too. The results are four waves: $\vec{k}_\rho(0) + \vec{K}_\rho \pm \vec{K}_\rho$ and $\vec{k}_\rho(0) - \vec{K}_\rho \pm \vec{K}_\rho$, of which two are new structures. The process can be repeated to infinity. Therefore, for a single grating, all the possible diffracted waves are included in the following periodic patterns:

$$\vec{k}_\rho(0) + m\vec{K}_\rho \qquad m = 0, \pm 1, \pm 2, \cdots \tag{3.62}$$

which can easily be generalized to the multi-grating case as shown in Eq. (3.61). However, one may argue that the pattern $m'\vec{k}_\rho(0) + m\vec{K}_\rho$ can also fit the above reasoning, and that they should be included in the grating equation, too. This puzzle can be resolved by investigating one example. Consider, for instance, the pattern $2\vec{k}_\rho(0) + \vec{K}_\rho$ ($m' = 2, m = 1$). It can be written as $\vec{k}_\rho(0) + (\vec{k}_\rho(0) + \vec{K}_\rho)$, which implies the outcome of the interaction of two waves, because $\vec{k}_\rho(0)$ corresponds to the incident wave, and $\vec{k}_\rho(0) + \vec{K}_\rho$ represents the $+1$ order diffraction. It is well known that in a linear medium two light waves cannot interact with each other and produce a new wave. Hence, we may exclude $2\vec{k}_\rho(0) + \vec{K}_\rho$. For the same reason, the collection $m'\vec{k}_\rho(0) + m\vec{K}_\rho$ with $m' \neq 1$ can be excluded.

Another important concept is Snell's law. Snell's law is the law governing the refraction directions of light at the surface of discontinuity between two homogeneous media. In Section 2.3, we used a generalized version of Snell's law with Eq. (3.17), though the grating medium was not homogeneous. We assumed that one of the wave vectors of the wavelets in medium G should have its transverse component matched to that of the incident wave. This actually implies that the periodic field structures at both sides of the boundary $z = 0$ should match each other at the boundary. This is exactly the essence of the Snell's law of refraction. We may consider the incident beam as the "cause" of the event; while the field in slab G as the "result". It is reasonable to say that they must be correlated with each other. It turns out that the most basic requirement of this correlation is that they have the same geometric pattern at the boundary. We have also

applied this generalized Snell's law in Eq. (3.33) and Eq. (3.34) of Section 3.2.5, which turned out to be justified – we did find the unique solution to Maxwell's equations and the corresponding boundary conditions.

From the grating equation, a few groups of useful equations can be derived. In solving a practical problem, the grating vectors may be given as a set of components, i.e., $K_{i,x}, K_{i,y}$ and $K_{i,z}$ with $i = 1, 2, \cdots, M$. Obviously, $K_{i,z}$ can be put away in this section, because only the directions of the waves are interested. The direction of a possible diffraction order $\mathbf{m}(J)$ can be represented in component form, according to Eq. (3.61):

$$k_x(J) = k_x(0) + \sum_{i=1}^{M} m_i(J) K_{i,x} \tag{3.63}$$

and

$$k_y(J) = k_y(0) + \sum_{i=1}^{M} m_i(J) K_{i,y} \tag{3.64}$$

The transverse component can thus be found as:

$$k_\rho(J) = \sqrt{k_x^2(J) + k_y^2(J)} \tag{3.65}$$

The diffraction angle $\theta_R(J)$ and $\theta_T(J)$ of the J-th reflection and transmission order can be found from:

$$\begin{cases} \cos\theta_R(J) &= \frac{\sqrt{k^2 n_R^2 - k_\rho^2(J)}}{k n_R} \\ \cos\theta_T(J) &= \frac{\sqrt{k^2 n_T^2 - k_\rho^2(J)}}{k n_T} \end{cases} \tag{3.66}$$

We also need expressions for $\alpha_i^+(J)$ and $\alpha_i^-(J)$ in Eq. (3.28). The following formulas can be used for computation:

$$\begin{cases} \cos\alpha_i^{\pm}(J) &= \frac{k_x(J)k_x(J_i^{\pm}) + k_y(J)k_y(J_i^{\pm})}{k_\rho(J)k_\rho(J_i^{\pm})} \\ \sin\alpha_i^{\pm}(J) &= \frac{k_x(J)k_y(J_i^{\pm}) - k_y(J)k_x(J_i^{\pm})}{k_\rho(J)k_\rho(J_i^{\pm})} \end{cases} \tag{3.67}$$

3.4 Modelling a Coupler with Sandwich Structure

In the previous sections, the physical process of single-slab diffraction has been modeled mathematically. The model can be directly used to analyze the performance of a coupler

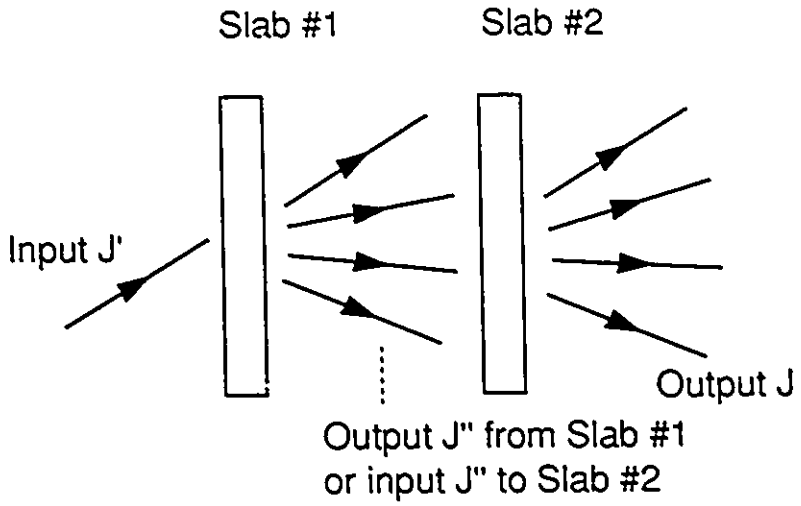

Figure 3.11: Inputs and outputs of a two-layer sandwich structure.

using a single grating-bearing slab. For couplers with multiple slabs, the model can not be directly applied. However fortunately, single slabs are the building blocks of a sandwich structure. The function of each building block can still be analyzed with a single slab model. Hence, what is needed is to find a way to feature the cascading of the individual slabs.

Consider the two-slab sandwich in Fig. 3.11. As in the case of single slab structure, the function of the sandwich as a whole can be , characterized by a Jones matrix $M_T(J, J')$, with which we have:

$$\vec{T}(J, J') = M_T(J, J')\vec{I}(J') \tag{3.68}$$

where the vectors are Jones vectors with two complex components. Obviously, according to the previous sections, each of the two slabs can be characterized with a set of Jones matrices. For the first slab, we may have $M_T^{(1)}(J'', J')$ for $J'' = 0, 1, 2, ...N''$. For the second slab, we may have $M_T^{(2)}(J, J'')$ where $J'' = 0, 1, 2, ...N''$ and $J = 0, 1, 2...N$. The outputs of the first slab are provoked by the input $\vec{I}(J')$ and, in turn, are the input of the second slab. Each input can be diffracted by the second slab and split into various orders of the output. Since it is assumed that the grating slab is a linear device, each output

order is the sum of the output provoked by all the individual inputs:

$$\begin{aligned}\vec{T}(J,J') &= \sum_{J''}\vec{T}(J,J'') \\ &= \sum_{J''}M_T^{(2)}(J,J'')\vec{T}(J'',J') \\ &= \{\sum_{J''}M_T^{(2)}(J,J'')M_T^{(1)}(J'',J')\}\vec{I}(J')\end{aligned} \tag{3.69}$$

Compared with Eq. (3.68), we have:

$$M_T(J,J') = \sum_{J'}M_T^{(2)}(J,J'')M_T^{(1)}(J'',J') \tag{3.70}$$

Apparently, both $M_T^{(2)}(J,J'')$ and $M_T^{(1)}(J'',J')$ can be found using the previously introduced algorithm, and $M_T(J,J')$ can thus be found without difficulty.

For simplicity, a characterization matrix $\mathcal{M}_T$ may be defined for slab or slab sandwich. It is a two-dimensional array with Jones matrices as its elements. The element matrix of row J and column J' is $M_T(J,J')$. With the definition, Eq. (3.70) can be expressed as:

$$\mathcal{M}_T = \mathcal{M}_T^{(2)}\mathcal{M}_T^{(1)} \tag{3.71}$$

which is the product of the two matrices for the two individual slabs. This result can be generalized to the case of n sandwiched slabs, after the matrices of each individual slab is found with the algorithm presented in the previous sections. The matrix characterizing the sandwich can be expressed as:

$$\mathcal{M}_T = \mathcal{M}_T^{(n)}\mathcal{M}_T^{(n-1)}\cdots\mathcal{M}_T^{(2)}\mathcal{M}_T^{(1)} \tag{3.72}$$

One problem we may have here is the neglected reflected diffraction orders. In the case of the two-layered structure, a more precise expression than Eq. (3.71) is:

$$\mathcal{M}_T = \mathcal{M}_T^{(2)}\mathcal{M}_T^{(1)} + \sum_{i=1}^{\infty}\mathcal{M}_T^{(2)}\{\mathcal{M}_R^{(1)}\mathcal{M}_R^{(2)}\}^i\mathcal{M}_T^{(1)} \tag{3.73}$$

where $\mathcal{M}_R^{(1)}$ and $\mathcal{M}_R^{(2)}$ are the reflection matrices. The physical insight that Eq. (3.73) provides is that light can be reflected by the second slab to the first and then back to

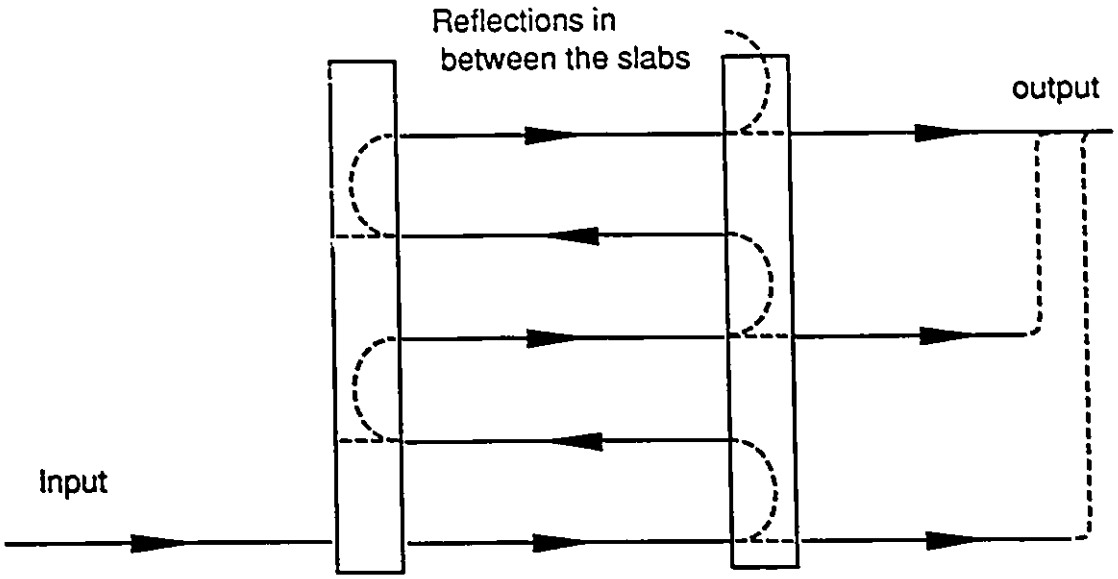

Figure 3.12: The reflections in between two sandwiched slabs.

the second. The reflections can happen more than once, as Fig. 3.12 shows. Actually, for precise modelling of multiple slab couplers, the most efficient treatment is to consider all the boundaries in between the slabs and solve a linear equation set similar to Eq. (3.36)-(3.39). In other words, the whole sandwich has to be considered as a single unit. However, for a well designed grating slab, the reflection diffractions can be very weak. In fact, it is a common practice to neglect the reflected diffractions of a transmission hologram. Apparently, the algorithm introduced in the previous sections can help to optimize the design of each grating slab so as to minimize the reflections. In this case, the matrix multiplication Eq. (3.72) can be employed for solving practical problems, for its simplicity.

3.5 Computation and Examples

The algorithm introduced in the previous sections has been implemented in FORTRAN. The resulting computer program is given in Appendix D. In this section, some technical details will be discussed, followed by two numerical examples.

Recall that in Section 3.2.3, we have introduced a one-dimensional index J to label the terms (or orders) in Eq. 3.11. This practice was first used in [50], but no detailed discussion was provided. It turns out that, in practice, the use of a single-number index is a rather important issue. The reason lies in the fact that we cannot include an infinite number of terms (or orders) in a practical computation program. Expression (3.11), thus all the other relevant expressions, have to be truncated. This means that we have to include only the "significant" terms and give up the rest. When the M-dimensional index $\mathbf{m}$ is used, truncation can be done by selecting a lower bound L_i and an upper bound U_i for each integer index m_i to limit the size of each dimension, i.e., we let

$$L_i \leq m_i \leq U_i \tag{3.74}$$

However, this is not a very efficient way, because it may lead to the inclusion of too many orders. The total number of the orders included is $\prod_{i=1}^{M}(U_i - L_i + 1)$. Suppose in order to include one more significant order into our consideration, K_1 has to be increased by 1. The actual increase in the total number will be $\prod_{i=2}^{M}(U_i - L_i + 1)$ which may be much larger than one. The extra terms added to the collection may not be significant at all and will simply waste the computation time. For a rough estimate, suppose the size of each dimension is $U_i + L_i + 1 = N_t$, the minimum increment in the total number will be N_t^{M-1}. This represents a rather rapid increase rate, and the computation time will increase even faster. To mitigate this problem, the most efficient way to keep the total number of terms as low as possible is to pick up the significant orders one by one, based on the experience and the understanding of the diffraction process. For example, for a two- grating slab, suppose the incident wave is in the direction of the order $\mathbf{m} = (0,0)$, then $(0,0)$ is always the most significant order. The second most important orders are $(-1,0)$, $(0,-1)$, $(1,0)$ and $(0,1)$, which are the direct neighbours of the incident wave. However, if it is known that the Bragg condition is satisfied between $(0,0)$ and $(1,0)$, we know that the order $(1,0)$ is more significant than the order $(-1,0)$. Similarly, if the Bragg condition is more closely satisfied between $(0,0)$ and $(0,-1)$, $(0,-1)$ is more significant than $(0,1)$. So in this case, the bottom-line truncation is to keep the three

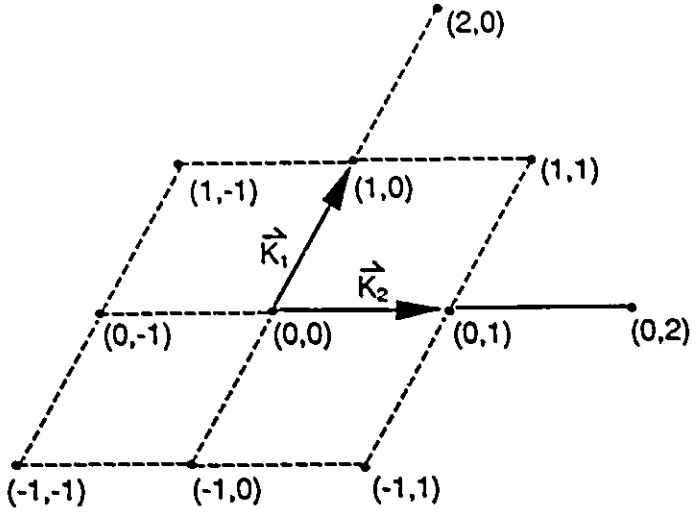

Figure 3.13: Diffraction orders of a two-grating system.

most important orders and neglect the rest. Obviously, this cannot be done by limiting the size of each dimension of m. It can only be done by investigating every individual diffraction order. For convenience in programing, a serial number can be assigned to each of the three orders. For example, $J = 0$ for $(0,0)$, $J = 1$ for $(1,0)$ and $J = 3$ for $(0,-1)$. Notice that, the assignment of J to m is not unique. There are many equivalent ways. For the same example, we may have $J = 0$ for $(0,-1)$, $J = 1$ for $(0,0)$ and $J = 2$ for $(1,0)$, etc. Therefore, a table, or a function in the form of $\mathrm{m}(J)$ is listed as an input parameter in the computation program. It serves as an interface through which a researcher can use his knowledge and understanding to make the simulation process efficient. The next most significant orders may be included for increasing the precision. These orders must be those neighbouring the orders of the higher priority. In the above mentioned example, the next most significant orders are $(-1,0)$, $(1,-1)$, $(0,-2)$, $(2,0)$, $(-1,-1)$ and $(1,1)$. An illustration about these orders is presented in Fig. 3.13. The number of orders under consideration can be further increased, at the expense of a longer computing time, until the required precision is achieved.

Another important issue is the validity of the theory and the computation program.

Presently, it is rather difficult to verify the theory by an experiment due to limitations in the optical measurements. For example, there has not been a way to measure the refractive index modulation directly. However, support may still be obtained by comparing the numerical results with those of the existing theories.

One important theory is the Kogelnik's coupled wave theory. It has been widely accepted as a theory that gives a good approximation to the diffraction of single volume gratings. Single grating diffraction is a special case of multi-grating diffraction that is modelled in this thesis. Therefore, comparison can be made between these two theories. The author has designed an example, possessing the desired qualities for Kogelnik's approximations, such as low modulation (0.001), presence of only two waves (achieved by using an incident angle of 60°), perpendicular polarization and near Bragg incidence. The refractive indices of region R and T are assumed to be 1.5 which matches the average index of region G. Computation results from both theories are shown in Fig. 3.14, where a very good match can be observed. The same result is also shown in Fig. 3.15 with a logarithmic scale. In both figures, the diffraction efficiency is plotted against the wavelength deviation from the Bragg condition. The example was originally proposed as a WDM filter. Since Kogelnik's theory is an approximate one, the mismatch in the results is not a surprise. The presented theory has also been compared with some existing rigorous theory. Perfect match is obtained. Fig. 3.16 shows a simulation result obtained by running the program listed in Appendix D of the thesis. It perfectly matches the result shown in Fig. 5 of [53]. This offers a strong support for the theory and the simulation program presented in this thesis.

Finally, a very effective way to check the validity is to apply the law of conservation of energy (or power). Since it is the light field that is simulated with Maxwell's equations, it is very much unlikely that this law happens to be satisfied when there is any mistake in the theory or the program. By checking the sum of the output power of all the output orders and comparing the sum with that of the input, a few mistakes in the program had been successfully located and corrected.

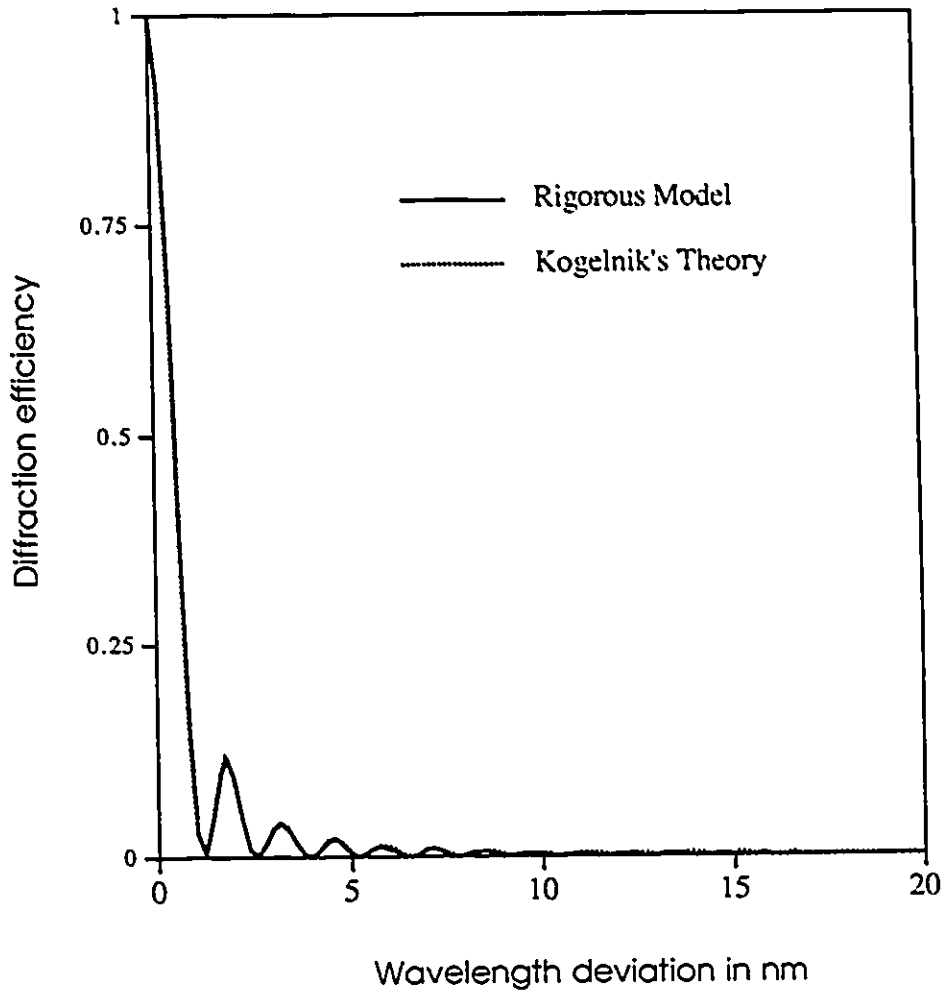

Figure 3.14: Comparison between numerical results of Kogelnik's theory and that of the theory presented in this thesis. In this example, $n_R = n_T = n_0 = 1.5$, $\Delta = 0.001$, $\lambda = 1.0\ \mu m$, $K_x = K_z = 0$, $K_y = 16.32\ \mu m^{-1}$ and the incident angle $\theta = 60°$.

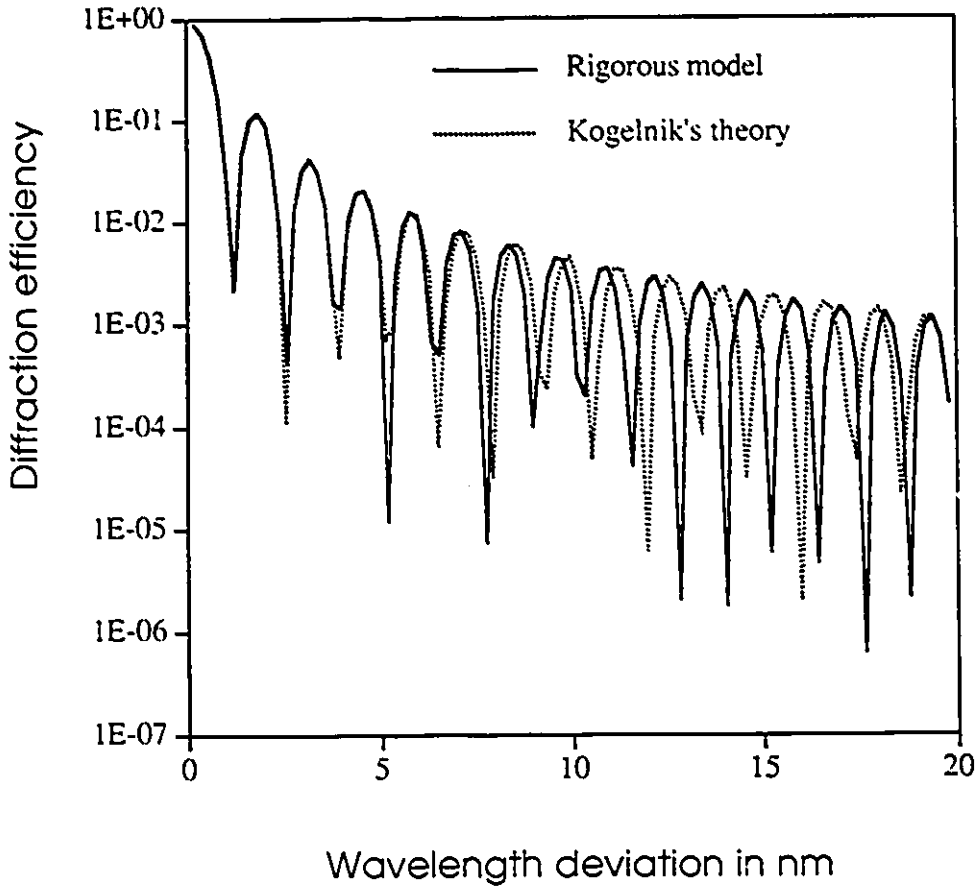

Figure 3.15: The same comparison as Fig. 3.14 in a lograrithmic scale.

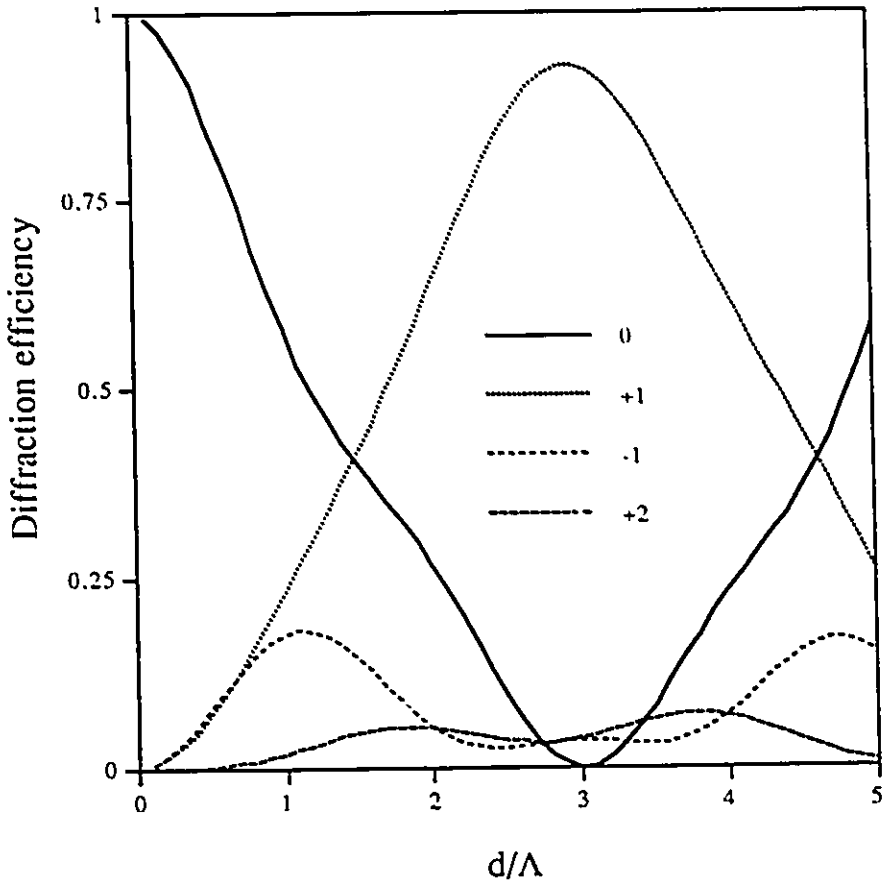

Figure 3.16: Simulation result for the example shown in Fig. 5 of [53], where $n_R = n_T = n_0 = 1.5$, $\lambda = 1.0\ \mu m$, $K_x = -3.273\ \mu m^{-1}$, $K_y = K_z = 0$, $\Delta = 0.0603$, $k_x(0) = 1.637\ \mu m^{-1}$ and $k_y(0) = 0$.

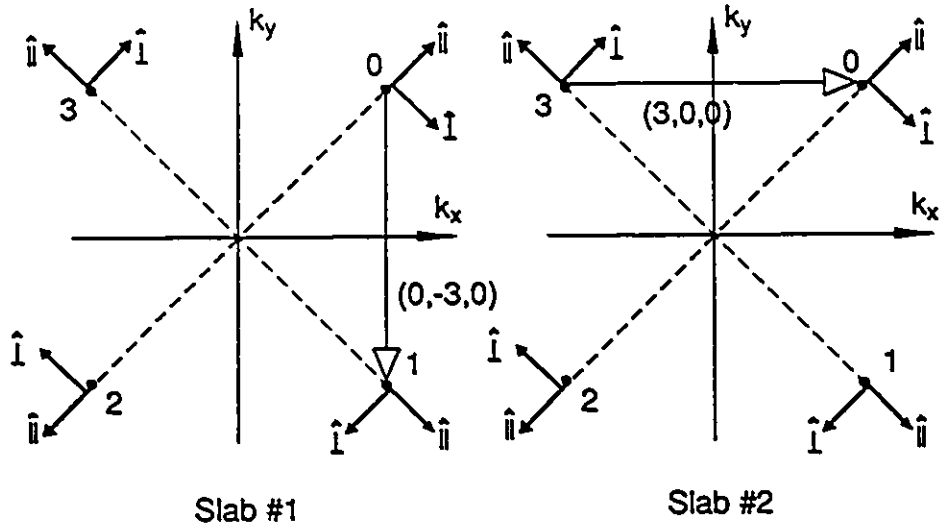

Figure 3.17: Grating vectors, wave vectors and the field vectors in a 4 × 4 coupler design.

Next we will show two computational examples through which more details about the computation technique will be presented. We will first show a design of a 4 × 4 coupler—a perfect example to start with because of the simplicity.

As shown in Section 2.3, the slab sandwich of a 4 × 4 coupler is composed of 2 identical single-grating slabs. The four input / output directions are arranged in such a way that two grating degenerations can be obtained. Here, we give a design based on the configuration shown in Fig. 2.4, assuming that the GRIN lenses have a diameter of 1.5 *mm* and a length of 3 *mm*. The fibers are mounted on the rims of the end surfaces of the lenses, and the four fibers are located in a pattern symmetrical about the axis of the lenses. So in the k-space, see Fig. 3.17, we have four wave vectors specified as:

$$\begin{cases} \vec{k}_{\rho,0} = (\kappa, \kappa) \\ \vec{k}_{\rho,1} = (\kappa, -\kappa) \\ \vec{k}_{\rho,2} = (-\kappa, -\kappa) \\ \vec{k}_{\rho,3} = (-\kappa, \kappa) \end{cases} \tag{3.75}$$

where $\kappa = \frac{2\pi n_R}{\lambda} \frac{1.5mm/2}{\sqrt{(1.5mm/2)^2+(3mm)^2}} \cos\frac{\pi}{4}$. Assume the refractive indices are matched, i,e.,

$n_R = n_0 = n_T = 1.5$, and $\lambda = 0.8\ \mu m$, then $\kappa = 2.0204\ (\frac{1}{\mu m})$. The grating vectors are chosen to be $(0, -4.0408\ (\frac{1}{\mu m}), 0)$ for the first slab and $(4.0408\ (\frac{1}{\mu m}), 0, 0)$ for the second slab, according to the Bragg condition. One important feature about this design is the perfect symmetry of the arrangement. This is an advantage, which we can exploit in the computation. First, only one slab need be evaluated, the second one is merely a rotated version of the first one. Secondly, only one incident direction needs be considered, the others are again the rotated version of the first one. Suppose we consider the first slab and the first incident direction—the one indicated by $\vec{k}_{\rho,0} = (2.0204\ (\frac{1}{\mu m}), 2.0204\ (\frac{1}{\mu m}))$; assume $\Delta = 0.025$; and neglect all the high order diffractions. We get the result shown in Fig. 3.18. Notice that in the figure, the reflections are not shown, because they are not significant in magnitude. Besides, for simplifying the presentation, we have not given the phase characteristics, assuming that only the power transmission properties are interesting in the application. Furthermore, for practical purpose, instead of using the complex amplitude coupling coefficient $t_{g,h}$ $(g, h = \perp, \parallel)$, we have defined the following set of quantities:

$$CT_{gh}(J, J') = |t_{gh}(J, J')|^2 \frac{\cos\theta_T(J)}{\cos\theta_R(J')} \tag{3.76}$$

These coefficients can be called polarization-dependent power transfer coefficients (PTCs). For example, $CT_{\perp\parallel}(J, J')$ is the coefficient of power transfer from order J', with a parallel polarization, to order J, with a perpendicular polarization. We may also define another set of coefficients:

$$PT_{gh}(J, J') = \angle[t_{gh}(J, J')] \quad for \ \ g, h = \perp, \parallel \tag{3.77}$$

which represents the phase of $t_{gh}(J, J')$. Similarly, for the reflection Jones matrices $M_R(J, J')$, we may have:

$$\begin{cases} CR_{gh}(J, J') = |r_{gh}|^2 \frac{\cos\theta_R(J)}{\cos\theta_R(J')} \\ PR_{gh}(J, J') = \angle(r_{gh}(J, J')) \\ g, h = \perp, \parallel \end{cases} \tag{3.78}$$

Since $t_{gh}(J, J')$ can be uniquely determined by $CT_{gh}(J, J')$ and $PT_{gh}(J, J')$, where $CT_{gh}(J, J')$

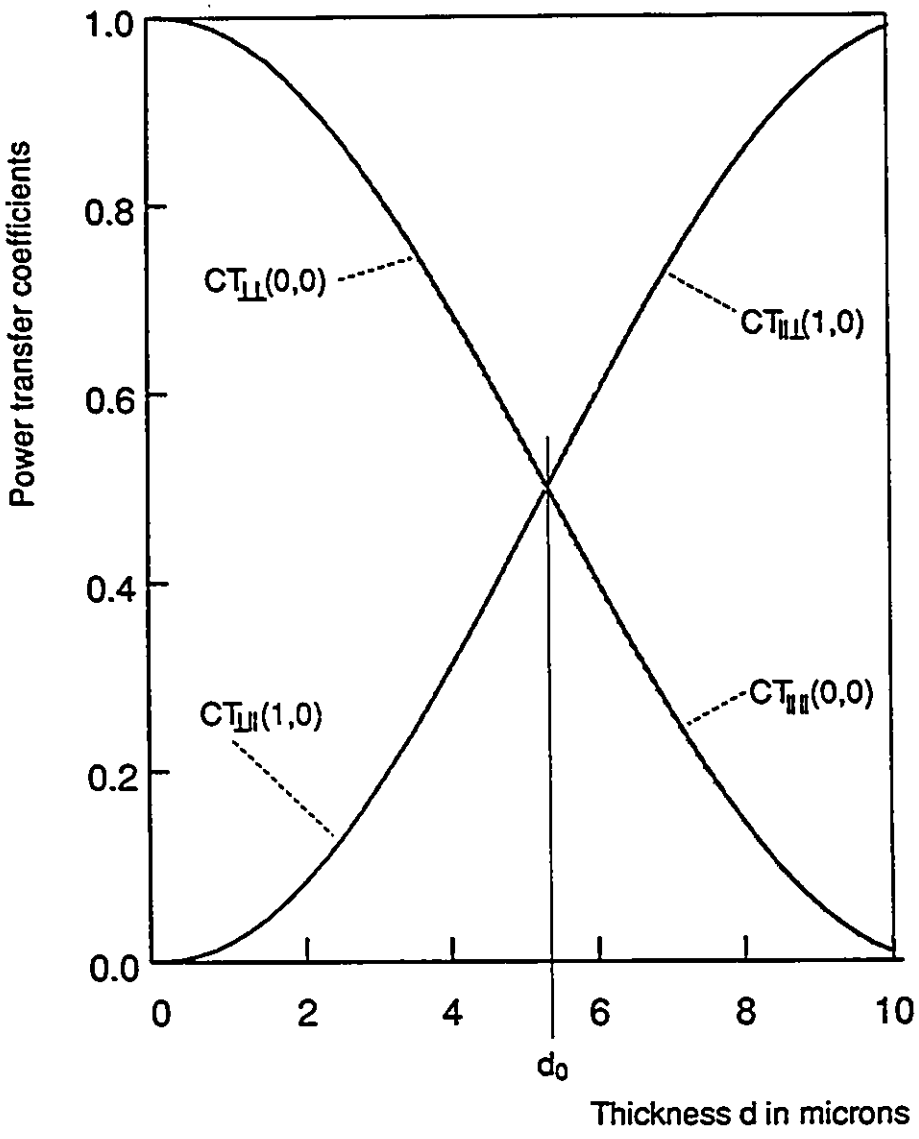

Figure 3.18: Computation results for a 4 × 4 coupler.

determines the amplitude, though it is mapped to the power domain; $PT_{g\lambda}(J, J')$ determines the phase, we may write the Jones matrices $M_T(J, J')$ as:

$$M_T(J,J') = \begin{bmatrix} (CT_{\perp\perp}(J,J');\ PT_{\perp\perp}(J,J')) & (CT_{\perp\parallel}(J,J');\ PT_{\perp\parallel}(J,J')) \\ (CT_{\parallel\perp}(J,J');\ PT_{\parallel\perp}(J,J')) & (CT_{\parallel\parallel}(J,J');\ PT_{\parallel\parallel}(J,J')) \end{bmatrix} \tag{3.79}$$

and similarly:

$$M_R(J,J') = \begin{bmatrix} (CR_{\perp\perp}(J,J');\ PR_{\perp\perp}(J,J')) & (CR_{\perp\parallel}(J,J');\ PR_{\perp\parallel}(J,J')) \\ (CR_{\parallel\perp}(J,J');\ PR_{\parallel\perp}(J,J')) & (CR_{\parallel\parallel}(J,J');\ PR_{\parallel\parallel}(J,J')) \end{bmatrix} \tag{3.80}$$

Apparently, the new way of writing Jones matrices is different from the way used in Section 3.2.6. However, it is equivalent to the former. In practice, the use of PTCs brings enormous convenience, because power is a more frequently used quantity than the field amplitude in any coupler application.

In this particular example, if we let $d = d_0 = 5.3125\ \mu m$, using the presentation with PTCs, we have the following computed matrices:

$$M_T(0,0) = \begin{bmatrix} (0.503; -0.55) & (0.000; -0.56) \\ (0.000; -0.56) & (0.502; -0.55) \end{bmatrix} \tag{3.81}$$

$$M_T(1,0) = \begin{bmatrix} (0.000; -0.60) & (0.497; -0.55) \\ (0.497; -0.54) & (0.001; -0.54) \end{bmatrix} \tag{3.82}$$

$$M_R(0,0) = \begin{bmatrix} (0.000; 0.00) & (0.000; 0.00) \\ (0.000; 0.00) & (0.000; 0.00) \end{bmatrix} \tag{3.83}$$

$$M_R(1,0) = \begin{bmatrix} (0.000; 0.00) & (0.000; 0.00) \\ (0.000; 0.00) & (0.000; 0.00) \end{bmatrix} \tag{3.84}$$

Since the phase characteristics are not so important, we may neglect the phase part and obtain a simpler representation:

$$M_T(0,0) = \begin{bmatrix} 0.503 & 0.000 \\ 0.000 & 0.502 \end{bmatrix} \tag{3.85}$$

$$M_T(1,0) = \begin{bmatrix} 0.000 & 0.497 \\ 0.497 & 0.000 \end{bmatrix} \tag{3.86}$$

$$M_R(0,0) = \begin{bmatrix} 0.000 & 0.000 \\ 0.000 & 0.000 \end{bmatrix} \tag{3.87}$$

$$M_R(1,0) = \begin{bmatrix} 0.000 & 0.000 \\ 0.000 & 0.000 \end{bmatrix} \tag{3.88}$$

Apparently, the reflections are very weak and insignificant. Therefore, next we will focus our attention on the transmission matrices. From the Expressions (3.85) and (3.86), using the symmetry of the coupler structure, we may have the following results for the first slab without doing any extra computation:

$$M_T(1,1) = M_T(2,2) = M_T(3,3) = \begin{bmatrix} 0.503 & 0.000 \\ 0.000 & 0.502 \end{bmatrix} \tag{3.89}$$

$$M_T(0,1) = M_T(3,2) = M_T(2,3) = \begin{bmatrix} 0.000 & 0.497 \\ 0.497 & 0.000 \end{bmatrix} \tag{3.90}$$

$$M_T(2,1) = M_T(1,2) = M_T(0,3) = M_T(3,0) = \begin{bmatrix} 0 & 0 \\ 0 & 0 \end{bmatrix} \tag{3.91}$$

$$M_T(2,0) = M_T(0,2) = M_T(1,3) = M_T(3,1) = \begin{bmatrix} 0 & 0 \\ 0 & 0 \end{bmatrix} \tag{3.92}$$

All these matrices can be put together to form a large matrix called the characteristic matrix. It characterizes the power transmission properties of the first slab:

$$\mathcal{M}_1 = \begin{pmatrix} & \vdots & \\ \cdots & M_T(J,J') & \cdots \\ & \vdots & \end{pmatrix} \tag{3.93}$$

$$= \begin{pmatrix} \begin{bmatrix} 0.503 & 0 \\ 0 & 0.502 \end{bmatrix} \begin{bmatrix} 0 & 0.497 \\ 0.497 & 0 \end{bmatrix} & 0 & 0 \\ \begin{bmatrix} 0 & 0.497 \\ 0.497 & 0 \end{bmatrix} \begin{bmatrix} 0.503 & 0 \\ 0 & 0.502 \end{bmatrix} & 0 & 0 \\ 0 & \begin{bmatrix} 0.503 & 0 \\ 0 & 0.502 \end{bmatrix} \begin{bmatrix} 0 & 0.497 \\ 0.497 & 0 \end{bmatrix} \\ 0 & \begin{bmatrix} 0 & 0.497 \\ 0.497 & 0 \end{bmatrix} \begin{bmatrix} 0.503 & 0 \\ 0 & 0.502 \end{bmatrix} \end{pmatrix} \tag{3.94}$$

In a similar way, for the second slab, we have:

$$\mathcal{M}_2 = \begin{pmatrix} \begin{bmatrix} 0.503 & 0 \\ 0 & 0.502 \end{bmatrix} & 0 & 0 & \begin{bmatrix} 0 & 0.497 \\ 0.497 & 0 \end{bmatrix} \\ 0 & \begin{bmatrix} 0.503 & 0 \\ 0 & 0.502 \end{bmatrix} \begin{bmatrix} 0 & 0.497 \\ 0.497 & 0 \end{bmatrix} & 0 \\ 0 & \begin{bmatrix} 0 & 0.497 \\ 0.497 & 0 \end{bmatrix} \begin{bmatrix} 0.503 & 0 \\ 0 & 0.503 \end{bmatrix} & 0 \\ \begin{bmatrix} 0 & 0.497 \\ 0.497 & 0 \end{bmatrix} & 0 & 0 & \begin{bmatrix} 0.503 & 0 \\ 0 & 0.502 \end{bmatrix} \end{pmatrix} \tag{3.95}$$

The characteristic matrix of the two-slab sandwich can be found as:

$$\mathcal{M} = \mathcal{M}_2\mathcal{M}_1 = \begin{pmatrix} \begin{bmatrix} 0.253 & 0 \\ 0 & 0.252 \end{bmatrix} \begin{bmatrix} 0 & 0.250 \\ 0.250 & 0 \end{bmatrix} & \begin{bmatrix} 0.247 & 0 \\ 0 & 0.247 \end{bmatrix} \begin{bmatrix} 0 & 0.250 \\ 0.250 & 0 \end{bmatrix} \\ \begin{bmatrix} 0 & 0.250 \\ 0.250 & 0 \end{bmatrix} \begin{bmatrix} 0.253 & 0 \\ 0 & 0.252 \end{bmatrix} & \begin{bmatrix} 0 & 0.250 \\ 0.250 & 0 \end{bmatrix} \begin{bmatrix} 0.247 & 0 \\ 0 & 0.247 \end{bmatrix} \\ \begin{bmatrix} 0.247 & 0 \\ 0 & 0.247 \end{bmatrix} \begin{bmatrix} 0 & 0.250 \\ 0.250 & 0 \end{bmatrix} & \begin{bmatrix} 0.253 & 0 \\ 0 & 0.252 \end{bmatrix} \begin{bmatrix} 0 & 0.250 \\ 0.250 & 0 \end{bmatrix} \\ \begin{bmatrix} 0 & 0.250 \\ 0.250 & 0 \end{bmatrix} \begin{bmatrix} 0.247 & 0 \\ 0 & 0.247 \end{bmatrix} & \begin{bmatrix} 0 & 0.250 \\ 0.250 & 0 \end{bmatrix} \begin{bmatrix} 0.253 & 0 \\ 0 & 0.252 \end{bmatrix} \end{pmatrix} \tag{3.96}$$

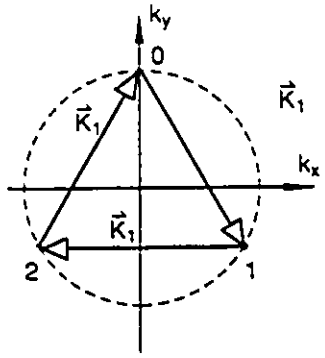

Figure 3.19: A design of 3×3 coupler.

This matrix represents a satisfactory 4×4 coupler. The power is virtually evenly distributed, and an important observation in this example is that a coupler made from holographic gratings can be made essentially polarization insensitive.

The second example is a 3×3 star coupler. In [30, 31], multiple gratings are arranged in a mesh-like pattern to build $N \times N$ couplers. As it is shown in Fig. 2.10, a 3×3 coupler consists of 3 gratings. Since we have assumed multiple gratings in the simulation model, the computation package can be used to simulate a 3×3 coupler. Furthermore, because the model is a three- dimensional one, we can easily add one more dimension to the grating-arrangement pattern. The design pattern is shown in Fig. 3.19. Again the configuration shown in Fig. 2.4 is used and the GRIN rod lenses have a diameter of 1.5 mm and a length of 3 mm. The coordinates of the wave vectors in the k-space, is determined as follows: let

$$\kappa = \frac{2\pi n_R}{\lambda} \frac{0.75\ mm}{\sqrt{(0.75\ mm)^2 + (3\ mm)^2}},$$

then

$$\vec{k}_{\rho,0} = (0, \kappa) \tag{3.97}$$

$$\vec{k}_{\rho,1} = (\frac{\sqrt{3}}{2}\kappa, -\frac{1}{2}\kappa) \tag{3.98}$$

$$\vec{k}_{\rho,2} = (-\frac{\sqrt{3}}{2}\kappa, -\frac{1}{2}\kappa) \tag{3.99}$$

This is again a symmetrical pattern. The grating vectors are:

$$\vec{K}_1 = (\frac{\sqrt{3}}{2}\kappa, -\frac{3}{2}\kappa, 0) \tag{3.100}$$

$$\vec{K}_2 = (-\sqrt{3}\kappa, 0, 0) \tag{3.101}$$

$$\vec{K}_3 = (\frac{\sqrt{3}}{2}\kappa, \frac{3}{2}\kappa, 0) \tag{3.102}$$

Now suppose the relative modulation indices $\Delta_1 = \Delta_2 = \Delta_3 = 0.018$, the phases $\phi_1 = \phi_2 = \phi_3 = 0$, and the incident wave is in the direction of $\vec{k}_{p,0}$, we then have the result shown in Fig. 3.20 where we notice that when the incident wave is perpendicularly polarized, the output power in the order J is $CT_{\perp\perp}(J,0) + CT_{\parallel\perp}(J,0)$. Similarly, when the incident wave is in a polarization state parallel to the incident plane, the output power in order J is $CT_{\perp\parallel}(J,0) + CT_{\parallel\parallel}(J,0)$. To split the input light as uniform as possible, the thickness d is chosen to be $d_0 = 6.750$ microns, as it is shown in Fig. 3.20. For this thickness, we have

$$M_T(0,0) = \begin{bmatrix} 0.307 & 0.000 \\ 0.000 & 0.350 \end{bmatrix} \tag{3.103}$$

$$M_T(0,0) = \begin{bmatrix} 0.091 & 0.256 \\ 0.256 & 0.069 \end{bmatrix} \tag{3.104}$$

where the phase has been neglected as we have done for the 4×4 coupler. Besides, the reflections are so weak that they can be basically omitted. When all the Jones matrices are put together, we may have a matrix characterizing the 3×3 coupler:

$$\mathcal{M} = \left(\begin{bmatrix} 0.307 & 0 \\ 0 & 0.350 \end{bmatrix} \begin{bmatrix} 0.091 & 0.256 \\ 0.256 & 0.069 \end{bmatrix} \begin{bmatrix} 0.091 & 0.256 \\ 0.256 & 0.069 \end{bmatrix} \right. \\ \begin{bmatrix} 0.091 & 0.256 \\ 0.256 & 0.069 \end{bmatrix} \begin{bmatrix} 0.307 & 0 \\ 0 & 0.350 \end{bmatrix} \begin{bmatrix} 0.091 & 0.256 \\ 0.256 & 0.069 \end{bmatrix} \\ \left. \begin{bmatrix} 0.091 & 0.256 \\ 0.256 & 0.069 \end{bmatrix} \begin{bmatrix} 0.091 & 0.256 \\ 0.256 & 0.069 \end{bmatrix} \begin{bmatrix} 0.307 & 0 \\ 0 & 0.350 \end{bmatrix} \right) \tag{3.105}$$

Also, notice that the symmetry of the Jones matrices results from the use of the natural coordinate systems introduced in Section 3.2.4, in which each diffraction order is described

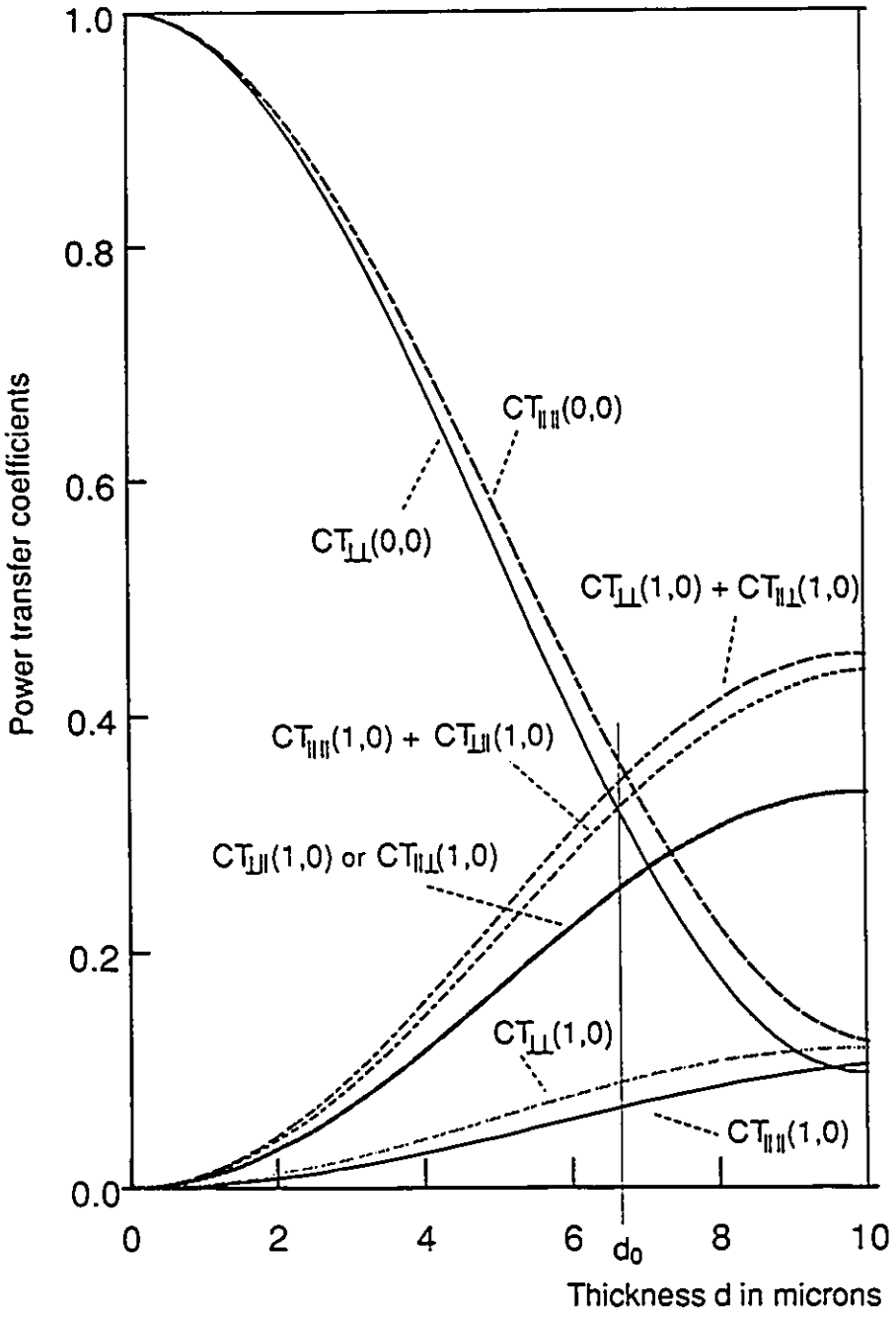

Figure 3.20: Computation results for a 3 × 3 coupler.

with respect to a reference based on its own parameters. Therefore, all the diffraction orders are treated "equal". It is discovered that with such natural reference systems, great convenience can be obtained to explore the symmetry of the design patterns.

3.6 Conclusion

In this chapter, we have presented a rigorous model for numerical simulation or analysis of the grating diffraction process in a grating-based component.

The derivation of the algorithm is strictly based on Maxwell's equations. The core of the algorithm is a set of linear equations, called mode equations. They form a generalized eigensystem. An important feature of the model is the use of natural reference systems which make the mode equations simple and the exploration of symmetrical structures easy. The grating slabs are characterized with a set of Jones matrices, which makes the study of polarization efficient. Furthermore, the model is a multiple grating diffraction model, which can be used for any single-slab holographic grating system. It has also been pointed out that a multi-slab structure can be depicted by the multiplication of characterization matrices of the individual slabs. Two examples are presented at the end of the chapter.

Chapter 4

Summary and Future Research Work

4.1 Summary

In this thesis, we have shown that

1. In order to get the desired efficiency, fiber mode matching has to be taken into account. Three possible configurations using lenses, GRIN lenses and fiber tapers are proposed. All of them meet the fiber mode matching requirement.

2. A holographic grating can be shared by waves from a number of pairs of fibers, which implies that a single grating can be used as a number of 2×2 couplers in parallel; the technique used to realize the sharing of a grating is termed grating degeneration in this thesis and is subject to the constraints imposed by the Bragg condition. Grating degeneration can be used to reduce the number of gratings required in a star coupler.

3. The grating system of a star coupler can be viewed as a network of gratings; the topology of such a network can be changed to a multi-stage one if multiple grating-bearing slabs are allowed to be sandwiched together in a cascade manner. This

design is termed as sandwich structure. It can be used for reducing the difficulty in the coupler implementation.

4. Grating degeneration and sandwich structure can be combined and applied in one design. By doing so, the required number of gratings can be significantly decreased. For example, a 16×16 coupler requires 256 gratings generally or 120 gratings when the zero orders are used, as in the design shown in [30]. However, in a design with grating degeneration and sandwich structure, a total number of 12 gratings are used and are distributed among four grating slabs with at most four gratings in one slab.

5. The number of gratings can be further reduced by using the so called quasi-Bragg diffraction. When a certain amount of violation of the Bragg condition is deliberately introduced in a coupler design, only two gratings are required in a 16×16 coupler. The key to this technique is to make the violation of Bragg conditions much smaller for the wanted waves than the unwanted ones.

6. The design of a wavelength-routing coupler requires arranging $2N$, rather than N, distinct directions, because the zeroth orders cannot be used for wavelength routing.

7. Grating degeneration can also be used in a routing coupler. In the example of 8×8 routing coupler, six, instead of sixteen gratings are used if the wavelengths of a WDM network can be used as design parameters.

In a second part of this thesis, a mathematical model for simulating or analyzing the diffraction of a grating system is presented. The model is rigorously based on the Maxwell's equations and thus can be used to study every aspect of the grating diffraction. The core of the algorithm is a set of model equations derived under a set of natural coordinate systems. These equations form a generalized eigen-system. A set of Jones matrices are used to characterize a grating system constructed on a dielectric slab. This makes it possible to take the polarization responsivity of the coupler into account.

4.2 Suggestions for the Future Work

The author believes that the work presented in this thesis is the point of departure for future research activities in a few distinct directions.

In one direction, experimental fabrication should be started as soon as possible. The first target should be to build a 4×4 multimode fiber star coupler. The significance of doing so is two-fold. Firstly, a 4×4 star is the simplest structure that contains the most important concepts presented in this work. Therefore, its fabrication is the easiest way to verify these concepts. In addition, the coupler does not introduce any unknown difficulties in the fabrication process. Though the four-fiber array alignment requires a special custom-made positioner, it is not a very difficult task because of the use of multimode fiber. The typical precision requirement for multi-mode fiber alignment is in the order of a few microns which can be achieved easily with the conventional mechanical designs. Secondly, multi-mode fiber star couplers are expected to be widely used in the near future in photonic local area networks (LANs), and therefore the fabrication of holographic multimode star couplers may have a high commercial value. In a LAN, the short transmission distance makes the fiber dispersion insignificant, the use of multi-mode fiber will thus likely be favoured, simply due to the lower cost. The core of this 4×4 coupler will be two identical holographic gratings sandwiched with one of them rotated about its normal line by 90°. Since the fiber tapers are relatively new components and are not widely used, the configuration shown in Fig. 2.3 and 2.4 are suggested. The recording material used for grating fabrication is likely to be DCG, because of its optical quality. Another advantage in using DCG is that the gelatin coating can be prepared with relatively simple facilities. This offers a control over various parameters of the fabricated grating slabs. Notice that DCG is the only available material in which such control can be obtained. With improvements in the alignment technique and skills, this coupler can be easily developed into a 4×4 single-mode fiber star coupler. There are obviously no fundamental reasons against this development. The next step to follow is to fabricate a 16×16 star coupler. For this coupler, the technique of quasi-Bragg diffraction can be

practiced. The benefit obtained would be that only two gratings have to be constructed on each of the four slabs, as shown in Fig. 2.31. Again, multimode fiber couplers should be tried first because of their commercial value. The version for single mode fibers should follow with the improvement of alignment techniques. In fact, a great deal of research work should be put on the issue of fiber-slab interfacing, especially for couplers with $N > 16$. Research in this area should never be neglected.

A second direction of future work is in the numerical analysis and design based on the model given in this thesis. This work will have the following aspects:

1. Optimization of the design parameters. Based on the understanding of the diffraction process, the simulation algorithm should be used to collect data for a numerical analysis. The result can thus help to arrive at the optimized parameters.

2. Grating system designs using quasi-Bragg diffraction. Although in Chapter 2 an intuitive geometric quantity is defined to measure the amount of violation of Bragg condition, a quantitative analysis is still necessary.

3. The bandwidth of a holographic grating can be estimated with the coupled-wave theory [39]. However the theory is an approximate one, and a study has yet to be done based on rigorous theories such as the one presented in this thesis. The study will show the true theoretical limit of the coupler performance under various conditions. It is also a complement to the experimental study which is subject to practical limitations.

4. Since light field is a vector field, it is not unusual that a component responds differently when its direction, or specifically, the polarization changes. The model given in this thesis can be used as a convenient tool to study this issue because of the use of Jones matrices. The author expects that under certain conditions, a coupler can be made insensitive to the polarization by setting the parameters properly, or by using cascaded elements that compensate or cancel the response of the individual components. On the other hand, conditions that result in the highest polarization

sensitivity are equally important, because components that respond to polarization are also useful. Furthermore the author expects that the reflection type gratings may have promising qualities in terms of polarization sensitivity. This has yet to be investigated in future research work.

Another research direction the author suggests is the design and fabrication of wavelength-routing couplers. As it has been pointed out, grating degeneration can be applied to a routing coupler which supports a shuffle topology. However, the author believes that the gratings are still not fully used. In the design given in Section 2.5, each of the gratings is used to convey traffic in one direction. It is understood that a grating can be used for two-way traffic, that is, if a grating is used for the traffic from port A to port B, it can also be used at the same time for the traffic from B to A. It is believed that if the shuffle topology can be modified in a proper way, traffics in both directions can be accommodated and this may result in a more simplified and a more efficient wavelength routing coupler.

Appendix A

Multi-Beam Spot-Diffusing And Fly-Eye Receivers For Indoor Infrared Wireless Communications—Concepts and Design Issues

The purpose of using wireless communications systems in an indoor environment is to eliminate wiring. As the number of personal computers, work stations and other user terminals increases, communication cable wiring becomes a considerable problem. A rewiring job not only involves substantial cost, but also loss of valuable time. In addition, exposed wiring can be potentially dangerous and unsightly. Obviously, employing wireless systems is at least one of the solutions to this wiring problem.

In implementation of a wireless system, a choice must be made between radio waves and infrared radiation. Since radio waves can penetrate most obstacles in a building structure, communication can be allowed theoretically between any two points in a building and even between neighbouring buildings. However, radio systems are subject to radio

wave control regulations, and they are also vulnerable to electromagnetic interference which is more than abundant in environments such as factories, metropolitan areas, etc.

Infrared radiation can be well confined within a room. This is disadvantageous in terms of wireless communications, because cables are still needed for communication links in between rooms. However, the absence of any potential interference makes an infrared system free from any governmental regulations, which makes an infrared system desirable in many circumstances.

There are basically two types of indoor infrared radiation systems. One uses diffused radiation [54] and the other employs line-of-sight transmission links [55]. The advantage of a diffused radiation system is its operational simplicity due to lack of alignment necessity. However, the negative aspects include inefficient power transmission, multipath effects and the wide angle acceptance of ambient lights. The bulk result is a low data rate. On the contrary, a line-of-sight system can have a bit rate a few orders of magnitude higher due to a higher power transmission efficiency, a small field-of-view and a single transmission path. Nevertheless, the line-of-sight can be easily blocked and the alignment requires high mechanical stability for the optical antenna systems. This, to some extent, contradicts the original purpose of a wireless system.

Some novel configurations have been proposed and implemented [56][57]. An interesting experimental LAN was reported as RADICOM [57], in which a satellite called "reflector" is mounted in the ceiling. This implies a broad 120° beam of 300 mW infrared power. The terminal station transceiver beam has a narrow beamwidth of about 10°. FSK modulation at two different subcarrier frequencies is used for the up-links and the down-links to help isolate the links in two directions. The system demonstrated data transmission up to 1 Mbps at a distance of 5 m with an error rate less than 10^{-7}. This system is basically a line-of-sight system, except the alignment operation of the "reflector" is eliminated due to the use of a wide beam and a wide acceptance angle. Besides, the installation of the active reflectors may turn out to be inconvenient.

A new configuration termed as spot-diffusing multi-line-of-sight was proposed by the

author in the summer of 1990. It includes two new concepts: one is called spot diffusing, the other is the use of multiple lines-of-sight and fly-eye receivers. Experimental work was conducted to test the feasibility of the concepts. Details about this work can be found in [58] [59].

Appendix B

High-Angular Tolerance Receiver For Atmospheric Optical Links

This work started when the author was working as a research associate in 1989. It was ended during the second term of the Ph.D. program in 1990. Some supplemental work was done later with the help of an undergraduate student. The details of the work were published in [60] through [63] and a patent [64] has been approved recently.

The work is based on the idea that an optical taper, a conical optical waveguide with one end larger than the other, can be used to increase the receiving area of a photodiode without increasing its intrinsic capacitance. A large area photodetector can increase the field of view of a receiver used in an atmospheric / free-space optical link, and hence make the alignment easier.

In fact, the optical taper used in this application is employed as a passive power collector. When power collecting is concerned, it is important to distinguish between a non-imaging collector and an imaging collector [65]. Typical imaging collectors are lenses and spherical mirrors.

Image forming components can retain the spatial information on the incoming light beams, but in the field of telecommunications, the spatial information is always lost in the channel anyway. Therefore, a non-imaging component can be used as an alternative

collector. It has been shown that, at the cost of losing the spatial information, a non-imaging system can have a higher light collecting power. To be more specific, an optical taper can have an equivalent $f^{\#}$ - a measure of the light collecting ability - close to 0.5 [66], which is a very difficult figure to achieve for an imaging lens. However, a non-imaging system has a disadvantage of causing dispersion, though this becomes significant only at very high bit rates.

A basic law that should be obeyed in passive light power collection is, as in the case of a star coupler, the second law of thermodynamics. Here it states that the field-of-view of the system multiplied by its geometric magnification in the receiving area remains a constant. The constant is only a function of the system $f^{\#}$. Therefore, given the $f^{\#}$, the greater the improvement in receiving area, the smaller the field-of-view [67].

The work presented in [62] is a paper published in the Canadian Journal of Electrical & Computer Engineering. It includes the original proposal, some analytic and experimental results. A later work [63] was published in the same journal, presenting a model for numerical simulations of the optical taper. This model is quite generalized, so that the taper shape can be taken into account.

Appendix C

Bibliography

References

[1] C. E. Catlett, "In search of gigabit applications," *IEEE Communications Magazine*, vol. 30, no. 4, pp. 42-51, April 1992.

[2] S. R. Nagel, "Optical fiber--the expanding medium," *IEEE Communications Magazine*, vol. 25, no. 4, pp. 33-43, April 1987.

[3] W. E. Burr, "The FDDI optical data link," *IEEE Communications Magazine*, vol. 24, no. 5, pp. 18-23, May 1986.

[4] Floyd E. Ross, "An overview of FDDI: the fiber distributed data interface," *IEEE Journal on Selected Areas in Communications*, vol. 7, no. 7, pp. 1043-1051, September 1989.

[5] R. Ballart and Y. C. Ching, "SONET: Now it's the standard optical network," *IEEE Communications Magazine*, vol. 27, no. 3, pp. 8-15, Match 1989.

[6] J. A. McEachern, "Gigabit networking on the public transmission network," *IEEE Communications Magazine*, vol. 30, no. 4, pp. 70-78, April 1992.

[7] P. Newman, "ATM technology for corporate networks," *IEEE Communications Magazine*, vol. 30, no. 4, pp. 90-101, April 1992.

[8] Anthony S. Acampora, Mark J. Karol, "An overview of lightwave packet networks," *IEEE Network Magazine*, vol. 3, no. 1, pp. 29-41, January 1989.

[9] Paul S. Henry, "High-capacity lightwave local area networks," *IEEE Communications Magazine*, vol. 27, no. 1, pp. 20–26, October 1989.

[10] B. S. Glance, et al., "Densely spaced FDM coherent star network with optical signals confined to equally spaced frequencies," *Journal of Lightwave Technology*, vol. 6, no. 11, pp. 1770–1781, November 1988.

[11] J. A. Valdmanis, et al., "Generation of optical pulses as short as 27 femtoseconds directly from a laser balancing self-phase modulation, group-velocity dispersion, saturable absorption, and saturable gain," *Optics Letters*, vol. 10, no. 3, pp. 131–133, March 1985.

[12] P. Simon, et al., "Generation of 30-fs tunable over the visible spectrum," *Optics Letters*, vol. 16, no. 20, pp. 1569–1571, October 1991.

[13] M. N. Islam, et al., "All-optical time-domain chirp switches," *Optics Letters*, vol. 16, no. 7, pp. 484–486, April 1991.

[14] T Morioka, et al., "Ultrafast polarization-independent optical demultiplexer using optical carrier frequency shift through crossphase modulation," *Electronics Letters*, vol. 28, no. 11, pp. 1070–1072, May 1992.

[15] M. Haner, et al., "Optical demultiplexing of terabit packets using a nonlinear waveguide grating coupler," *Proceedings of Optical Fiber Communications Conference*, pp. 15–16, February, 1992.

[16] A. M. Weiner, et al., "Encoding and decoding of femtosecond pulses," *Optics Letters*, vol. 13, no. 4, pp. 300–302, April 1988.

[17] J. A. Salehi, "Pseudorandom light from a mode-locked laser," *Optics Letters*, vol. 14, no. 3, pp. 174–176, February 1989.

[18] N. Vethanayagam and R. I. MacDonald, "Demonstration of a novel optical code-division multiple-access system at 800 megachips per second," *Optics Letters*, vol. 16, no. 13, pp. 1010–1012, July 1991.

[19] E. Savov, W. Steenaart and A. Javed, "Photonic switching using spatial light modulators—a feasibility study," *1988 IEEE GLOBCOM*, vol. 2, pp. 29.4.1–29.4.5, November 1988.

[20] A. A. M. Saleh "Reflective single-mode fiber-optic passive star couplers," *Journal of Lightwave Technology*, vol. 6, no. 3, pp. 392–398, March 1988.

[21] M. Irshid and M. Kavehrad, "Distributed optical passive star couplers," *IEEE Photonic Technology Lett.*, vol. 3, no. 3, pp. 247–249, March 1991.

[22] Jin Au Kong, *Theory of electromagnetic waves*, John Wiley & Sons, Toronto,1975.

[23] T. H. Wood, et al. "Broadband Upgrade of a single-fiber fiber-in-the-loop system using three-levels of multiplexing," *Proceedings of Optical Fiber Communications Conference*, PD16, pp. 375–378, February 1992.

[24] S. K. Scheen and T. G. Giallorenzi, "Single-mode fiber-optical power divider: Encapsulated etching technique," *Optics Letters*, vol. 4, no. 1, pp. 29–31, January 1979.

[25] B. S. Kawasaki, K. O. Hill, and R. G. Lamont, "Biconical taper single-mode fiber coupler," *Optics Letters*, vol. 6, no. 7, pp. 327–328, July 1981.

[26] R. A. Bergh, G. Kotler, and H. J. Show, "Single-mode fiber optic directional coupler," *Electronic Lett.*, vol. 16, no. 7, pp. 260–261, March 1980.

[27] C. Dragone, "Efficient $N \times N$ star coupler using Fourier optics," *Journal of Lightwave Technology*, vol. LT-7, no. 3, pp. 479–489, March 1989.

[28] C. Dragone, et al.,"Efficient multichannel integrated optical star coupler on silicon," *IEEE Photonic Technology Lett.*, vol. 1, no. 8, pp. 241–243, August 1989.

[29] Ken K. H. Lee and W. Steenaart, "Analysis of $N \times N$ passive optical star coupler based on the normal modes of N input waveguides," *Journal of Lightwave Technology*, vol. 10, no. 12, pp. 1800–1806, December 1992.

[30] M. Tabiani and M. Kavehrad, "An efficient $N \times N$ passive optical star coupler," *IEEE Photonic Technology Lett.*, vol. 2, no. 11 pp. 826–829, November 1990.

[31] M. Tabiani and M. Kavehrad, "Theory of an efficient $N \times N$ passive optical star coupler," *Journal of Lightwave Technology*, vol. LT-9, no. 4, pp. 448–455, April 1991.

[32] B. J. Chang and C. D. Leonard, "Dichromated gelatin for the fibrication of holographic optical elements," *Applied Optics*, vol. 18, no. 14, pp. 2407–2417, July 1979.

[33] G. Yun and M. Kavehrad, "$N \times N$ passive fiber star coupler using grating degeneration and sandwich structures," *IEEE Photonic Technology Lett.*, vol. 4, no. 9 pp. 1035–1037, September 1992.

[34] G. Yun and M. Kavehrad, "Grating degeneration technique and sandwich structure for holographic $N \times N$ passive star couplers," *Journal of Lightwave Technology*, vol. LT-10, no. 11, pp. 1562–1569, November 1992.

[35] M. Kavehrad and G. Yun, "Grating degeneration and cascading for efficient $N \times N$ optical star coupler," Patent pending, application filed, January 1992.

[36] N. Amitay, et. al., "Optical fiber tapers—a novel approach to self aligned beam expansion and single-mode hardware," *Journal of Lightwave Technology*, vol. LT-5, no. 1, pp. 70–76, January 1987.

[37] N. Amitay, et. al., "Optical fiber tapers at $1.3\mu m$ for self-aligned beam expansion and sigle-mode hardware," *Journal of Lightwave Technology*, vol. LT-5, no. 8, pp. 1123–1127, August 1987.

[38] Jack D. Gaskill. *Linear Systems, Fourier Transforms, and Optics*, John Wiley & Sons, Inc., New York, 1978.

[39] H. Kogelnik, "Coupled wave theory for thick hologram gratings," *The Bell System Technical Journal*, vol. 48, no. 9, pp. 2909–2947, November 1969.

[40] Robert J. Collier et al., *Optical Holography*, Academic Press, New York, 1971.

[41] M. Kavehrad and M. Tabiani, "Selective-broadcast optical passive star coupler design for dense WDM networks," *IEEE Photonics Technology Letters*, vol. 3, no. 5, pp. 487–489, May 1991.

[42] M. Kavehrad and M. Tabiani, "A selective-broadcast passive star coupler for self-routing dense wavelength division multiplexed optical networks," *Journal of Lightwave Technology*, vol. LT-9, no. 10, pp. 1278–1288, October 1991.

[43] B. E. A. Saleh and M. Carl Teich, *Fundamentals of Photonics*, John Wiley & Sons, Inc., New York, 1991.

[44] Eugene Hecht and Alfred Zajac, *Optics*, Addison-Wesley Publising Company, Inc., Ontario,1974.

[45] T. K. Gaylord and M. G. Moharam, "Planar dielectric grating diffraction theories," *Applied Physics B*, B. 28, no. 1, pp. 1–14, May 1982.

[46] R. Magnusson and T. K. Gaylord, "Analysis of multiwave diffraction of thick gratings," *Journal of Optical Society of America*, vol. 67, no. 9, pp. 1165–1170, September 1977.

[47] M. G. Moharam and T. K. Gaylord, "Three-dimensional vector coupled-wave analysis of planar grating diffraction," *Journal of Optical Society of America*, vol. 73, no. 9, pp. 1105–1112, September 1983.

[48] K. Rokushima and J. Yamakita, "Analysis of anisotropic dielectric gratings," *Journal of Optical Society of America*, vol. 73, no. 7, pp. 901–908, July 1983.

[49] E. N. Glytsis and T. K. Gaylord, "Rigorous three-dimensional coupled-wave diffraction analysis of single and cascaded anisotropic gratings," *Journal of Optical Society of America*, vol. 4, no. 11, pp. 2061 2081, November 1987.

[50] E. N. Glytsis and T. K. Gaylord, "Three-dimensional (vector) rigorous coupled-wave analysis of anisotropic grating diffraction," *Journal of Optical Society of America*, vol. 7, no. 8, pp. 1399 1420, August 1990.

[51] Zvi Zylberberg and Emanuel Marom, "Rigorous coupled-wave analysis of pure reflection gratings," *Journal of Optical Society of America*, vol. 73, no. 3, pp. 392–398, March 1983.

[52] M. G. Moharam and T. K. Gaylord, "Comments on analysis of reflection gratings," *Journal of Optical Society of America*, vol. 73, no. 3, pp. 399–401, March 1983.

[53] M. G. Moharam and T. K. Gaylord, "Rigorous coupled-wave analysis of planar-grating diffraction," *Journal of Optical Society of America*, vol. 71, no. 7, pp. 811–818, July 1981.

[54] F. R. Gfeller and U. Bapst, "Wireless in-house data communication via diffuse infrared radiation," *Proceedings of the IEEE*, vol. 67, no. 11, pp. 1474–1486, November 1979.

[55] T.S. Chu and M.J. Gans, "High speed infrared local wireless communication," *IEEE Communication Magazine*, vol. 25, no. 8, pp. 4–10, August 1987.

[56] Ch-Sun Yen and Richard D. Crawford, "The use of directed optical beams in wireless computer communications," *IEEE Globecom'85*, New Orleans, pp. 1181–1184, December 1985.

[57] Y. Nakata , et al, "In-house wireless communication system using infrared radiation," *Proc. of the seventh International Conference on Computer Communications*, Sydney, Australia, pp. 333–338, October 1984.

[58] G. Yun and M. Kavehrad, "Spot-Diffusing and Fly-Eye Receivers for Indoor Infrared Wireless Communications," *IEEE International Conference on Selected Topics in Wireless Communications*, Vancouver, pp. 262–265, June 1992.

[59] G. Yun and M. Kavehrad, "Indoor Infrared Wireless Communications using Spot-Diffusing and Fly-Eye Receivers," accepted by *Canadian Electrical and Computer Engineering Journal* in August, 1992.

[60] G. Yun and M. Kavehrad, "Efficient optical receivers for free-space / atmospheric optical communications," *15-th Biennial Symposium on Communications*, in Kingston, Session D. 3, pp. 180–183, May 1990.

[61] G. Yun and M. Kavehrad, "Application of Optical Tapers to Receivers in Free Space / Atmospheric Optical Links," *IEEE Military Communications Conference*, in Monterey, CA, vol. 3, pp. 45.1.1–45.1.5, September 1990.

[62] M. Kavehrad and G. Yun "High Angular Tolerance Receiver for Atmospheric Optical Links," *Canadian Electrical and Computer Engineering Journal*, vol. 16, no. 2, pp. 63–67, April 1991.

[63] X. Huang, G. Yun and M. Kavehrad "Modelling of optical tapers for high-angular-tolerance optical receivers application," *Canadian Electrical and Computer Engineering Journal*, vol. 17, No. 2, pp. 65–70, April 1992.

[64] M. Kavehrad and G. Yun, "Application of optical tapers to free-space / atmospheric optical line-of-sight communication links," US patent approved, September 1992.

[65] R. Winston, "Light collection within the framework of geometrical optics," *Journal of Optical Society of America*, vol. 60, no. 2, pp. 245–247, February 1970.

[66] D. E. Williamson, "Cone channel condenser optics," *Journal of Optical Society of America*, vol. 42, no. 10, pp. 712–715, October 1952.

[67] A. Rabl, "Comparision of solar concentrators," *Solar energy*, vol. 18, no. 2, pp. 93-111, February 1976.

Appendix D

List of symbols

$\vec{a}$	Amplitude vector of a plane wave component, defined by Eq. 3.30
$\vec{a}_l$	Eigen vector corresponding to q_l
$a_{l,\tau}$	Projection of $\vec{a}_l$ in the direction of $\hat{\tau}$
$a_{l,\rho}$	Projection of $\vec{a}_l$ in the direction of $\hat{\rho}$
$a_{l,z}$	Projection of $\vec{a}_l$ in the direction of $\hat{z}$
a_δ	qa_τ
a_τ	Projection of $\vec{a}$ in the direction of $\hat{\tau}$
a_ρ	Projection of $\vec{a}$ in the direction of $\hat{\rho}$
a_z	Projection of $\vec{a}$ in the direction of $\hat{z}$
A	Two-dimensional array defined by Eq. 3.23 through 3.26
a	Defined by Eq. 3.29, a column vector
A_i	Scalar amplitude of the field from the i-th input fiber
A'_i	Scalar amplitude of the field of the i-th output fiber
B	Two-dimensional array defined by Eq. 3.23 through 3.26
c	Speed of light
c_{ij}	Element (i-th row, j-th column) of matrix C
c_R	Element of matrix C_R, defined by Eq. 3.52
c_T	Element of matrix C_T, defined by Eq. 3.53

C	power coupling matrix of a star coupler
C_l	Complex constant coefficient for mode l
C_R	Coupling matrix for reflection diffraction
C_T	Coupling matrix for transmission diffraction
$CR_{\perp\perp}$	Polarization-dependent power coupling coefficient for reflection diffraction, defined by Eq. 3.78
$CR_{\perp\parallel}$	Polarization-dependent power coupling coefficient for reflection diffraction, defined by Eq. 3.78
$CR_{\parallel\perp}$	Polarization-dependent power coupling coefficient for reflection diffraction, defined by Eq. 3.78
$CR_{\parallel\parallel}$	Polarization-dependent power coupling coefficient for reflection diffraction, defined by Eq. 3.78
$CT_{\perp\perp}$	Polarization-dependent power coupling coefficient for transmission diffraction, defined by Eq. 3.76
$CT_{\perp\parallel}$	Polarization-dependent power coupling coefficient for transmission diffraction, defined by Eq. 3.76
$CT_{\parallel\perp}$	Polarization-dependent power coupling coefficient for transmission diffraction, defined by Eq. 3.76
$CT_{\parallel\parallel}$	Polarization-dependent power coupling coefficient for transmission diffraction, defined by Eq. 3.76
d	Thickness of grating slab
$E(x,y)$	Light field distribution on a plane perpendicular to the z-axis
$E^-(x,y)$	Light field distribution at the input side of a transparency
$E^+(x,y)$	Light field distribution at the output side of a transparency
$E'(x,y)$	Light field distribution on a plane perpendicular to the z-axis
$E(\vec{r})$	Electric field (when scalar field is assumed)
$\vec{E}(\vec{r})$	Electric field
$\mathcal{E}_b$	Optical energy required for one information bit

f	Focal length
$\mathcal{F}_{2D}\{\cdot\}$	Two dimensional Fourier transformation
G	Region defined by the grating slab
H	Power coupling matrix of an ideal lossless star coupler
$H(\lambda)$	Transfer function in wavelength domain
$H_d(\lambda)$	Transfer function of a grating when only the dispersion is considered.
$H_B(\lambda)$	Transfer function of a grating when only the Bragg effect is considered.
$\vec{H}$	H-field vector
$\vec{H}_1$	H-field in medium 1
$\vec{H}_2$	H-field in medium 2
I	Number of columns of a shuffleNet (chapter 2)
$\vec{I}$	Amplitude vector of the incident wave
$I_\perp$	Projection of $\vec{I}$ in the direction perpendicular to the incident plane
$I_\parallel$	Projection of $\vec{I}$ in the direction parallel to the incident plane
j	$\sqrt{-1}$
J	Serial number of mode $\mathrm{m}(J)$
J_i^-	Serial number of order $\mathrm{m}-\mathrm{u}_i$
J_i^+	Serial number of order $\mathrm{m}+\mathrm{u}_i$
k	$2\pi/\lambda$
$\vec{k}$	Wave vector of a plane wave
$\vec{k}_{rec}$	Wave vector of a plane wave in construction
$\vec{k}_{i,rec}$	The i-th wave vector in construction
k_x	Projection of $\vec{k}$ in the direction of x-axis
k_y	Projection of $\vec{k}$ in the direction of y-axis
k_z	Projection of $\vec{k}$ in the direction of z-axis
$\vec{k}_\rho$	Transverse component of $\vec{k}$
$\vec{k}_i$	Wave vector of the i-th ($i=1,2,\ldots$)direction
$\vec{k}_{i,\rho}$	Transverse component of $\vec{k}_i$

$k_{i,x}$	x-component of $\vec{k}_i$
$k_{i,y}$	y-component of $\vec{k}_i$
$k_{i,z}$	z-component of $\vec{k}_i$
$\vec{K}$	Grating vector
K_x	Projection of $\vec{K}$ in the direction of x-axis
K_y	Projection of $\vec{K}$ in the direction of y-axis
K_z	Projection of $\vec{K}$ in the direction of z-axis
$\vec{K}_\rho$	Transverse component of $\vec{K}$
$\vec{K}_i$	Grating vector of the i-th grating
$\vec{K}_{ij}$	Grating vector relating $\vec{k}_i$ and $\vec{k}_j$
$\vec{\mathbf{K}}^T$	A column vector of vectors, defined by Eq. 3.16
$\mathbf{K}_z^T$	A column vector, z-component of $\vec{\mathbf{K}}^T$
L	Integer, size of matrices $\mathbf{A}$ or $\mathbf{B}$
$\mathbf{m}$	A row vector of indices, order of diffraction
M	Number of couplers a message has to pass through in an optical bus (in chapter 1) or the number of superimposed gratings in a dielectric slab (Chapter 3)
M_R	Jones matrix for the reflection diffraction
M_T	Jones matrix for the transmission diffraction
$\mathcal{M}_R$	Characteristic matrix for reflection diffraction
$\mathcal{M}_R^{(i)}$	Reflection characteristic matrix for the i-th slab
$\mathcal{M}_T$	Characteristic matrix for transmission diffraction
$\mathcal{M}_T^{(i)}$	Transmission characteristic matrix for the i-th slab
n	Number of stages for star coupler construction
$n(\vec{r})$	Refractive index of a grating slab
n_0	Average refractive index in region G
n_R	Refractive index of region R
n_T	Refractive index of region T

$\hat{n}$	Unit vector in the direction of a normal line
N	Number of input / output ports
p	Total input power from all the input ports of a star coupler (Chapter 1)
p	Degree of graph of a shufflenet (Chapter 2)
p_i	Input power at the i-th ($i = 1, 2, \ldots, N$) input port of a star coupler
p_i'	Output power at the i-th ($i = 1, 2, \ldots, N$) output port of a star coupler
$p_i^{(j)}$	Output power in the i-th ($i = 1, 2, \ldots, N$) output direction at the output side of the j-th ($j = 0, 1, 2, \ldots$) slab
$p(x, y)$	Aperture function of the slab
P_r	Optical power received by a receiver
P_t	Optical transmission power
$P(\xi, \eta)$	Fourier transformation of $p(x, y)$
$PR_{\perp\perp}$	Polarization-dependent phase coupling coefficient for reflection diffraction, defined by Eq. 3.78
$PR_{\perp\parallel}$	Polarization-dependent phase coupling coefficient for reflection diffraction, defined by Eq. 3.78
$PR_{\parallel\perp}$	Polarization-dependent phase coupling coefficient for reflection diffraction, defined by Eq. 3.78
$PR_{\parallel\parallel}$	Polarization-dependent phase coupling coefficient for reflection diffraction, defined by Eq. 3.78
$PT_{\perp\perp}$	Polarization-dependent phase coupling coefficient for transmission diffraction, defined by Eq. 3.77
$PT_{\perp\parallel}$	Polarization-dependent phase coupling coefficient for transmission diffraction, defined by Eq. 3.77
$PT_{\parallel\perp}$	Polarization-dependent phase coupling coefficient for transmission diffraction, defined by Eq. 3.77
$PT_{\parallel\parallel}$	Polarization-dependent phase coupling coefficient for transmission diffraction, defined by Eq. 3.77

Q	Volume grating selectivity factor
q	Eigenvalue
q_l	The l-th eigenvalue
$\vec{r}$	Position vector
$r_{\perp\perp}$	Element of the matrix M_R, defined by Eq. 3.51
$r_{\perp\parallel}$	Element of the matrix M_R, defined by Eq. 3.51
$r_{\parallel\perp}$	Element of the matrix M_R, defined by Eq. 3.51
$r_{\parallel\parallel}$	Element of the matrix M_R, defined by Eq. 3.51
R	Region of reflections
$\vec{R}$	Amplitude vector of a reflection order
$R_\perp$	Projection of $\vec{R}$ in the direction perpendicular to the plane of diffraction of that order
$R_\parallel$	Projection of $\vec{R}$ in the direction parallel to the plane of diffraction of that order
S	Entropy measured at the input side of a star coupler
S'	Entropy measured at the output side of a star coupler
t_{ij}	Transmission amplitude coupling coefficient (Chapter 2)
$t_{\perp\perp}$	Element of the matrix M_T, defined by Eq. 3.50
$t_{\perp\parallel}$	Element of the matrix M_T, defined by Eq. 3.50
$t_{\parallel\perp}$	Element of the matrix M_T, defined by Eq. 3.50
$t_{\parallel\parallel}$	Element of the matrix M_T, defined by Eq. 3.50
T	Region of transmission
$\vec{T}$	Amplitude vector of a transmission order
$T_\perp$	Projection of $\vec{T}$ in the direction perpendicular to the plane of diffraction of that order
$T_\parallel$	Projection of $\vec{T}$ in the direction parallel to the plane of diffraction of that order
$T'_\perp$	Phase shifted version of $T_\perp$, defined by 3.44
$T'_\parallel$	Phase shifted version of $T_\parallel$, defined by 3.45
$\mathbf{u}_i$	Unit row vector of size M with its non-zero element (1) placed

	at the i-th position
$\vec{V}$	$\frac{\vec{k}}{kn_0} - q\hat{z}$
V_z	z-component of $\vec{V}$
$\hat{x}$	Unit vector in the direction of the x-axis
$\hat{y}$	Unit vector in the direction of the y-axis
$\hat{z}$	Unit vector in the direction of the z-axis
α	Excess loss of 2×2 couplers
α_{ij}	Excess loss factor corresponding to η_{ij}
α_i^-	Angle between $\hat{\rho}(J)$ and $\hat{\rho}(J_i^-)$
α_i^+	Angle between $\hat{\rho}(J)$ and $\hat{\rho}(J_i^+)$
β	Defined by Eq. 2.27
γ	Coupling factor defined in [30]
δ	Degree of violation against Bragg condition (chapter 2)
δ_{ij}	Degree of violation against Bragg condition, when $\vec{k}_i$ and $\vec{k}_j$ are considered (Chapter 2) or Kronecker delta (chapter 3)
Δ	Relative modulation index of a volume phase grating
Δ_i	Relative modulation index of the grating with $\vec{K}_i$
Δ_{ij}	Relative modulation index of the grating with $\vec{K}_{ij}$
Δ_{max}	Maximum available relative index modulation
$\bar{\Delta}$	Routing matrix
ϵ	Dielectric constant
ϵ_0	Permittivity of vacuum
ϵ_1	Dielectric constant of medium 1
ϵ_2	Dielectric constant of medium 2
η	Diffraction efficiency of a grating or power coupling coefficient of a 2×2 coupler or spatial frequency in the direction of y axis (chapter 2)
η_{ri}	Coupling coefficient of the 2×2 coupler of the

	i-th ($i = 1, 2, \ldots, N$) user at the receiver side of the optical bus
η_{ti}	Coupling coefficient of the 2×2 coupler of the
	i-th ($i = 1, 2, \ldots, N$) user at the transmitter side of the optical bus
η_{ij}	Element (i-th row, j-th column) of matrix H
θ	An angle
θ_R	Angle of reflection
θ_T	Angle of transmission
λ	Wavelength in vacuum
λ_i	The i-th wavelength in a multi-wavelength system
λ_{rec}	Wavelength in construction
Λ	Grating period
Λ_ρ	Grating period in the transverse direction
μ	Relative permeability
μ_0	Permeability of vacuum
μ_1	Relative permeability of medium 1
μ_2	Relative permeability of medium 2
ξ	Spatial frequency in the direction of x axis
$\hat{\rho}$	Unit vector defined by Eq. 3.22
$\hat{\tau}$	Unit vector defined by Eq. 3.22
ϕ_i	Initial phase of the grating corresponding to $\vec{K}_i$
Φ_R	Power coupling matrix for a reflection order, defined by Eq. 3.58
Φ_T	Power coupling matrix for a transmission order, defined by Eq. 3.56
$\psi(x, y)$	Fiber transverse mode
$\Psi(\xi, \eta)$	Fourier transformation of $\psi(x, y)$
ω	Angular frequency of light field

Appendix E

Program Listing

```
C To run to the program, an input file has to be prepared
C in the following format:
C
C cgd.out,
C tms0.out, rflc0.out,
C tms1.out, rflc1.out,
C tms2.out, rflc2.out,
C tms3.out, rflc3.out,
C tms4.out, rflc4.out,
C tms5.out, rflc5.out,
C tms6.out, rflc6.out,
C tms7.out, rflc7.out,
C tms8.out, rflc8.out,
C tms9.out, rflc9.out,
C Npt,
C MM, NOD, d0, NR, N0, NT, lambda,
C Delta(1),Kx(1),Ky(1),Kz(1),phi(1),
C Delta(2),Kx(2),Ky(2),Kz(2),phi(2),
C Delta(3),Kx(3),Ky(3),Kz(3),phi(3),
C Delta(4),Kx(4),Ky(4),Kz(4),phi(4),
C kx0,ky0,
C M1(0),M2(0),M3(0),M4(0),
C M1(1),M2(1),M3(1),M4(1),
C M1(2),M2(2),M3(2),M4(2),
C M1(3),M2(3),M3(3),M4(3),
C M1(4),M2(4),M3(4),M4(4),
C M1(5),M2(5),M3(5),M4(5),
C M1(6),M2(6),M3(6),M4(6),
C M1(7),M2(7),M3(7),M4(7),
C M1(8),M2(8),M3(8),M4(8),
C M1(9),M2(9),M3(9),M4(9),
C Ip(1,0),Ip(1,1),Ip(1,2),Ip(1,3),Ip(1,4),Ip(1,5),Ip(1,6),Ip(1,7),Ip(1,8),Ip(1,9),
C Ip(2,0),Ip(2,1),Ip(2,2),Ip(2,3),Ip(2,4),Ip(2,5),Ip(2,6),Ip(2,7),Ip(2,8),Ip(2,9),
C Ip(3,0),Ip(3,1),Ip(3,2),Ip(3,3),Ip(3,4),Ip(3,5),Ip(3,6),Ip(3,7),Ip(3,8),Ip(3,9),
C Ip(4,0),Ip(4,1),Ip(4,2),Ip(4,3),Ip(4,4),Ip(4,5),Ip(4,6),Ip(4,7),Ip(4,8),Ip(4,9),
C Im(1,0),Im(1,1),Im(1,2),im(1,3),Im(1,4),Im(1,5),Im(1,6),Im(1,7),Im(1,8),Im(1,9),
C Im(2,0),Im(2,1),Im(2,2),Im(2,3),Im(2,4),Im(2,5),Im(2,6),Im(2,7),Im(2,8),Im(2,9),
C Im(3,0),Im(3,1),Im(3,2),Im(3,3),Im(3,4),Im(3,5),Im(3,6),Im(3,7),Im(3,8),Im(3,9),
C Im(4,0),Im(4,1),Im(4,2),Im(4,3),Im(4,4),Im(4,5),Im(4,6),Im(4,7),Im(4,8),Im(4,9),
C
C where,
C cgd.out:   file name, character of length equal or less
C         than 12, for output data of the initial set-up
C         and mornitoring the run.
C
C tmsJ.out: file name, character of length equal or less
C         than 12, for output data of the transmission Jones
C         matricix of order J.
C
C rflcJ.out: file name, charact    of length equal or less
C         than 12, for output data of the reflection Jones
C         matrix of order J.
C
C Npt:      number of points, integer.
C
C MM:       number of gratings, integer, no greater than 4.
C
C NOD:      number of diffracted order, integer, no greater
C         than 9.
C
C d0:       Initial thickness.
C
C NR:       Refractive index of region R.
C
C N0:       Average refractive index of region G.
C
```

```
C NT:       Refractive index of region T.
C
C lambda:   Wavwlength.
C
C Delta(I): Relative modulation index of the I-th grating, real.
C
C Kx(I):    x-component of the grating vector of the
C           I-th grating, real.
C
C Ky(I):    y-component of the grating vector of the
C           I-th grating, real.
C
C Kz(I):    z-component of the grating vector of the
C           I-th grating, real.
C
C kx0:      x-component of the wave vector of the incident
C           wave, real.
C
C ky0:      y-component of the wave vector of the incident
C           wave, real.
C
C MI(J):    the I-th element of the index-vector of the J-th
C           order, integer.
C
C Ip(I,J)   integer, serial number of the neighbouring order of
C           the order with serial number J, in the positive
C           direction of grating #I.
C
C Im(I,J)   integer, serial number of the neighbouring order of
C           the order with serial number J, in the negative
C           direction of grating #I.
C
      PROGRAM CGD
C
      character ifname*12, ofname*12, ot(0:9)*12,or(0:9)*12
      integer Npt
      INTEGER M(4,0:9),MM,NOD,I
      REAL D,NR,N0,NT,D0
      REAL LAMBDA
      REAL DD(4),KKX(4),KKY(4),KKZ(4),PHI(4),KX0,KY0
      REAL KX(0:9),KY(0:9),KR(0:9),COR(0:9),COT(0:9)
      INTEGER IP(4,0:9),IM(4,0:9)
      REAL SIP(4,0:9),SIM(4,0:9),COP(4,0:9),COM(4,0:9)
      COMPLEX DET
      COMPLEX CA(40,40),CB(40,40),CAB(40,40)
      COMPLEX CQ(40),CV(40,40),CC(40,40),CD(40,2)
      REAL AR(40,40),AI(40,40)
      REAL BR(40,40),BI(40,40)
      REAL QR(40),QI(40),VR(40,40),VI(40,40)
      COMPLEX MR(2,2,0:9),MT(2,2,0:9)
      REAL CR(2,2,0:9),PR(2,2,0:9),CT(2,2,0:9),PT(2,2,0:9)
CC
      write(*,*) 'input file name:'
      read(*,*) ifname
        OPEN(7, file=ifname)
      read(7,*) ofname
      do j=0,9
       read(7,*) ot(j),or(j)
      end do
        open(8, file=ofname)
C
      read (7,*) Npt
      READ (7,*) MM,NOD,D0,NR,N0,NT,LAMBDA
      read (7,*) DD(1),KKX(1),KKY(1),KKZ(1),PHI(1)
      read (7,*) DD(2),KKX(2),KKY(2),KKZ(2),PHI(2)
      read (7,*) DD(3),KKX(3),KKY(3),KKZ(3),PHI(3)
```

```
      read (7,*) DD(4),KKX(4),KKY(4),KKZ(4),PHI(4)
      read (7,*) KX0,KY0
      read (7,*) M(1,0),M(2,0),M(3,0),M(4,0)
      read (7,*) M(1,1),M(2,1),M(3,1),M(4,1)
      read (7,*) M(1,2),M(2,2),M(3,2),M(4,2)
      read (7,*) M(1,3),M(2,3),M(3,3),M(4,3)
      read (7,*) M(1,4),M(2,4),M(3,4),M(4,4)
      read (7,*) M(1,5),M(2,5),M(3,5),M(4,5)
      read (7,*) M(1,6),M(2,6),M(3,6),M(4,6)
      read (7,*) M(1,7),M(2,7),M(3,7),M(4,7)
      read (7,*) M(1,8),M(2,8),M(3,8),M(4,8)
      read (7,*) M(1,9),M(2,9),M(3,9),M(4,9)
      do I=1,4
      read (7,*) Ip(I,0),Ip(I,1),Ip(I,2),Ip(I,3),Ip(I,4),
     x          Ip(I,5),Ip(I,6),Ip(I,7),Ip(I,8),Ip(I,9)
      end do
      do I=1,4
      read (7,*) Im(I,0),Im(I,1),Im(I,2),Im(I,3),Im(I,4),
     x          Im(I,5),Im(I,6),Im(I,7),Im(I,8),Im(I,9)
      end do
C
      WRITE(8,5) MM,NOD
    5 FORMAT(///5X,'MM=',I2,4X,'NOD=',I2)
      WRITE(8,4) D0,NR,N0,NT,LAMBDA
    4 FORMAT(/5X,'D0=',F8.5,' NR=',F8.5,' N0=',F8.5,' NT=',F8.5,
     x' LAMBDA=',F8.5/)
      DO I=1,MM
      WRITE(8,25) I,DD(I),KKX(I),KKY(I),KKZ(I),PHI(I)
   25 FORMAT(5X,'I=',I2,'  DD=',F8.5,'  KKX=',F8.5,'  KKY=',
     X F8.5,'  KKZ=',F8.5,'  PHI=',F8.5//)
      END DO
      WRITE(8,35) KX0,KY0
   35 FORMAT(5X,'INCIDENT:',' KX0=',F8.5,' KY0=',F8.5)
C
C****Computing the grating equation****
C
      CALL GRATEQ(MM,M,NOD,LAMBDA,KKX,KKY,KX0,KY0,KX,KY,KR,
     X NR,N0,NT,COR,COT)
C
C
C****Find the adjacent orders****
C
      CALL ADJOR(MM,M,NOD,KX,KY,KR,IP,IM,SIP,SIM,COP,COM)
C
C
C
C****Computing the "matrices"****
C
      NN=4*(NOD+1)
      CALL MTRX(MM,NOD,NN,M,N0,LAMBDA,KR,DD,KKZ,PHI,IP,IM,
     XSIP,SIM,COP,COM,CA,CB)
C
C****Prepare for EISPACK
C
      CALL MTRX2(NN,CA,CB,CAB,AR,AI,BR,BI)
C
C****Find the eigen values and vectors****
C
      CALL CEIGEN(NN,BR,BI,QR,QI,VR,VI,CQ,CV)

C
C****Boundary conditions****
C
      do j=0,NOD
       open(2*j+9,file=ot(j))
       open(2*j+10,file=or(j))
```

```
      write(2*j+9,53) j
      write(2*j+10,53) j
   53 format('J=',I2)
      write(2*j+9,54)
   54 format(2x,'d',7x,'CT(1,1)',2x,'PT(1,1)',2x,'CT(2,1)',2x,'PT(2,1)',
     x 2x,'CT(1,2)',2x,'PT(1,2)',2x,'CT(2,2)',2x,'PT(2,2)')
      write(2*j+10,56)
   56 format(2x,'d',7x,'CR(1,1)',2x,'PR(1,1)',2x,'CR(2,1)',2x,'PR(2,1)',
     x 2x,'CR(1,2)',2x,'PR(1,2)',2x,'CR(2,2)',2x,'PR(2,2)')
      end do
c
      do 100 i=1,Npt
      write(6,*) i
      D=I*d0
      CALL COEFCTS(MM,NOD,NN,M,D,NR,N0,NT,LAMBDA,KKZ,KR,COR,COT,
     X CV,CQ,CC,CD)
C
C
C****Solve boundary coditons****
C
      CALL  CMIVS(CC,CD,NN,2,DET)
      IF(DET.EQ.0.0) THEN
      WRITE(6,*) 'SORRY, DET=0.O'
      END IF
C
C
C****Computing Jones matrices****
C
      CALL JONESMTX(NOD,NN,N0,D,LAMBDA,COR,COT,CQ,CV,CD,MR,MT)
C
C
C****Computing coupling coeficients****
C
      CALL PCPLMTRX(NOD,NR,NT,COR,COT,MR,MT,CR,CT,PR,PT)
c
      do j=0,NOD
      write(2*j+9,78)  d,ct(1,1,j),pt(1,1,j),ct(2,1,j),pt(2,1,j),
     x ct(1,2,j),pt(1,2,j),ct(2,2,j),pt(2,2,j)
      write(2*j+10,78) d,cr(1,1,j),pr(1,1,j),cr(2,1,j),pr(2,1,j),
     x cr(1,2,j),pr(1,2,j),cr(2,2,j),pr(2,2,j)
   78 format(1x,1F7.3,8F9.5)
      end do
c
  100 continue
C
C
      close(7)
      close(8)
      do j=0,NOD
       close(2*j+9)
       close(2*j+10)
      end do
      stop
      END
C
C
C This is a subroutine for computing grating equation
C
      SUBROUTINE GRATEQ(MM,M,NOD,LAMBDA,KKX,KKY,KX0,KY0,KX,KY,KR,
     X NR,N0,NT,COR,COT)
C
      INTEGER M(4,0:NOD),MM,NOD
      REAL KKX(MM),KKY(MM),KX0,KY0,KX(0:NOD),KY(0:NOD),KR(0:NOD)
      REAL NR,N0,NT,LAMBDA,COR(0:NOD),COT(0:NOD)
C
      PI=3.141592654
```

```
C
      JJ=0
      DO J=0,NOD
C                 Transversal components of J-th order:
      KX(J)=KX0
      KY(J)=KY0
      DO 20 I=1,MM
      KX(J)=KX(J)+M(I,J)*KKX(I)
      KY(J)=KY(J)+M(I,J)*KKY(I)
   20 CONTINUE
C                              "k_rho":
      KR(J)=SQRT(KX(J)**2+KY(J)**2)
C                              Get rid of the "insignificant" orders:
      X=KR(J)*LAMBDA/2.0/PI/NR
      Y=KR(J)*LAMBDA/2.0/PI/NT
      IF(X.GE.1.0) GOTO 30
      IF(Y.LT.1.0) GOTO 10
   30 NOD=NOD-1
      DO  K=J,NOD
      DO  I=1,MM
      M(I,K)=M(I,K+1)
      END DO
      END DO
      J=J-1
   10 JJ=JJ+1
      END DO
C                 Cosine of the diffraction orders:
      DO J=0,NOD
      COR(J)=SQRT(1-(KR(J)*LAMBDA/2.0/PI/NR)**2)
      COT(J)=SQRT(1-(KR(J)*LAMBDA/2.0/PI/NT)**2)
      END DO
C
      WRITE(8,40)
   40 FORMAT(//2X,'J',2X,'M1',2X,'M2',2X,'M3',2X,'M4',2X,
     x 'KX',8X,'KY',8X,'KRHO',6X,'COR',7X,'COT')
      DO J=0,NOD
      WRITE(8,45) J,M(1,J),M(2,J),M(3,J),M(4,J),
     x KX(J),KY(J),KR(J),COR(J),COT(J)
   45 FORMAT(1X,5(I2,2X),5(F8.5,2X))
      END DO

C
      RETURN
      END
C
C****A sub. finding the next door neighbors****
C
      SUBROUTINE ADJOR(MM,M,NOD,KX,KY,KR,IP,IM,
     X SIP,SIM,COP,COM)
C
      INTEGER M(4,0:NOD),IP(4,0:NOD),IM(4,0:NOD)
      REAL KX(0:NOD),KY(0:NOD),KR(0:NOD)
      REAL SIP(4,0:NOD),SIM(4,0:NOD),COP(4,0:NOD),COM(4,0:NOD)
C                              Initializing:
      DO 5 I=1,MM
      DO 5 J=0,NOD
      SIP(I,J)=5.5555
      SIM(I,J)=5.5555
      COP(I,J)=5.5555
      COM(I,J)=5.5555
    5 CONTINUE
C
      DO 30 J=0,NOD
      DO 20 I=1,MM
C
C           SIP(I,J): sine of the angle of the positive neighbor
```

```
C          SIM(I,J): sine of the angle of the negative neighbor
C          COP(I,J): cosine of the angle of the positive neighbor
C          COM(I,J): cosine of the angle of the negative neighbor
    IF(IM(I,J).EQ.-1) GOTO 10
    K=IM(I,J)
    SIM(I,J)=(KY(K)*KX(J)-KX(K)*KY(J))/KR(K)/KR(J)
    COM(I,J)=(KX(K)*KX(J)+KY(K)*KY(J))/KR(K)/KR(J)
  10 IF (IP(I,J).EQ.-1) GOTO 20
    K=IP(I,J)
    SIP(I,J)=(KY(K)*KX(J)-KX(K)*KY(J))/KR(K)/KR(J)
    COP(I,J)=(KX(K)*KX(J)+KY(K)*KY(J))/KR(K)/KR(J)
C
  20 CONTINUE
  30 CONTINUE
C                          Print
    WRITE(8,22)
  22  FORMAT(//5X,'IP=')
    DO I=1,MM
    WRITE(8,21) (IP(I,J),J=0,NOD)
    END DO
  21  FORMAT(10X,9(I8,1X))
    WRITE(8,23)
  23  FORMAT(//5X,'IM=')
    DO I=1,MM
    WRITE(8,21) (IM(I,J),J=0,NOD)
    END DO
    WRITE(8,24)
  24  FORMAT(//5X,'SIP=')
    DO I=1,MM
    WRITE(8,40) (SIP(I,J),J=0,NOD)
    END DO
    WRITE(8,26)
  26  FORMAT(//5X,'SIM=')
    DO I=1,MM
    WRITE(8,40) (SIM(I,J),J=0,NOD)
    END DO
    WRITE(8,27)
  27  FORMAT(//5X,'COP=')
    DO I=1,MM
    WRITE(8,40) (COP(I,J),J=0,NOD)
    END DO
    WRITE(8,28)
  28  FORMAT(//5X,'COM=')
    DO I=1,MM
    WRITE(8,40) (COM(I,J),J=0,NOD)
    END DO
  40  FORMAT(10X,9(F8.5,1X))
C
    RETURN
    END
C
C****This is a subroutine for computing the complex
C                    matrices of the mode eqs****
C
    SUBROUTINE MTRX(MM,NOD,NN,M,N0,LAMBDA,KR,DD,KKZ,PHI,IP,IM,
   XSIP,SIM,COP,COM,CA,CB)
C
    INTEGER M(4,0:NOD),IP(4,0:NOD),IM(4,0:NOD)
    REAL LAMBDA,VR,VZ,N0
    REAL KR(0:NOD),DD(MM),KKZ(MM),PHI(MM)
    REAL SIP(4,0:NOD),SIM(4,0:NOD),COP(4,0:NOD),COM(4,0:NOD)
    COMPLEX C,CA(NN,NN),CB(NN,NN)
C
    PI=3.141592654
C
C            Initializing CA and CB
```

```
C               NN: size of CA and CB,NN=4*(1+NOD)
      DO 10 K=1,NN
      DO 10 L=1,NN
      CA(K,L)=0.0
      IF (L.EQ.K) THEN
      CB(K,L)=1.0
      ELSE
      CB(K,L)=0.0
      END IF
   10 CONTINUE
C
      DO 100 J=0,NOD
C                 VZ: M*K_z
      VZ=0.0
      DO I=1,MM
      VZ=VZ+M(I,J)*KKZ(I)
      END DO
      VZ=VZ*LAMBDA/2.0/PI/N0
      VR=KR(J)*LAMBDA/2.0/PI/N0
C
C FIRST, DD=0
      CA(1+4*J,1+4*J)=-2.0*VZ
      CA(1+4*J,2+4*J)=1.0-VR*VR-VZ*VZ
C SECOND, DD=0
      CA(2+4*J,1+4*J)=1.0
C THIRD, DD=0
      CA(3+4*J,3+4*J)=-VZ
      CA(3+4*J,4+4*J)=VR-1.0/VR
C FOURTH, DD=0
      CA(4+4*J,3+4*J)=-VR
      CA(4+4*J,4+4*J)=-VZ
C DD<>0
      DO 20 I=1,MM
C
      IF (IM(I,J).GT.-1) THEN
      C=CMPLX(COS(PHI(I)),SIN(PHI(I)))
      C=DD(I)*C
C
      CA(1+4*J,2+4*IM(I,J))=C*COM(I,J)
      CA(1+4*J,3+4*IM(I,J))=-C*SIM(I,J)
      CA(3+4*J,4+4*IM(I,J))=-C/VR
      CA(4+4*J,2+4*IM(I,J))=-C*VR*SIM(I,J)
      CA(4+4*J,3+4*IM(I,J))=-C*VR*COM(I,J)
      CA(4+4*J,4+4*IM(I,J))=-C*ZV
      CB(4+4*J,4+4*IM(I,J))=C
      END IF
C
      IF (IP(I,J).GT.-1) THEN
      C=CMPLX(COS(PHI(I)),-SIN(PHI(I)))
      C=DD(I)*C
C
      CA(1+4*J,2+4*IP(I,J))=C*COP(I,J)
      CA(1+4*J,3+4*IP(I,J))=-C*SIP(I,J)
      CA(3+4*J,4+4*IP(I,J))=-C/VR
      CA(4+4*J,2+4*IP(I,J))=-C*VR*SIP(I,J)
      CA(4+4*J,3+4*IP(I,J))=-C*VR*COP(I,J)
      CA(4+4*J,4+4*IP(I,J))=-C*VZ
      CB(4+4*J,4+4*IP(I,J))=C
      END IF
C

   20 CONTINUE
C
  100 CONTINUE
C
      RETURN
```

```
      END
C
C**** A sub for preparing a pair of real matrice for EISPACK****
C
      SUBROUTINE MTRX2(NN,CA,CB,CAB,AR,AI,BR,BI)
      REAL AR(NN,NN),AI(NN,NN),BR(NN,NN),BI(NN,NN)
      COMPLEX CAB(NN,NN),CA(NN,NN),CB(NN,NN)
      COMPLEX DET
C
      DO I=1,NN
      DO J=1,NN
      CAB(I,J)=0.0
      IF(I.EQ.J) CAB(I,J)=1.0
      END DO
      END DO
C                       Split CB into real and imaginary parts:
      DO K=1,NN
      DO L=1,NN
      AR(K,L)=REAL(CA(K,L))
      BR(K,L)=REAL(CB(K,L))
      AI(K,L)=IMAG(CA(K,L))
      BI(K,L)=IMAG(CB(K,L))
      END DO
      END DO
C
C                       print the result for checking:
      WRITE(8,59)
   59 FORMAT(//'A=')
      DO K=1,NN
      WRITE (8,55) (AR(K,L),L=1,NN)
      WRITE (8,55) (AI(K,L),L=1,NN)
      END DO
C                       print the result for checking:
      WRITE(8,57)
   57 FORMAT(//'B=')
      DO K=1,NN
      WRITE (8,55) (BR(K,L),L=1,NN)
      WRITE (8,55) (BI(K,L),L=1,NN)
      END DO
   55 FORMAT(1X,12E9.2E2)
C
C
C                       Inverse of CB: CAB=Inv(CB)
      CALL CMIVS(CB,CAB,NN,NN,DET)
      IF(DET.EQ.0.0) WRITE(6,15)
   15 FORMAT(5X,'SORRY, FAIL AT CMRVS')
C                       CB=Inv(CB)*CA:
      CALL CMMLT (CAB,CA,CB,NN)
C
      DO K=1,NN
      DO L=1,NN
      AR(K,L)=REAL(CA(K,L))
      BR(K,L)=REAL(CB(K,L))
      AI(K,L)=IMAG(CA(K,L))
      BI(K,L)=IMAG(CB(K,L))
      END DO
      END DO
C
      RETURN
      END


C****This a subroutine for finding inverse of a complex matrix
C                 or solution to a set of linear equations****
C
      SUBROUTINE CMIVS(A,B,N,M,DET)
```

```
      COMPLEX A(N,N),B(N,M),TEMP,DET
C
      DET=(1.0,0.0)
C
      DO 5 K=1,N
      IF(K.EQ.N) GOTO 10
C
      TEST=CABS(A(K,K))
      L=K
      KP1=K+1
C
C FIND THE LARGEST ELEMENT
C
      DO 15 I=KP1,N
      IF(TEST.GE.CABS(A(I,K))) GOTO 15
      TEST=CABS(A(I,K))
      L=I
   15 CONTINUE
C
      IF(L.EQ.K) GOTO 10
C
C CHANGE POSITIONS:
      DO J=1,N
      TEMP=A(L,J)
      A(L,J)=A(K,J)
      A(K,J)=TEMP
      END DO
      DO J=1,M
      TEMP = B(L,J)
      B(L,J)=B(K,J)
      B(K,J)=TEMP
      END DO
      DET=-DET
C
   10 DET=DET*A(K,K)
      IF(CABS(DET).EQ.0.0) GOTO 20
C
      IF(K.EQ. N) GOTO 25
      DO J=KP1,N
      A(K,J) = A(K,J)/A(K,K)
      END DO
C
   25 DO J=1,M
      B(K, J)=B(K,J)/A(K,K)
      END DO
C
      DO 35 I=1,N
      IF(I.EQ.K) GOTO 35
C
      IF(K.EQ.N) GOTO 30
      DO J=KP1,N
      A(I,J)=A( I, J )-A(I,K)*A( K ,J)
      END DO
   30 DO J=1,M
      B(I,J)=B(I,J)-A ( I,K )*B ( K ,J)
      END DO
   35 CONTINUE
C
    5 CONTINUE
C
   20 RETURN
      END
C
C****This is a subroutine for complex matrix multiplication****
C
      SUBROUTINE CMMLT (A,B,C,M)
```

```
      COMPLEX A(M,M),B(M,M),C(M,M),S
C
      DO 10 I=1,M
      DO 10 J=1,M
      S=0.0
      DO L=1,M
      S=S+A(I,L)*B(L,J)
      END DO
      C(I,J)=S
   10 CONTINUE
C
      RETURN
      END
C
C*****This is a subroutine computing the set of linear equations
C                    derived from the boundary conditions*****
C
      SUBROUTINE COEFCTS(MM,NOD,NN,M,D,NR,N0,NT,LAMBDA,KKZ,KR,COR,COT,
     X CA,CQ,CC,CD)
C
      INTEGER LL,MM,NOD,NN,M(4,0:NOD)
      REAL D,NR,N0,NT,LAMBDA,SIR,SIT
      REAL KKZ(0:NOD),KR(0:NOD),COR(0:NOD),COT(0:NOD)
      COMPLEX CX,CY,CJ,CQ(NN),CA(NN,NN),CC(NN,NN),CD(NN,2)
C
      LL=4*(NOD+1)
      CJ=(0.0,1.0)
      PI=3.141592654
C
C     write(6,48)
C  48 format(1x,'C=')
C
      DO 10 J=0,NOD
C
      Z=0.0
      DO I=1,MM
      VZ=VZ+M(I,J)*KKZ(I)
      END DO
      VZ=VZ*LAMBDA/2.0/PI/N0
      VR=KR(J)*LAMBDA/2.0/PI/N0
C
      SIR=KR(J)*LAMBDA/2.0/PI/NR
      SIT=KR(J)*LAMBDA/2.0/PI/NT
C
      DO 20 L=1,LL
      CC(4*J+1,L)=( COR(J)+(N0/NR)*(VZ+CQ(L)) )*CA(4*J+2,L)
      CX=( -COT(J)+(N0/NT)*(VZ+CQ(L)) )*CA(4*J+2,L)
      CY=2.0*PI*CJ*N0*CQ(L)*D/LAMBDA
      CC(4*J+2,L)=CX*CEXP(CY)
      CC(4*J+3,L)=(1.0+(N0/NR)*(VZ+CQ(L))*COR(J))*CA(4*J+3,L)
     X-SIR*COR(J)*CA(4*J+4,L)
      CX=( -1.0+(N0/NT)*(VZ+CQ(L))*COT(J) )*CA(4*J+3,L)
     X-SIT*COT(J)*CA(4*J+4,L)
      CC(4*J+4,L)=CX*CEXP(CY)
   20 CONTINUE
C
C     write(6,50) (real(cc(1+4*J,I)),I=1,II)
C     write(6,50) (imag(cc(1+4*j,I)),I=1,II)
C     write(6,50) (real(cc(2+4*j,I)),I=1,II)
C     write(6,50) (imag(cc(2+4*j,I)),I=1,II)
C     write(6,50) (real(cc(3+4*j,I)),I=1,II)
C     write(6,50) (imag(cc(3+4*j,I)),I=1,II)
C     write(6,50) (real(cc(4+4*j,I)),I=1,II)
C     write(6,50) (imag(cc(4+4*j,I)),I=1,II)
C
C  50 format(2x,8E10.3E1)
```

```
C
      DO I=1,4
      CD(4*J+I,1)=0.0
      CD(4*J+I,2)=0.0
      END DO
   10 CONTINUE
      CD(1,1)=2.0*COR(0)
      CD(3,2)=2.0*COR(0)
C
C     WRITE(6,63)
C  63 FORMAT(2X,'CD=')
C     DO I=1,NN
C     WRITE(6,65) (CD(I,J),J=1,2)
C  65 FORMAT(1X,4E10.3E1)
C     END DO
C
      RETURN
      END
C
C*****This is a sub. for computing the John's matrices*****
C
      SUBROUTINE JONESMTX(NOD,NN,N0,D,LAMBDA,COR,COT,CQ,CA,CD,MR,MT)
      INTEGER NOD,NN
      REAL N0,D,LAMBDA
      REAL COR(0:NOD),COT(0:NOD)
      COMPLEX CJ,CX
      COMPLEX CQ(NN),CA(NN,NN),CD(NN,2)
      COMPLEX MR(2,2,0:NOD),MT(2,2,0:NOD)
C
C     WRITE(6,63)
C  63 FORMAT(2X,'CD=')
C     DO I=1,NN
C     WRITE(6,65) (CD(I,J),J=1,2)
C  65 FORMAT(1X,4E10.3E1)
C     END DO
C           MR: John's matrix for the J-th reflection
C           MT: John's matrix for the J-th transmission
      PI=3.141592654
      CJ=(0.0,1.0)
C
      DO 20 J=0,NOD
C
      DO 10 I=1,2
      MR(1,I,J)=0.0
      MR(2,I,J)=0.0
      MT(1,I,J)=0.0
      MT(2,I,J)=0.0
      DO L=1,NN
      MR(1,I,J)=MR(1,I,J)+CD(L,I)*CA(4*J+2,L)
      MR(2,I,J)=MR(2,I,J)-CD(L,I)*CA(4*J+3,L)
      CX=2.0*PI*N0*CJ*CQ(L)*D/LAMBDA
      MT(1,I,J)=MT(1,I,J)+CD(L,I)*CA(4*J+2,L)*CEXP(CX)
      MT(2,I,J)=MT(2,I,J)+CD(L,I)*CA(4*J+3,L)*CEXP(CX)
      END DO
      MR(2,I,J)=MR(2,I,J)/COR(J)
      MT(2,I,J)=MT(2,I,J)/COT(J)
   10 CONTINUE
   20 CONTINUE
      MR(1,1,0)=MR(1,1,0)-1.0
      MR(2,2,0)=MR(2,2,0)+1.0
C
C     DO J=0,NOD
C     write(8,79) J
C  79 format(1x,'J=',I2)
C     WRITE(8,*) 'D     M(0)     M(1)'
C     WRITE(8,81) D,((MT(I,K,J),I=1,2),K=1,2)
```

```
C  81 FORMAT(1X,9F8.5)
C    WRITE(8,82) ((MT(I,K,J),I=1,2),K=1,2)
C  82 FORMAT(5X,'MT=',8F8.5)
C    END DO
C
     RETURN
     END
C
C*****This is a sub for Computing the power coupling matrices*****
C
     SUBROUTINE PCPLMTRX(NOD,NR,NT,COR,COT,MR,MT,CR,CT,PR,PT)
C
     INTEGER NOD
     REAL X,Y
     REAL NR,NT,COR(0:NOD),COT(0:NOD)
     REAL CR(2,2,0:NOD),CT(2,2,0:NOD),PR(2,2,0:NOD),PT(2,2,0:NOD)
     COMPLEX MR(2,2,0:NOD),MT(2,2,0:NOD)
C
C                CR: coupling matrix in reflection region
C                PR: phase corresponding to CR
C                CT: power coupling matrix in transmission region
C                PT: phase corresponding to CT
     DO J=0,NOD
     DO K=1,2
     DO I=1,2
     X=REAL(MR(I,K,J))
     Y=AIMAG(MR(I,K,J))
     CR(I,K,J)=(X*X+Y*Y)*COR(J)/COR(0)
     CR(I,K,J)=(CR(I,K,J))
     IF(CR(I,K,J).LT.1.0E-8) THEN
     PR(I,K,J)=0.0
     ELSE
     PR(I,K,J)=ATAN(Y/X)
     END IF
c
     X=REAL(MT(I,K,J))
     Y=AIMAG(MT(I,K,J))
     CT(I,K,J)=(X*X+Y*Y)*NT*COT(J)/NR/COR(0)
     CT(I,K,J)=(CT(I,K,J))
     IF(CT(I,K,J).LT.1.0E-8) THEN
     PT(I,K,J)=0.0
     ELSE
     PT(I,K,J)=ATAN(Y/X)
     END IF
     END DO
     END DO
     END DO
C
C    DO J=0,NOD
C    WRITE(6,72) J
C  72 FORMAT(1X,'J=',I2)
C    WRITE(6,71) ((CR(I,K,J),I=1,2),K=1,2)
C  71 FORMAT(5X,'CR=',4F10.5)
c    WRITE(6,74) ((PR(I,K,0),I=1,2),K=1,2)
c  74 FORMAT(5X,'PR=',4F10.5)
C    WRITE(6,73) ((CT(I,K,J),I=1,2),K=1,2)
C  73 FORMAT(5X,'CT=',4F10.5)
C    WRITE(6,76) ((PT(I,K,J),I=1,2),K=1,2)
C  76 FORMAT(5X,'PT=',4F10.5)
C    END DO
C
     RETURN
     END
CC
C
C*****This is a subroutine for the eigenvalues and
```

```
C                vectors of a pair of complex matrices****
C
      SUBROUTINE CEIGEN(NN,BR,BI,QR,QI,VR,VI,CQ,CV)
      REAL BR(NN,NN),BI(NN,NN),QR(NN),QI(NN),VR(NN,NN),VI(NN,NN),
     X     FV2(40),FV3(40)
      COMPLEX CQ(NN),CV(NN,NN)
C
      WRITE(8,57)
   57 FORMAT(//'B=')
      DO K=1,NN
      WRITE (8,55) (BR(K,L),L=1,NN)
      WRITE (8,55) (BI(K,L),L=1,NN)
      END DO
   55 FORMAT(1X,12E10.3E1)
C
      CALL CG(NN,NN,BR,BI,QR,QI,1,VR,VI,FV2,FV3,IERR)
C
C
      WRITE(8,58)
   58 FORMAT(//'Q=')
      WRITE(8,56) (QR(L),L=1,NN)
      WRITE(8,56) (QI(L),L=1,NN)
      WRITE(8,59)
   59 FORMAT(//'V=')
      DO K=1,NN
      WRITE(8,56) (VR(K,L),L=1,NN)
      WRITE(8,56) (VI(K,L),L=1,NN)
      END DO
   56 FORMAT(1X,12E9.2E2)
C                Build complex array CQ & CV:
C
      DO K=1,NN
      CQ(K)=CMPLX(QR(K),QI(K))
      DO L=1,NN
      CV(K,L)=CMPLX(VR(K,L),VI(K,L))
      END DO
      END DO
C
C
      RETURN
      END
```

```
      SUBROUTINE CG(NM,N,AR,AI,WR,WI,MATZ,ZR,ZI,FV2,FV3,IERR)
C
      INTEGER N,NM,IS1,IS2,IERR,MATZ
      REAL AR(NM,N),AI(NM,N),WR(N),WI(N),ZR(N,N),ZI(N,N),
     X  FV2(40),FV3(40)
C
      IF (N .LE. NM) GO TO 10
      IERR = 10 * N
      GO TO 20
C
   10 IS1 = 1
      IS2 = N
      CALL CORTH(NM,N,IS1,IS2,AR,AI,FV2,FV3)
      CALL COMQR2(NM,N,IS1,IS2,FV2,FV3,AR,AI,WR,WI,ZR,ZI,IERR)
C
   20 RETURN
      END

      SUBROUTINE CORTH(NM,N,LOW,IGH,AR,AI,ORTR,ORTI)
C
      INTEGER I,J,M,N,II,JJ,LA,MP,NM,IGH,KP1,LOW
      REAL AR(NM,N),AI(NM,N),ORTR(IGH),ORTI(IGH)
      REAL F,G,H,FI,FR,SCALE
      REAL SQRT,CABS,ABS
      COMPLEX CMPLX
C
      LA = IGH - 1
      KP1 = LOW + 1
      IF (LA .LT. KP1) GO TO 200
C
      DO 180 M = KP1, LA
      H = 0.0
      ORTR(M) = 0.0
      ORTI(M) = 0.0
      SCALE = 0.0
C     ********** SCALE COLUMN (ALGOL TOL THEN NOT NEEDED) **********
      DO 90 I = M, IGH
   90 SCALE = SCALE + ABS(AR(I,M-1)) + ABS(AI(I,M-1))
C
      IF (SCALE .EQ. 0.0) GO TO 180
      MP = M + IGH
C     ********** FOR I=IGH STEP -1 UNTIL M DO -- **********
      DO 100 II = M, IGH
      I = MP - II
      ORTR(I) = AR(I,M-1) / SCALE
      ORTI(I) = AI(I,M-1) / SCALE
      H = H + ORTR(I) * ORTR(I) + ORTI(I) * ORTI(I)
  100 CONTINUE
C
      G = SQRT(H)
      F = CABS(CMPLX(ORTR(M),ORTI(M)))
      IF (F .EQ. 0.0) GO TO 103
      H = H + F * G
      G = G / F
      ORTR(M) = (1.0 + G) * ORTR(M)
      ORTI(M) = (1.0 + G) * ORTI(M)
      GO TO 105
C
  103 ORTR(M) = G
      AR(M,M-1) = SCALE
C     ********** FORM (I-(U*UT)/H) * A **********
  105 DO 130 J = M, N
      FR = 0.0
      FI = 0.0
C     ********** FOR I=IGH STEP -1 UNTIL M DO -- **********
      DO 110 II = M, IGH
```

```
      I = MP - II
      FR = FR + ORTR(I) * AR(I,J) + ORTI(I) * AI(I,J)
      FI = FI + ORTR(I) * AI(I,J) - ORTI(I) * AR(I,J)
  110 CONTINUE
C
      FR = FR / H
      FI = FI / H
C
      DO 120 I = M, IGH
      AR(I,J) = AR(I,J) - FR * ORTR(I) + FI * ORTI(I)
      AI(I,J) = AI(I,J) - FR * ORTI(I) - FI * ORTR(I)
  120 CONTINUE
C
  130 CONTINUE
C     ********** FORM (I-(U*UT)/H)*A*(I-(U*UT)/H) **********
      DO 160 I = 1, IGH
      FR = 0.0
      FI = 0.0
C     ********** FOR J=IGH STEP -1 UNTIL M DO -- **********
      DO 140 JJ = M, IGH
      J = MP - JJ
      FR = FR + ORTR(J) * AR(I,J) - ORTI(J) * AI(I,J)
      FI = FI + ORTR(J) * AI(I,J) + ORTI(J) * AR(I,J)
  140 CONTINUE
C
      FR = FR / H
      FI = FI / H
C
      DO 150 J = M, IGH
      AR(I,J) = AR(I,J) - FR * ORTR(J) - FI * ORTI(J)
      AI(I,J) = AI(I,J) + FR * ORTI(J) - FI * ORTR(J)
  150 CONTINUE
C
  160 CONTINUE
C
      ORTR(M) = SCALE * ORTR(M)
      ORTI(M) = SCALE * ORTI(M)
      AR(M,M-1) = -G * AR(M,M-1)
      AI(M,M-1) = -G * AI(M,M-1)
  180 CONTINUE
C
  200 RETURN
      END
C
C
      SUBROUTINE COMQR2(NM,N,LOW,IGH,ORTR,ORTI,HR,HI,WR,WI,ZR,ZI,IERR)

      INTEGER I,J,K,L,M,N,EN,II,JJ,LL,NM,NN,IGH,IP1,
     X        ITS,LOW,LP1,ENM1,IEND,IERR
      REAL HR(NM,N),HI(NM,N),WR(N),WI(N),ZR(NM,N),ZI(NM,N),
     X     ORTR(IGH),ORTI(IGH)
      REAL SI,SR,TI,TR,XI,XR,YI,YR,ZZI,ZZR,NORM,MACHEP
      REAL SQRT,CABS,ABS
      INTEGER MIN0
      COMPLEX Z3
      COMPLEX CSQRT,CMPLX
      REAL REAL,AIMAG
C
C     ********** MACHEP IS A MACHINE DEPENDENT PARAMETER SPECIFYING
C     THE RELATIVE PRECISION OF FLOATING POINT ARITHMETIC.**********
      MACHEP = 1.0E-32
C
      IERR = 0
C
C     ********** INITIALIZE EIGENVECTOR MATRIX **********
      DO 100 I = 1, N
```

```
C
      DO 100 J = 1, N
      ZR(I,J) = 0.0
      ZI(I,J) = 0.0
      IF (I .EQ. J) ZR(I,J) = 1.0
  100 CONTINUE
C     ********** FORM THE MATRIX OF ACCUMULATED TRANSFORMATIONS
C     FROM THE INFORMATION LEFT BY CORTH **********
      IEND = IGH - LOW - 1
      IF (IEND) 180, 150, 105
C     ********** FOR I=IGH-1 STEP -1 UNTIL LOW+1 DO -- **********
  105 DO 140 II = 1, IEND
      I = IGH - II
      IF (ORTR(I) .EQ. 0.0 .AND. ORTI(I) .EQ. 0.0) GO TO 140
      IF (HR(I,I-1) .EQ. 0.0 .AND. HI(I,I-1) .EQ. 0.0) GO TO 140
C     ********** NORM BELOW IS NEGATIVE OF H FORMED IN CORTH **********
      NORM = HR(I,I-1) * ORTR(I) + HI(I,I-1) * ORTI(I)
      IP1 = I + 1
C
      DO 110 K = IP1, IGH
      ORTR(K) = HR(K,I-1)
      ORTI(K) = HI(K,I-1)
  110 CONTINUE
C
      DO 130 J = I, IGH
      SR = 0.0
      SI = 0.0
C
      DO 115 K = I, IGH
      SR = SR + ORTR(K) * ZR(K,J) + ORTI(K) * ZI(K,J)
      SI = SI + ORTR(K) * ZI(K,J) - ORTI(K) * ZR(K,J)
  115 CONTINUE
C
      SR = SR / NORM
      SI = SI / NORM
C
      DO 120 K = I, IGH
      ZR(K,J) = ZR(K,J) + SR * ORTR(K) - SI * ORTI(K)
      ZI(K,J) = ZI(K,J) + SR * ORTI(K) + SI * ORTR(K)
  120 CONTINUE
C
  130 CONTINUE
C
  140 CONTINUE
C
C     ********** CREATE REAL SUBDIAGONAL ELEMENTS **********
  150 L = LOW + 1
C
      DO 170 I = L, IGH
      LL = MIN0(I+1,IGH)
      IF (HI(I,I-1) .EQ. 0.0) GO TO 170
      NORM = CABS(CMPLX(HR(I,I-1),HI(I,I-1)))
      YR = HR(I,I-1) / NORM
      YI = HI(I,I-1) / NORM
      HR(I,I-1) = NORM
      HI(I,I-1) = 0.0
C
      DO 155 J = I, N
      SI = YR * HI(I,J) - YI * HR(I,J)
      HR(I,J) = YR * HR(I,J) + YI * HI(I,J)
      HI(I,J) = SI
  155 CONTINUE
C
      DO 160 J = 1, LL
      SI = YR * HI(J,I) + YI * HR(J,I)
      HR(J,I) = YR * HR(J,I) - YI * HI(J,I)
```

```
      HI(J,I) = SI
  160 CONTINUE
C
      DO 165 J = LOW, IGH
      SI = YR * ZI(J,I) + YI * ZR(J,I)
      ZR(J,I) = YR * ZR(J,I) - YI * ZI(J,I)
      ZI(J,I) = SI
  165 CONTINUE
C
  170 CONTINUE
C     ********** STORE ROOTS ISOLATED BY CBAL **********
  180 DO 200 I = 1, N
      IF (I .GE. LOW .AND. I .LE. IGH) GO TO 200
      WR(I) = HR(I,I)
      WI(I) = HI(I,I)
  200 CONTINUE
C
      EN = IGH
      TR = 0.0
      TI = 0.0


C     ********** SEARCH FOR NEXT EIGENVALUE **********
  220 IF (EN .LT. LOW) GO TO 680
      ITS = 0
      ENM1 = EN - 1
C     ********** LOOK FOR SINGLE SMALL SUB-DIAGONAL ELEMENT
C                FOR L=EN STEP -1 UNTIL LOW DO -- **********
  240 DO 260 LL = LOW, EN
      L = EN + LOW - LL
      IF (L .EQ. LOW) GO TO 300
      IF (ABS(HR(L,L-1)) .LE.
     X    MACHEP * (ABS(HR(L-1,L-1)) + ABS(HI(L-1,L-1))
     X          + ABS(HR(L,L)) +ABS(HI(L,L)))) GO TO 300
  260 CONTINUE
C     ********** FORM SHIFT **********
  300 IF (L .EQ. EN) GO TO 660
      IF (ITS .EQ. 30) GO TO 1000
      IF (ITS .EQ. 10 .OR. ITS .EQ. 20) GO TO 320
      SR = HR(EN,EN)
      SI = HI(EN,EN)
      XR = HR(ENM1,EN) * HR(EN,ENM1)
      XI = HI(ENM1,EN) * HR(EN,ENM1)
      IF (XR .EQ. 0.0 .AND. XI .EQ. 0.0) GO TO 340
      YR = (HR(ENM1,ENM1) - SR) / 2.0
      YI = (HI(ENM1,ENM1) - SI) / 2.0
      Z3 = CSQRT(CMPLX(YR**2-YI**2+XR,2.0*YR*YI+XI))
      ZZR = REAL(Z3)
      ZZI = AIMAG(Z3)
      IF (YR * ZZR + YI * ZZI .GE. 0.0) GO TO 310
      ZZR = -ZZR
      ZZI = -ZZI
  310 Z3 = CMPLX(XR,XI) / CMPLX(YR+ZZR,YI+ZZI)
      SR = SR - REAL(Z3)
      SI = SI - AIMAG(Z3)
      GO TO 340
C     ********** FORM EXCEPTIONAL SHIFT **********
  320 SR = ABS(HR(EN,ENM1)) + ABS(HR(ENM1,EN-2))
      SI = 0.0
C
  340 DO 360 I = LOW, EN
      HR(I,I) = HR(I,I) - SR
      HI(I,I) = HI(I,I) - SI
  360 CONTINUE
C
      TR = TR + SR
```

```
      TI = TI + SI
      ITS = ITS + 1
C     ********** REDUCE TO TRIANGLE (ROWS) **********
      LP1 = L + 1
C
      DO 500 I = LP1, EN
      SR = HR(I,I-1)
      HR(I,I-1) = 0.0
      NORM = SQRT(HR(I-1,I-1)*HR(I-1,I-1)+HI(I-1,I-1)*HI(I-1,I-1)
     X       +SR*SR)
      XR = HR(I-1,I-1) / NORM
      WR(I-1) = XR
      XI = HI(I-1,I-1) / NORM
      WI(I-1) = XI
      HR(I-1,I-1) = NORM
      HI(I-1,I-1) = 0.0
      HI(I,I-1) = SR / NORM
C
      DO 490 J = I, N
      YR = HR(I-1,J)
      YI = HI(I-1,J)
      ZZR = HR(I,J)
      ZZI = HI(I,J)
      HR(I-1,J) = XR * YR + XI * YI + HI(I,I-1) * ZZR
      HI(I-1,J) = XR * YI - XI * YR + HI(I,I-1) * ZZI
      HR(I,J) = XR * ZZR - XI * ZZI - HI(I,I-1) * YR
        HI(I,J) = XR * ZZI + XI * ZZR - HI(I,I-1) * YI
  490 CONTINUE
C
  500 CONTINUE
C
      SI = HI(EN,EN)
      IF (SI .EQ. 0.0) GO TO 540
      NORM = CABS(CMPLX(HR(EN,EN),SI))
      SR = HR(EN,EN) / NORM
      SI = SI / NORM
      HR(EN,EN) = NORM
      HI(EN,EN) = 0.0
      IF (EN .EQ. N) GO TO 540
      IP1 = EN + 1
C
      DO 520 J = IP1, N
      YR = HR(EN,J)
      YI = HI(EN,J)
      HR(EN,J) = SR * YR + SI * YI
      HI(EN,J) = SR * YI - SI * YR
  520 CONTINUE
C     ********** INVERSE OPERATION (COLUMNS) **********
  540 DO 600 J = LP1, EN
      XR = WR(J-1)
      XI = WI(J-1)
C
      DO 580 I = 1, J
      YR = HR(I,J-1)
      YI = 0.0
      ZZR = HR(I,J)
      ZZI = HI(I,J)
      IF (I .EQ. J) GO TO 560
C
      YI = HI(I,J-1)
      HI(I,J-1) = XR * YI + XI * YR + HI(J,J-1) * ZZI
  560 HR(I,J-1) = XR * YR - XI * YI + HI(J,J-1) * ZZR
      HR(I,J) = XR * ZZR + XI * ZZI - HI(J,J-1) * YR
      HI(I,J) = XR * ZZI - XI * ZZR - HI(J,J-1) * YI
  580 CONTINUE
C
```

```
      DO 590 I = LOW, IGH
      YR = ZR(I,J-1)
      YI = ZI(I,J-1)
      ZZR = ZR(I,J)
      ZZI = ZI(I,J)
      ZR(I,J-1) = XR * YR - XI * YI + HI(J,J-1) * ZZR
      ZI(I,J-1) = XR * YI + XI * YR + HI(J,J-1) * ZZI
      ZR(I,J) = XR * ZZR + XI * ZZI - HI(J,J-1) * YR
      ZI(I,J) = XR * ZZI - XI * ZZR - HI(J,J-1) * YI
  590 CONTINUE
C
  600 CONTINUE
C
      IF (SI .EQ. 0.0) GO TO 240
C
      DO 630 I = 1, EN
      YR = HR(I,EN)
      YI = HI(I,EN)
      HR(I,EN) = SR * YR - SI * YI
      HI(I,EN) = SR * YI + SI * YR
  630 CONTINUE
C
      DO 640 I = LOW, IGH
      YR = ZR(I,EN)
      YI = ZI(I,EN)
      ZR(I,EN) = SR * YR - SI * YI
      ZI(I,EN) = SR * YI + SI * YR
  640 CONTINUE
C
      GO TO 240
C     ********** A ROOT FOUND **********
  660 HR(EN,EN) = HR(EN,EN) + TR
      WR(EN) = HR(EN,EN)
      HI(EN,EN) = HI(EN,EN) + TI
      WI(EN) = HI(EN,EN)
      EN = ENM1
      GO TO 220
C     ********** ALL ROOTS FOUND. BACKSUBSTITUTE TO FIND
C                VECTORS OF UPPER TRIANGULAR FORM **********
  680 NORM = 0.0
C
      DO 720 I = 1, N
C
      DO 720 J = I, N
      NORM = NORM + ABS(HR(I,J)) + ABS(HI(I,J))
  720 CONTINUE
C
      IF (N .EQ. 1 .OR. NORM .EQ. 0.0) GO TO 1001
C     ********** FOR EN=N STEP -1 UNTIL 2 DO -- **********
      DO 800 NN = 2, N
      EN = N + 2 - NN
      XR = WR(EN)
      XI = WI(EN)
      ENM1 = EN - 1
C     ********** FOR I=EN-1 STEP -1 UNTIL 1 DO -- **********
      DO 780 II = 1, ENM1
      I = EN - II
      ZZR = HR(I,EN)
      ZZI = HI(I,EN)
      IF (I .EQ. ENM1) GO TO 760
      IP1 = I + 1
C
      DO 740 J = IP1, ENM1
      ZZR = ZZR + HR(I,J) * HR(J,EN) - HI(I,J) * HI(J,EN)
      ZZI = ZZI + HR(I,J) * HI(J,EN) + HI(I,J) * HR(J,EN)
  740 CONTINUE
```

```
C
 760  YR = XR - WR(I)
      YI = XI - WI(I)
      IF (YR .EQ. 0.0 .AND. YI .EQ. 0.0) YR = MACHEP * NORM
      Z3 = CMPLX(ZZR,ZZI) / CMPLX(YR,YI)
      HR(I,EN) = REAL(Z3)
      HI(I,EN) = AIMAG(Z3)
 780  CONTINUE
C
 800  CONTINUE
C     ********** END BACKSUBSTITUTION **********
      ENM1 = N - 1
C     ********** VECTORS OF ISOLATED ROOTS **********
      DO 840 I = 1, ENM1
      IF (I .GE. LOW .AND. I .LE. IGH) GO TO 840
      IP1 = I + 1
C
      DO 820 J = IP1, N
      ZR(I,J) = HR(I,J)
      ZI(I,J) = HI(I,J)
 820  CONTINUE
C
 840  CONTINUE
C     ********** MULTIPLY BY TRANSFORMATION MATRIX TO GIVE
C           VECTORS OF ORIGINAL FULL MATRIX.
C           FOR J=N STEP -1 UNTIL LOW+1 DO -- **********
      DO 880 JJ = LOW, ENM1
      J = N + LOW - JJ
      M = MIN0(J-1,IGH)
C
      DO 880 I = LOW, IGH
      ZZR = ZR(I,J)
      ZZI = ZI(I,J)
C
      DO 860 K = LOW, M
      ZZR = ZZR + ZR(I,K) * HR(K,J) - ZI(I,K) * HI(K,J)
      ZZI = ZZI + ZR(I,K) * HI(K,J) + ZI(I,K) * HR(K,J)
 860  CONTINUE
C
      ZR(I,J) = ZZR
      ZI(I,J) = ZZI
 880  CONTINUE
C
      GO TO 1001
C     ********** SET ERROR -- NO CONVERGENCE TO AN
C           EIGENVALUE AFTER 30 ITERATIONS **********
 1000 IERR = EN
 1001 RETURN
      END
```